**„Dunărea de Jos" University of Galaţi**
**Doctoral School of Mechanical and Industrial Engineering**

# Doctoral Thesis

**- Summary -**

# Rheological and *pVT* Behavior of Polymer/MWCNT Nanocomposites

**PhD candidate,**
**Nicoleta-Violeta CRISTEA**, Eng.
„Dunărea de Jos" University of Galaţi

**Scientific coordinator**,
Professor **Cătălin FETECĂU**, Ph.D. Eng.
„Dunărea de Jos" University of Galaţi

**I4 Serie: Industrial Engineering** **No. 79**

**GALAŢI**
**2021**

**„Dunărea de Jos" University of Galaţi**
**Doctoral School of Mechanical and Industrial Engineering**

# Doctoral Thesis

**- Summary -**

# Rheological and *pVT* Behavior of Polymer/MWCNT Nanocomposites

**PhD candidate,**
**Nicoleta-Violeta CRISTEA**, Eng.
„Dunărea de Jos" University of Galaţi

| | |
|---|---|
| **Chairman** | Professor **Elena SCUTELNICU**, Ph.D. Eng.<br>„Dunărea de Jos" University of Galaţi |
| **Scientific coordinator** | Professor **Cătălin FETECĂU**, Ph.D. Eng.<br>„Dunărea de Jos" University of Galaţi |
| **Official referents** | Professor **Cristian-Vasile DOICIN**, Ph.D. Eng.<br>„Politehnica" University of Bucharest |
| | Professor **Maria-Carmen LOGHIN**, Ph.D. Eng.<br>„Gheorghe Asachi" University of Iaşi |
| | Professor **Mihaela BUCIUMEANU**, Ph.D. Eng.<br>„Dunărea de Jos" University of Galaţi |

**I4 Serie: Industrial Engineering** **No. 79**

**GALAŢI**
**2021**

# TABLE OF CONTENTS

# ABSTRACT

I hereby declare that this thesis contains no material which has been accepted for the award of any other degree or diploma at any university or equivalent institution and that, to the best of my knowledge and belief, this thesis contains no material previously published or written by another person, except where due reference is made in the text of the thesis. This thesis includes experimental results that can be found in the 17 manuscripts published in peer-reviewed journals.

The scope of this thesis was to add knowledge on the rheological properties, specific volume and thermal conductivity of various polymers/multi-walled carbon nanotubes (MWCNT) nanocomposites in order to provide reliable data for CAD/CAE simulation. The rheological data obtained from the capillary rheometer has great significance because this technique provides insight on the effect of shear rate on viscosity over a wide range of shear rates that are commonly encountered in the manufacturing processes. The pressure-Volume-Temperature (*pVT*) diagrams were determined in order to predict the volumetric shrinkage of the nanocomposites at slow cooling rates and at various temperature ranges. Additionally, thermal conductivity (*TC*) measurements were performed to investigate de effect of MWCNTs on the *TC* of the polymer/MWCNT nanocomposites.

The ideas, development and writing up of all the manuscripts in the thesis were the principal responsibility of myself, the candidate, working within the Doctoral School of Dunarea de Jos University of Galati under the supervision of Professor Cătălin Fetecău and Professor Felicia Stan. The inclusion of co-authors reflects the fact that the work came from active collaboration between researchers and acknowledges input into team-based research.

**Chapter one** covers the state-of-the-art after a short introduction on the main material data needed for the injection molding simulation. The states-of-the art were presented into three parts for better understanding the three types of measurements for determining the physical properties: viscosity, specific volume and thermal conductivity. The first part provides brief background, valuable information and the related research studies in the rheological behavior of the polymer/carbon nanotube nanocomposites. The second part presents the types of measurements to determine the *pVT* diagrams and a brief review of the available articles that studied the influence of pressure and temperature on the specific volume. Lastly, the third part of the state-of-the-art shows the various types of methods to determine the thermal conductivity and, from the literature review, the influence of CNTs on the *TC* was presented.

A small description of the materials tested and the characterization methods discussed in this thesis are presented in **Chapter two**. The nanocomposites analyzed in this thesis are thermoplastics such as low-density polyethylene (LDPE), high-density polyethylene (HDPE), ethylene vinyl acetate (EVA), polypropylene (PP) and thermoplastic polyurethane (TPU) filled with 0.1, 0.3, 0.5, 1, 3, and 5 wt.% of MWCNTs. Five types of measurements were performed on the polymer/MWCNT nanocomposites, such as: *DSC*, bulk density, capillary rheometry, specific volume and thermal conductivity. The rheological, *pVT* and *TC* behavior of the nanocomposites were performed using very complex equipment, i.e., the Rheograph 75 (RG75) high-pressure capillary rheometer (Göttfert, Germany).

**Chapter three** presents the thermal properties of the polymer/MWCNT nanocomposites analyzed. The addition of MWCNTs was found to influence the degree of crystallinity due to an increased number of nucleating sites; however, no trend was observed as a function of MWCNT loading. A small increase of the melting temperature was observed when the MWCNT loading increased for the nanocomposites that have a LDPE, HDPE, and PP matrix. Meanwhile, the melting temperature slightly decreased with increasing MWCNT loading for the EVA and TPU/MWCNT nanocomposites.

The rheological behavior of the polymer/MWCNT nanocomposites analyzed is presented and discussed in **Chapter four**. The viscosity decreased with increasing temperature for all polymer/MWCNT nanocomposites, more significantly at low shear rates. Whereas, at higher shear rates, the molecules disentangle and align, meaning that the mobility of polymer molecules increases and the dependency of viscosity on temperature decreases. The addition of MWCNTs was found to increase the viscosity, especially for the nanocomposites with higher MWCNT loadings, and to decrease the shear-thinning index, which can have an impact on the processability of the melt due to miscibility of the blend.

The results in **Chapter five** show that the nanocomposites with the LDPE, HDPE, and PP matrix, the specific volume is nearly constant with increasing nanotube loading up to 1 wt.%, where a further increase of MWCNT loading results in a decrease in the specific volume. However, the specific volume of the EVA/MWCNT nanocomposites has similar values only at low MWCNT loadings (0.1, 0.3, and 0.5 wt.%) with a decreasing trend with increasing the MWCNT loading. Regarding the *pVT* data of the TPU/MWCNT nanocomposites, the specific volume in the solid state has lower values at 1 wt.% than the ones found at low MWCNT loadings. The reduction of the specific volume with the addition of MWCNTs can be explained by the nanotubes that do not expand or contract as the temperature changes and counteract shrinkage effects due to molecular orientation. Also, the effect of MWCNTs on the specific volume slightly decreases by increasing pressure.

Beside the temperature and pressure, the thermal conductivity is also influenced by addition to the MWCNT loading and is thouroughly discussed in **Chapter six**. When the effects of temperature and pressure were separated from that of the MWCNTs, the results indicated a moderate enhancement in the thermal conductivity of the polymer/MWCNT nanocomposite (24–46%) with increasing MWCNT loading from 0.1 to 5 wt.%, although MWCNTs can exhibit thermal conductivity as high as 3000 W/m·K.

**Chapter seven** presents the analytical modeling of material properties of the polymer/MWCNT nanocomposites, i.e., the rheological and specific volume behavior using the Cross–WLF and 2-domain Tait models, respectively. The shear-thinning index calculated by the Cross–WLF model indicated that the polymer/MWCNT nanocomposites are suitable for injection molding. Furthermore, the values of shear-thinning index indicate that the nanotubes are in a state of good dispersion and aligned in the flow direction. Regarding the 2-domain Tait model, the specific volume at zero pressure was found to be nearly constant with increasing nanotube loading up to 1 wt.%, where a further increase of MWCNT loading results in a decrease in the specific volume.

Finally, in **Chapter eight**, the summary of the conclusions described at the end of each chapter are presented, followed by the original contributions of the author and potential and future research directions.

**Keywords:** *low-density polyethylene, high-density polyethylene, ethylene vinyl acetate, polypropylene, thermoplastic polyurethane, carbon nanotubes, DSC, shear viscosity, shear-thinning, specific volume, thermal conductivity*

# LIST OF ORIGINAL PUBLICATIONS

## ▪ Articles in ISI Journals

1. **Stanciu N.V.**, Stan F., Sandu I.L., Fetecău C., Ţurcanu A.M., **2021**, *Thermal, Rheological, Mechanical, and Electrical Properties of Polypropylene/Multi-Walled Carbon Nanotube Nanocomposites*, **Polymers**, Vol. 13, 187, https://doi.org/10.3390/polym13020187.
2. Stan F., **Stanciu N.V.**, Constantinescu A.M., Fetecău C., **2021**, *3D Printing of Flexible and Stretchable Parts using Multiwall Carbon Nanotube/Polyester-Based Thermoplastic Polyurethane*, **Journal of Manufacturing Science and Engineering Transactions of ASME**, Vol. 143, 051002-1-9, https://doi.org/10.1115/1.4048442.
3. **Stanciu N.V.**, Roşculeţ T.R, Fetecău C., Ţapu C., **2020**, *Forensic Facial Reconstruction using 3D Printing*, **Materiale Plastice**, Vol. 57(4), pp. 248–257, https://doi.org/10.37358/MP.20.4.5424.
4. **Stanciu N.V.**, Stan F., Fetecău C., **2020**, *Experimental Investigation of the Melt Shear Viscosity, Specific Volume and Thermal Conductivity of Low-Density Polyethylene/Multi-Walled Carbon Nanotube Composites Using Capillary Flow*, **Polymers**, Vol. 12, 1230, https://doi.org/10.3390/polym12061230.
5. **Stanciu N.V.**, Stan F., Sandu I.L., Susac F., Fetecău C., Roşculeţ T.R., **2019**, *Mechanical, Electrical and Rheological Behavior of Ethylene-Vinyl Acetate/Multi-Walled Carbon Nanotube Composites*, **Polymers**, Vol. 11, 1300, https://doi.org/10.3390/polym11081300.
6. Stan F., **Stanciu N.V.**, Fetecău C., Sandu I.L., **2019**, *Mechanical Recycling of Low-Density Polyethylene/Carbon Nanotube Composites and its Effect on Material Properties*, **Journal of Manufacturing Science and Engineering-Transactions of the ASME**, Vol. 141, 091004-1-7, https://doi.org/10.1115/1.4044101.
7. **Stanciu N.V.**, Stan F., Fetecău C., **2018**, *Melt Shear Rheology and pVT Behavior of Polypropylene/Multi-Walled Carbon Nanotube Composites*, **Materiale Plastice**, Vol. 55, pp. 482–487, https://doi.org/10.37358/MP.18.4.5058.
8. Stan F., **Stanciu N.V.**, Fetecău C., **2017**, *Melt Rheological Properties of Ethylene-Vinyl Acetate/Multi-Walled Carbon Nanotube Composites*, **Composites Part B Engineering**, Vol. 110, pp. 20–31, https://doi.org/10.1016/j.compositesb.2016.10.071.

## ▪ Published papers in conference proceedings

1. Stan F., Sandu I.L., Ţurcanu A.M., **Stanciu N.V.**, Fetecău C., **2021**, *The Influence of Carbon Nanotube and Reprocessing on the Morphology and Properties of High Density Polyethylene/Carbon Nanotube Composites*, **the 2021 Manufacturing Science and Engineering Conference (MSEC2021)**, Virtual, Online, 21-25 June 2021, in press.
2. Stan F., **Stanciu N.V.**, Fetecău C., **2019**, *On the 3D Printability of Multi-Walled Carbon Nanotube/High Density Polyethylene Composites*, **Proceedings of the 2019 Manufacturing Science and Engineering Conference (MSEC2019)**, Penn State Erie, The Behrend College, Erie, PA, USA, 10-14 June 2019, Paper No. MSEC2019-2776, https://doi.org/10.1115/MSEC2019-2776.
3. **Stanciu N.V.**, Stan F., Fetecău C., Susac, F., **2019**, *On the Feasibility of Printing 3D Composite Objects Based on Polypropylene/Multi-Walled Carbon Nanotubes*, **9th International Conference on Manufacturing Science and Education**, Sibiu, Romania, 5-7 June 2019. Published in MATEC Web of Conference, Vol. 290, 03017, https://doi.org/10.1051/matecconf/201929003017.

4. Fetecău C., Stan F., Timotin P., **Stanciu N.V.**, Roşculeţ R.T., **2018**, *Mechanical Behavior of LDPE/MWCNT Composites after Fatigue and Cryogenic Treatment*, **Proceedings of the 2018 Manufacturing Science and Engineering Conference (MSEC2018)**, Collage Station, TX, USA, 18-22 June 2018, Paper No. MSEC2018-6532, V002T04A014, https://doi.org/10.1115/MSEC2018-6532.
5. Stan F., **Stanciu N.V.**, Fetecău C., Sandu I.L., **2018**, *Characterization of Welding Attributes in Friction Spot Stir Welding of High-Density Polyethylene/Multi-Walled Carbon Nanotube Composites*, **Proceedings of the 2018 Manufacturing Science and Engineering Conference (MSEC2018)**, Collage Station, TX, USA, 18-22 June 2018, Paper No. MSEC2018-6317, V002T04A006, https://doi.org/10.1115/MSEC2018-6317.
6. Stan F., Fetecău C., **Stanciu N.V.**, Roşculeţ T.R., Sandu I.L., **2017**, *Investigation of Structure-Property Relationships in Thermoplastic Polyurethane/Multiwalled Carbon Nanotube Composites*, **ASME 2017 12th International Manufacturing Science and Engineering Conference (MSEC2017)**, Vol. 2: Additive Manufacturing; Materials, Los Angeles, California, USA, 4-8 June 2017, Paper No. MSEC2017-2760, pp. V002T03A016, https://doi.org/10.1115/MSEC2017-2760.
7. Stan F., Fetecău C., **Stanciu N.V.**, **2017**, *Fabrication of Micro-Channels in PMMA by Tip-Based Microfabrication Technique: Depth and Friction Analysis*, **ASME 2017 12th International Manufacturing Science and Engineering Conference (MSEC2017)**, Vol. 2: Additive Manufacturing; Materials, Los Angeles, California, USA, 4-8 June 2017, Paper No. MSEC2017-2763, V002T03A017, https://doi.org/10.1115/MSEC2017-2763.
8. Cristea A., Fetecău C., **Stanciu N.V.**, **2017**, *Experimental Research on the Durability of the Cutting Tools for Cutting-Off Steel Profiles*, **ImanE&E**, 21st edition, 25-26 May 2017, Iaşi, România (MATEC Web of Conferences), https://doi.org/10.1051/matecconf/201711201021.
9. Fetecău C., Stan F., **Cristea N.V.**, Sandu I.L., **2016**, *An Analysis of Interfacial Adhesion Between TPU/MWCNT Composites and ABS by Over Injection Molding*, **ASME 2016 Manufacturing Science and Engineering Conference (MSEC2016) & 44rd North American Manufacturing Research Conference (NAMRC44) of SME**, Virginia Tech University, USA, 27 June – 1 July 2016, Paper No. MSEC2016-8571, V001T02A050, https://doi.org/10.1115/MSEC2016-8571.

## ▪ Published papers/ posters at national/ international conferences

1. **Stanciu N.V.**, Stan F., Fetecău C., **2020**, *Determination of Transition Temperature of Polymer/MWCNT Nanocomposites Based on the pVT Data*, **Scientific Conference of Doctoral Schools**, SCDS-UDJG 2020, 18-19 June 2020, Galaţi, România.
2. **Stanciu N.V.,** Constantinescu A.M., Stan F., Fetecău C., **2019**, *3D Printing of Flexible Circuits Based on EVA/CNT Composite*, **Salonul inovării şi cercetării Ugal Invent 2019**, 16-18 October 2019, Galaţi, România.
3. **Stanciu N.V.**, Constantinescu A.M., Stan F., Fetecău C., **2019**, *Mechanical and Electrical Properties of 3D Printed Sandwich Structures using Polyoxymethylene/MWCNT Composites and Poly(lactic) Acid*, **Polymer Processing in Engineering Conference**, 7-9 October 2019, Galaţi, România.
4. Sandu I.L., **Stanciu N.V.**, Stan F., Fetecău C., **2019**, *Effect of Multiple Recycling on the Mechanical and Rheological Properties of Ethylene-Vinyl Acetate/Multi-Walled Carbon Nanotube Composites*, **Polymer Processing in Engineering Conference**, 7-9 October 2019, Galaţi, România.
5. Manole I., Sandu I.L., Stan F., **Stanciu N.V.**, Fetecău C., **2019**, *Fabrication of Composites from Plastic Waste*, **23rd International Exhibition of Inventics - Inventica**, 25-28 June 2019, Iași, România.

6. **Stanciu N.V.**, Stan F., Fetecău C., **2019**, *3D-Printing of Flexible Parts Based on LDPE/MWCNT Composites*, **Scientific Conference of Doctoral Schools**, SCDS-UDJG 2019, 7-8 June 2019, Galaţi, România.
7. **Stanciu N.V.**, Manole I., Stan F., Fetecău C., **2019**, *3D Printing of Flexible Strain Sensor Using Thermoplastic Polyurethane/Multi-Walled Carbon Nanotube Composites*, **11th edition of „Euroinvent"**, 16-18 May 2019, Iași, România.
8. Stan F., **Stanciu N.V.**, Sandu I.L., Fetecău C., Şerban A., **2019**, *Effect of Low- and Extreme Low-Temperature on Mechanical Properties of 3D Printed Polyethylene Terephthalate Glycol Copolymer*, **The Romanian Journal of Technical Sciences – Applied Mechanics**, Vol. 64, pp. 21–42.
9. **Stanciu N.V.**, Stan F., Fetecău C., Şerban A., **2018**, *Fabrication and Characterization of LDPE and HDPE Filaments for 3D Printing*, **Journal of Engineering Sciences and Innovation**, Vol. 3, pp. 299–312.
10. **Stanciu N.V.**, Stan F., Fetecău C., **2018**, *Fabrication of Polymer/Carbon Nanotube Filaments for 3D Printing*, **22nd International Exhibition of Inventics – Inventica**, 27-29 June 2018, Iași, România.
11. **Stanciu N.V.**, Stan F., Fetecău C., **2018**, *Pressure-Volume-Temperature Properties of High Density Polyethylene/Multi-Walled Carbon Nanotube Composites*, **Scientific Conference of Doctoral Schools**, SCDS-UDJG 2018, 7-8 June 2018, Galaţi, România.
12. **Stanciu N.V.**, Stan F., Fetecău C., **2018**, *Fabrication of Polymer/Carbon Nanotube Filaments for 3D Printing*, Euroinvent, **10th European Exhibition of Creativity and Innovation**, 17-19 May 2018, Iași, România.
13. Fetecău C., Stan F., **Stanciu N.V.**, **2017**, *Fixture Device for Delamination Testing of Two-Component Structure,* **Salonul inovării şi cercetării Ugal Invent 2017**, 19-20 October 2017, Galaţi, România.
14. **Stanciu N.V.**, Stan F., Fetecău C., **2017**, *On the Rheological Behavior of HDPE/MWCNT Nanocomposites*, **Rheology Summer School**, 18-23 June 2017, Gura Humorului, Suceava, România, ISSN: 2066-5790.
15. **Stanciu N.V.**, **2016**, *Fixture Device for Mode-I Delamination Testing*, **DAC-Xchange: Bright Minds meets Bright Future**, 4-6 October 2016, Stuttgart, Germany.

# 1. STATE-OF-THE-ART

## 1.1. Introduction

When filler is added to a polymer as reinforcement, the reinforcing filler component (*strong* and *stiff*) is supposed to bear most of the load or stress applied to the system while the polymer (*low strength*, *fairly tough* and *extensible*) should effectively transmit the load to the filler [1]. Advanced engineering materials with nano-sized fillers embedded inside the polymer matrix are named *nanocomposites* [2]. Nanocomposites are introduced in applications, such as medicine, food packaging, tissue engineering, agriculture, aerospace, and automotive industries [3,4] due to their exceptional mechanical [5-8], electrical [9-12], and thermal [13-15] properties, easy fabrication and cost-effectiveness [16,17].

The rheological parameters (viscosity, shear stress, shear rate, power-law index, $n$) are very important in deciding the suitable processing techniques and temperatures [26] in the manufacturing processes (injection molding or extrusion) [27]. The addition of fillers usually increases the viscosity **Error! Reference source not found.**, which can have an impact on the processability of the melt due to miscibility of the blend [26], thus the filler also becomes an important parameter [1].

Pressure-Volume-Temperature ($pVT$) data provides the specific volume, $V_{sp}$, at different pressure and temperature, as well as the variation of the glass transition temperature, $T_g$, with pressure [29]. The free volume available to molecules is reduced by increasing pressure or decreasing temperature, thus resulting in an increase in the intermolecular interactions [29]. It is expected that the viscosity would be less temperature sensitive for the filled polymer composites than the unfilled polymer [1] due to the fact that the free volume change is limited to the polymer fraction of the composite [1].

Rheological and $pVT$ data provide essential information for process simulation, which is an important part of the process setup and product design [30]. The quality of the molded part is influenced by the $pVT$ behavior [31] and can be an aid to design engineers to know how the polymer will behave inside the mold. Softwares such as Autodesk Moldflow and Moldex3D provide quantitative predictions based on reliable data to improve the flow, shrinkage or warpage problems in the molded parts [31,32]. Based on the volumetric change of the polymer, the volumetric shrinkage of the molded part can be predicted by the $pVT$ data. If the rheological behavior inside the mold can be simulated then the time, cost and material can be reduced as opposed to the trial and error method [32,33].

The rheological and $pVT$ data are temperature dependent, thus a deviation of calculated flow lines and shrinkage results in deviations in the simulated temperature history due to inaccurate thermal conductivity ($TC$) data [34]. The $TC$ data are necessary to reduce the occurrence of hot spots in injection molding specimens and for optimizing the heat transfer, thus less scrap rates [34]. The thermal conductivities of nanocomposites are strongly influenced by the filler type, size and shape [15,35,36], but also by the crystalline structure and interatomic interactions [15,37]. A major setback of the thermally conductive polymer nanocomposites is the high filler loading needed to achieve an appropriate level of $TC$ [15], causing the nanocomposite to be brittle, have poor processability and a high cost [15,37,38].

## 1.2. Review on the rheological behavior

The following review highlights the rheological behavior of polymer/CNT nanocomposites in terms of investigating the effect of CNTs on the viscosity. Since the rheological properties of polymer/CNT nanocomposites have been investigated by a numerous scientific reports, the discussion was focused on the most significant matrices. However, most papers investigated the viscosity at low

shear rates, thus providing little data regarding the viscosity at the medium and high shear rates that appear in the manufacturing processes.

*Han* et al. (2009) [68] showed that the complex viscosity and the storage and loss moduli of HDPE/multi-walled carbon nanotubes (MWCNTs) slightly increased with increasing MWCNT loading up to 5 wt.%, then significantly increased with further increasing the MWCNT loading (Figure 1.1), suggesting a rheological percolation threshold at 5 wt.%.

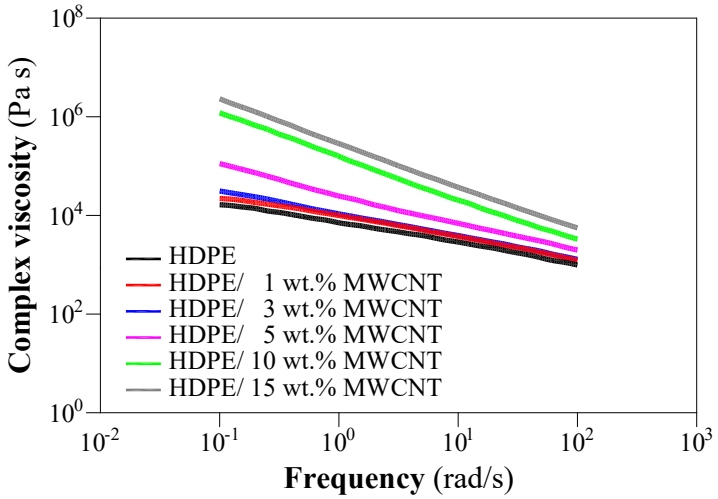


**Figure 1.1.** *Complex viscosity as a function of frequency for the HDPE/MWCNT nanocomposites*
Recreated from [68]

## 1.3. Review on the *pVT* behavior

In the following review, the *pVT* behavior of polymers and various composites was studied since no data regarding the specific volume behavior of polymers/CNT nanocomposites was found.

*Heidari* (2018) [102] measured the *pVT* properties of neat UHMWPE and filled with 10 wt.% nanohydroxyapatite (nHA) using SWO PVT 100 apparatus. Figure 1.2 shows that the specific volume decreased with the addition of the filler and with increasing pressure. Also, the specific volume increased with increasing temperature.

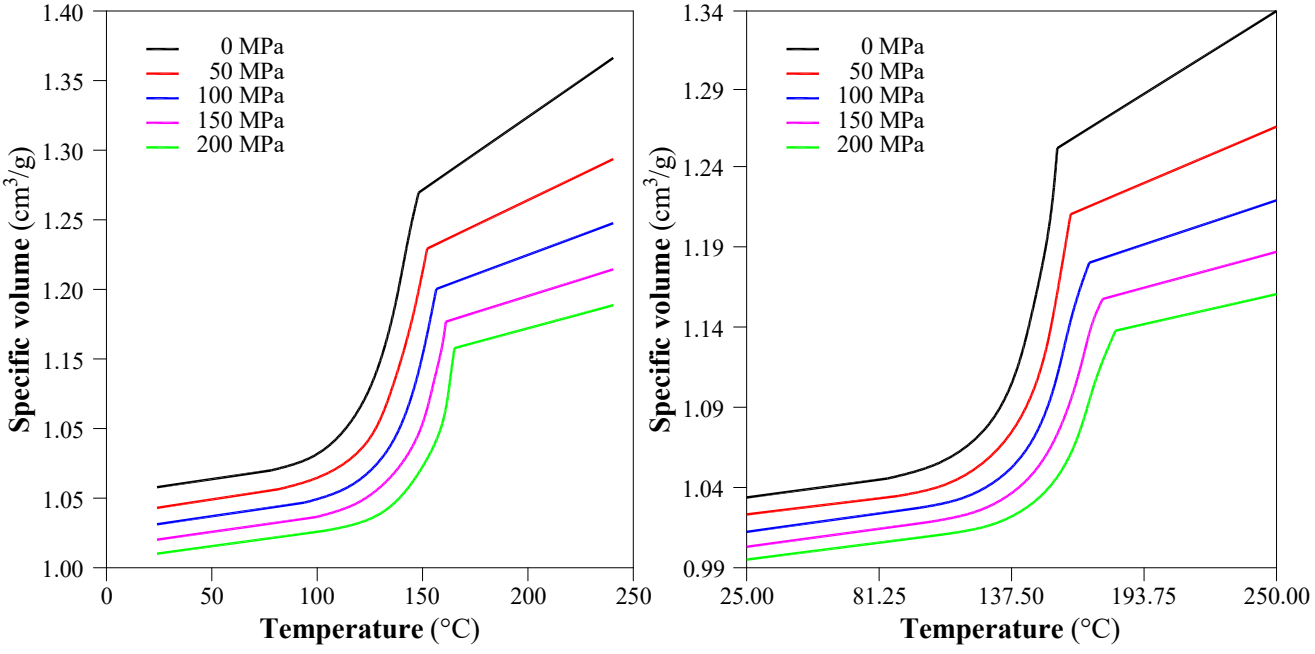


*a) UHMWPE* *b) UHMWPE with 10 wt.% nHA*

**Figure 1.2.** *Specific volume of (a) UHMWPE and (b) UHMWPE with 10 wt.% nHA as a function of pressure and temperature*
Recreated from [102]

## 1.4. Review on the *TC* behavior

From literature review, the first factor that affects the thermal conductivity of polymers/CNT nanocomposites is the temperature; if the temperature is increased, often the *TC* of polymer/CNT nanocomposites increases up to a certain limit [107]. Additionally, the increase of defects in the CNT network and poor dispersion significantly reduces the value of thermal conductivity [107].

*Ali* et al. (2016) [112] studied the effect of MWCNTs on the *TC* of polylactic acid (PLA)/MWCNT nanocomposites modified with liquid natural rubber (LNR). Figure 1.3.a shows that the *TC* increased with increasing MWCNT loading up to 3.5 wt.% by forming conducting path in the matrix. Further increasing the MWCNT loading to 4 wt.%, the *TC* decreased since the extended shape of MWCNTs reduced the crystallization of matrix with increasing the temperature. The *TC* of the nanocomposites with ≤3.5 wt.% of MWCNTs decreased with increasing the temperature due to the presence of defects and large boundaries at the matrix/MWCNT interface, which increased the thermal resistivity. Figure 1.3.b shows that, at higher MWCNT loading in the PLA/LNR matrix, a decrease in the thermal conductivity value is observed due to the presence of MWCNT agglomeration that will block the phonon travels. The optimum value of *TC* at 30 °C was found at PLA/LNR filled with 3.5 wt.% of MWCNTs. At higher loadings than 3.5 wt.%, the poor MWCNT dispersion in the nanocomposites leads to a decrease in *TC* values, showing that the MWCNT dispersion in the matrix has an important role in enhancing thermal conductivity.

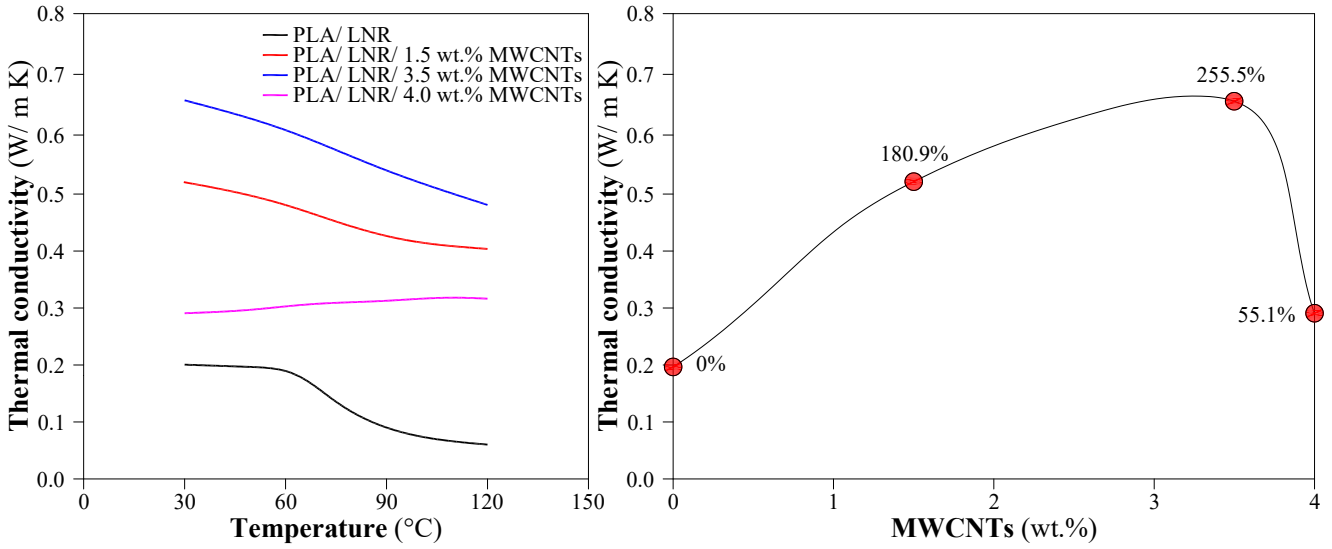


*a) temperature* *b) MWCNT loading*

**Figure 1.3.** *Thermal conductivity of PLA/LNR as a function of (a) temperature and (b) MWNCT loading at 30 °C*
Recreated from [112]

## 1.5. Conclusions and research directions

Polymer/carbon nanotube (CNT) nanocomposites have attracted substantial research and industrial interests owing to the CNTs outstanding thermal conductivity, electrical conductivity and mechanical properties. The increased usage of CNTs in polymers has opened up a new necessity for the manufacturing industry: the integration of polymer/CNT nanocomposites data in a CAD/CAE simulation for extrusion or injection molding process. Reliable numerical simulations of the melt manufacturing processes (e.g., injection molding and extrusion) can be performed using reliable material information (e.g., physical, mechanical, and rheological properties and specific volume) for each polymer/CNT nanocomposites.

In the last years, numerous investigations have been conducted to characterize the polymer/CNT nanocomposites. However, the material property data for numerical simulation may be acquired by

combining the physical, thermal, and mechanical properties from different sources. This compromise may lead to very serious errors since the material properties are influenced by many factors, such as polymer matrix, CNTs type, dispersion and alignment of CNTs within the polymer matrix etc.

From literature review, the rheological behavior of polymer/CNT nanocomposites revealed important details about the characteristics of the interface and the extent of polymer–nanotube interfacial interactions. Generally, the shear viscosity increased with increasing CNT loading due to the fact that the addition of CNTs blocks the movement and extensional activities of the macromolecular chains; therefore the rheological percolation threshold of the polymer-based CNT composites can be achieved under a CNT loading of 5 wt.%. The effect of CNTs is more important at low shear rates, while, at higher shear rates, the shear-thinning effect is enhanced regardless of CNT loading due to the CNT orientation. The general behavior reported is that, with increasing the CNT loading, a transition from a liquid-like to solid-like rheological response is observed, where the Newtonian plateau fades and the storage and loss moduli curves flatten in the low frequency region.

Studies regarding the *pVT* behavior of polymer/CNT nanocomposites were not available in the literature; therefore the *pVT* behavior of polymers and other nanocomposites was discussed. Generally, the specific volume decreases with increasing pressure and decreasing temperature. Also, the specific volume was influenced by the filler added in the polymer matrix.

Generally, the thermal conductivity of polymer/CNT nanocomposites increased with increasing temperature and increasing the CNT loading due to the changes at the interface between the polymer and CNTs. However, no information regarding the thermal conductivity dependency on pressure of polymer/CNT nanocomposites was found in literature.

A single source of material property data is needed for engineering calculations and simulations of manufacturing process, such as the injection molding process. The literature showed that the *pVT* and *TC* behaviors of polymer/CNT nanocomposites were barely investigated amongst the mechanical and rheological characterization, meaning that a reliable numerical simulation can not be performed. Therefore, the **main objective** of this thesis is to determine the material properties as analytical models that can be used in processing simulation and material properties prediction since they are affected by crystallinity, filler addition, processing conditions etc.

The objective was partly fulfilled by characterizing the polymer-based CNT composites through differential scanning calorimetry (*DSC*), capillary rheometry and *pVT* and *TC* measurements (Figure 1.4). The *DSC*[1] scans were performed to study the thermal transitions (melting/crystallization behavior, the degree of crystallinity, glass transitions etc.) of the polymer-based CNT composites. The rheological parameters (viscosity, shear stress, shear rate, power-law index) were determined due to their importance in deciding the suitable processing techniques and temperatures in the manufacturing processes. The *pVT* diagrams were drawn to provide the specific volume at different pressures and temperatures, as well as the variation of the glass transition temperature with pressure. Lastly, the *TC* behavior based on pressure, temperature and MWCNT loading was investigated since it is an important parameter to reduce the occurrence of hot spots in injection molding specimens and for optimizing the heat transfer. However, the mechanical and electrical properties of the polymer/CNT nanocomposites are not presented in this work, but can be found in various research articles affiliated to the Center of Excellence Polymer Processing, Dunarea de Jos University of Galati.

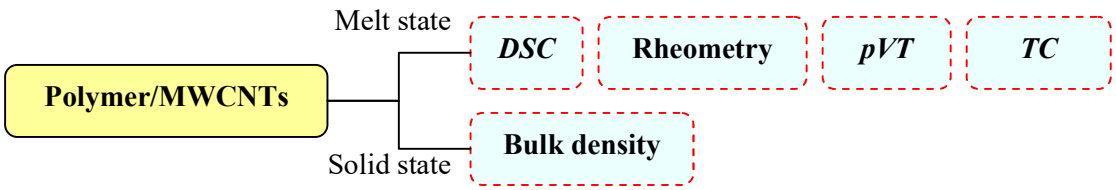


**Figure 1.4.** *Representation of the measurements performed*

[1] The *DSC* measurements were performed by the Institute of Macromolecular Chemistry "Petru Poni" (Iasi, Romania).

# 2. MATERIALS AND CHARACTERIZATION METHODS

## 2.1. Materials

The materials analyzed in this thesis are thermoplastics, such as low-density polyethylene (LDPE), high-density polyethylene (HDPE), ethylene vinyl acetate (EVA), polypropylene (PP) and thermoplastic polyurethane (TPU). The polymer matrices are filled with 0.1, 0.3, 0.5, 1, 3, and 5 wt.% of multi-walled carbon nanotubes (MWCNTs, Nanocyl NC7000™) [113], designed for extrusion and/or injection molding processes and supplied by Nanocyl S.A. (Belgium) [114-118].

The NC7000™ carbon nanotubes were produced by Catalytic Chemical Vapor Deposition (CCVD) method, with an average diameter of 9.5 nm and length of 1.5 μm [113]. Industrial NC7000™ CNTs are used in transportation, electronics (packaging, EMI-shielding, sensors), energy (Lithium-ion), and industrial applications (dynamic rubber parts, coatings and heating elements) [113].

Plasticyl™ masterbatches are thermoplastic/ multi-walled carbon nanotubes concentrates, mostly used for applications that require superior electrical conductivity and electrostatic discharge properties [113]. Table 2.1 presents the grade of the thermoplastic used in the processing of the nanocomposites, the mixing temperature and name of the masterbatches used for the extrusion of the pellets. Nanocomposites with 1–5 wt.% of MWCNTs were obtained by successive dilutions of commercially available masterbatches (10, 15 or 20 wt.% of MWCNTs) on a 48 mm twin screw extruder and the compounds with 0.1–0.5 wt.% of MWCNTs were made from the 1–5 wt.% nanocomposites. The compound dilutions were performed by Nanocyl S.A. in order to preserve the industrial character of the dilution process.

**Table 2.1.** *Polymer grades analyzed*

| Thermoplastic | Grade | Mixing temperature (°C) | Masterbatch |
|---|---|---|---|
| **LDPE** | ExxonMobil™ LDPE LD 655 | 135 | LDPE2001 |
| **HDPE** | Bormed™ HE9621-PH | 220 | HDPE1501 |
| **EVA** | EVATANE® 2020 | 170 | EVA2001 |
| **PP** | Moplen HP400R | 230 | PP2001 |
| **TPU** | Estane® 54610 | 170 | TPU1001 |

### 2.1.1. LDPE/MWCNT nanocomposites

The LDPE/MWCNT nanocomposites analysed were obtained by successive dilutions of LDPE2001 (Nanocyl S.A., Belgium) conductive masterbatch, which is LDPE (grade ExxonMobil™ LD 655, [129]) filled with 20 wt.% of MWCNTs [114]. LDPE2001 is ideal for extrusion and injection molding processes due to its low viscosity and high flow [114]. The main characteristics of LDPE2001 given in the technical data sheet (TDS) [114] are a density of 0.93 g/cm$^3$ and a MFI (190 °C, 21.6 kg, 4 mm) of 10.1±2.1 g/10 min. The matrix properties include a typical value of density of 0.913 g/cm$^3$, a MFI (190 °C, 2.16 kg) of 150 g/10 min and a peak melting temperature of 101 °C [129].

### 2.1.2. HDPE/MWCNT nanocomposites

The HDPE/MWCNT nanocomposites analysed were obtained by successive dilutions of HDPE1501 (Nanocyl S.A., Belgium) masterbatch, which is HDPE (grade Bormed™ HE9621-PH, [130])

filled with 15 wt.% of MWCNTs [115]. The main characteristics of HDPE1501 given in the TDS [115] are a MVR (190 °C, 21.6 kg, 4 mm) of 25.0±3 g/10 min and a melting point of 135 °C. The matrix properties include a typical value of density of 0.964 g/cm$^3$, a MFR (190 °C, 2.16 kg) of 12 g/10 min and a peak melting temperature of 133 °C [130].

### 2.1.3. EVA/MWCNT nanocomposites

The EVA/MWCNT nanocomposites analysed were obtained by successive dilutions of EVA2001 (Nanocyl S.A., Belgium), which is a conductive masterbatch based on EVA (grade EVATANE® 20–20, containing 20 wt.% of VA [135]) filled with 20 wt.% of MWCNTs [116]. The main characteristic of EVA2001 given in the technical data sheet [116] is a MFI (230 °C, 20 kg, 4 mm) of 6±1.2 g/10 min. EVATANE® 20–20 properties include a typical value of density of 0.95 g/cm$^3$ and a MFI (190 °C, 2.16 kg) of 17–23 g/10 min [135].

### 2.1.4. PP/MWCNT nanocomposites

The PP/MWCNT nanocomposites analysed were obtained by successive dilutions of PP2001 (Nanocyl S.A., Belgium) conductive masterbatch, which is PP (grade Moplen HP400R [136]) filled with 20 wt.% of MWCNTs [117]. The main characteristics of PP2001 given in the TDS [117] are a density of 0.872 g/cm$^3$ and a melting point of 165 °C. Moplen HP400R is a homopolymer polypropylene that exhibit high fluidity combined with a good stiffness, suitable for food contact and used for injection molding applications [136]. Its properties include a density of 0.9 g/cm$^3$, a MFR (230 °C, 2.16 kg) of 25 g/10 min and a MVR (230 °C, 2.16 kg) of 34 cm$^3$/10 min [136].

### 2.1.5. TPU/MWCNT nanocomposites

The TPU/MWCNT nanocomposites analysed were obtained by successive dilutions of TPU1001 (Nanocyl S.A., Belgium) masterbatch, which is TPU (grade Estane® 54610, [139]) filled with 10 wt.% of MWCNTs [118]. The main characteristics of TPU1001 given in the technical data sheet [118] are a MVR (190 °C, 15 kg, 4 mm) of 25.6±3 cm$^3$/10 min and a density of 1.216 g/cm$^3$. Estane® 54610 is an aromatic polyester-based thermoplastic polyurethane that exhibit good physical properties, chemical resistance and a wide processing window and is mainly used in calendering and film extrusion [139]. Its properties include a tensile strength of 37.2 MPa, a melting temperature of 120 °C and a glass transition temperature of -25 °C [139].

## 2.2. Characterization

### 2.2.1. Differential Scanning Calorimetry

**Differential scanning calorimetry** (*DSC*) measurements were used to study the influence of the MWCNT loading on the thermal transitions (melting/crystallization behavior, the degree of crystallinity, glass transitions etc.) of the composites. Literature shows that CNT loading significantly affects the thermal domains of the polymers [144,145]. After the *DSC* curves were obtained, the crystallinity degree, $\chi$, was calculated [146]

$$\chi = \frac{\Delta H_p}{\Delta H_c \cdot (1-\varphi)} \cdot 100 \ (\%), \tag{2.1}$$

where $\Delta H_p$ is the melt enthalpy of tested polymer, in J/g, $\Delta H_c$ – melt enthalpy of fully crystalline material as reference, in J/g, and $\varphi$ – weight fraction of MWCNTs.

### 2.2.2. Bulk density

The bulk density of the polymer/CNT nanocomposites was measured on a AB-204-S/FACT balance (Mettler Toledo, USA) equipped with a density determination kit. The bulk density of the sample was calculated based on the Archimedes's principle. The same pellets were weighed in air, then in ethanol. The bulk density is calculated with [148]

$$\rho = \frac{A}{A-E}(\rho_0 - \rho_L) + \rho_L \ \text{(g/cm}^3\text{)}, \tag{2.2}$$

where $A$ and $E$ are the weights (g) of the pellets measured in air, respectively in ethanol, $\rho_0$ is the density of ethanol (varies with temperature) and $\rho_L$ is the density of air, $\rho_L = 0.0012$ g/cm$^3$. The reported results of the bulk density are the averages and the standard deviations of ten measurements.

### 2.2.3. Capillary rheometry

The flow behavior and viscosity of the polymer/CNT nanocomposites were determined on a Rheograph 75 high-pressure capillary rheometer (Göttfert, Germany) that can make measurements at temperatures up to 400 °C, shear rates up to $10^7$ s$^{-1}$, in accordance to ASTM D3835. Before rheological measurements, the nanocomposites were dried in a vacuum oven (Raypa, Spain) to eliminate any moisture using the drying conditions presented in Table 2.2.

**Table 2.2.** *Vacuum drying conditions*

| Thermoplastic | Temperature (°C) | Time (h) |
|---|---|---|
| **LDPE** | 80 | 2 |
| **HDPE** | | |
| **TPU** | | 4 |
| **PP** | | |
| **EVA** | 60 | 3 |

For each temperature, three capillary dies were used that have a 1 mm diameter round-hole and three length-diameter ratios ($L/D$) of 30/1, 20/1 and 10/1 with 180° entrance angle. Then the linear Bagley and Weißenberg-Rabinowitsch corrections were performed using the WinRheo II software (Göttfert, Germany). For each temperature, the shear viscosity was determined using the true shear rate and shear stress. Table 2.3 shows the investigated temperature and shear rate ranges for the polymer/CNT nanocomposites analysed.

**Table 2.3.** *Experimental conditions for viscosity measurements*

| Thermoplastic | Temperature ranges (°C) | Shear rate ranges (s$^{-1}$) |
|---|---|---|
| **LDPE** | 110 – 150 | 50 – 5000 |
| **HDPE** | 170 – 230 | 75 – 5000 |
| **EVA** | 120 – 180 | 100 – 5000 |
| **PP** | 190 – 230 | 10 – 10000 |
| **TPU** | 180 – 210 | 10 – 5000 |

### 2.2.4. Specific volume

In this thesis, the pressure-Volume-Temperature ($pVT$) diagrams of the polymer/CNT nanocomposites was determined using the RG75 capillary rheometer equipped with a $pVT$ device (the

*pVT* capillary die is blocked by a capillary plug); procedure standardized in ISO 17744. The *pVT* measurements were based on the isothermal compression in order of decreasing temperature (Table 2.4) and increasing pressures from 10 to 1250 bar.

The experimental *pVT* data were then fitted to the modified 2-domain Tait model [31] using the WinRHEO II software. The obtained *pVT* diagrams (i) represent the existent relationship between pressure, specific volume and temperature; (ii) show transition temperatures as a function of temperature and pressure and (iii) can be used to determine the compressibility and volumetric thermal-expansion coefficients.

**Table 2.4.** *pVT diagram experimental conditions*

| Thermoplastic | MWCNTs (wt.%) | Loading temperature (°C) | Testing temperatures (°C) |
|---|---|---|---|
| **LDPE** | 0.1 – 3 | 110 | 30 – 160 |
| | 5 | 115 | |
| **HDPE** | 0.1 – 1 | 138 | 50 – 200 |
| | 3, 5 | 140 | |
| **EVA** | 0.1 – 1 | 110 | 50 – 180 |
| | 3, 5 | 115 | |
| **PP** | 0.1 – 5 | 190 | 80 – 220 |
| **TPU** | 0.1 – 5 | 140 | 50 – 180 |

### 2.2.5. Thermal conductivity

Thermal conductivity (*TC*) measurements of the polymer/CNT nanocomposites were conducted using a RG75 capillary rheometer equipped with a lockable die and a thermal conductivity probe, which was inserted into the nanocomposite melt. The *TC* probe consists of a thin walled piston with a thermocouple and a heating element in the centre and generates a defined heat flow through the sample with a 69 volts DC power supply. Thermal conductivity measurements were according to ASTM D5930. Measurements were made at various testing temperatures (Table 2.5), in decreasing order, and at increasing pressures from 100 to 500 bar. Before the measurements, the nanocomposites were dried under the vacuum drying conditions presented in Table 2.2.

The thermal conductivity, $\lambda$ (W/m·K), was calculated from the slope of the measurement points in the time range of 60 and 120 s (inset of Figure 2.4) and their respective temperatures. Two fixed values are used in the software based on the dimensions of the *TC* probe [149]: the specific heat energy of the probe, $Q = 159.765$ W/m, and the correction constant of the probe, $C = 0.51$.

**Table 2.5.** *Experimental conditions for TC measurements*

| Thermoplastic | MWCNTs (wt.%) | Loading temperature (°C) | Testing temperatures (°C) |
|---|---|---|---|
| **LDPE** | 0.1 – 0.5 | 110 | 50 – 140 |
| | 1 – 5 | 115 | |
| **HDPE** | 0.1 – 0.5 | 140 | 80 – 200 |
| | 1 – 5 | 145 | |
| **EVA** | 0.1 – 1 | 110 | 50 – 180 |
| | 3, 5 | 115 | |
| **TPU** | 0.1 – 5 | 140 | 60 – 210 |
| **PP** | 0.1 – 5 | 190 | 70 – 200 |

# 3. THERMAL PROPERTIES OF POLYMER/MWCNT NANOCOMPOSITES

## 3.1. Experimental results

### 3.1.1. Thermal behavior of LDPE/MWCNT nanocomposites

The typical *DSC* curves corresponding to the first heating, cooling, and second heating scans for the LDPE/MWCNT nanocomposites are shown in Figure 3.1. The first heating scan displays a shouldered peak at around 80–87 °C and an endothermic peak at around 104–107 °C while the second heating scan only shows an endothermic peak at around 102–103 °C. In the cooling scan, the crystallization temperature of the nanocomposites is nearly constant at around 90 °C for the nanotube loadings up to 1 wt.% while, at higher nanotube loadings, is shifted towards lower values due to the variations in the nucleation activity of the CNTs [150].

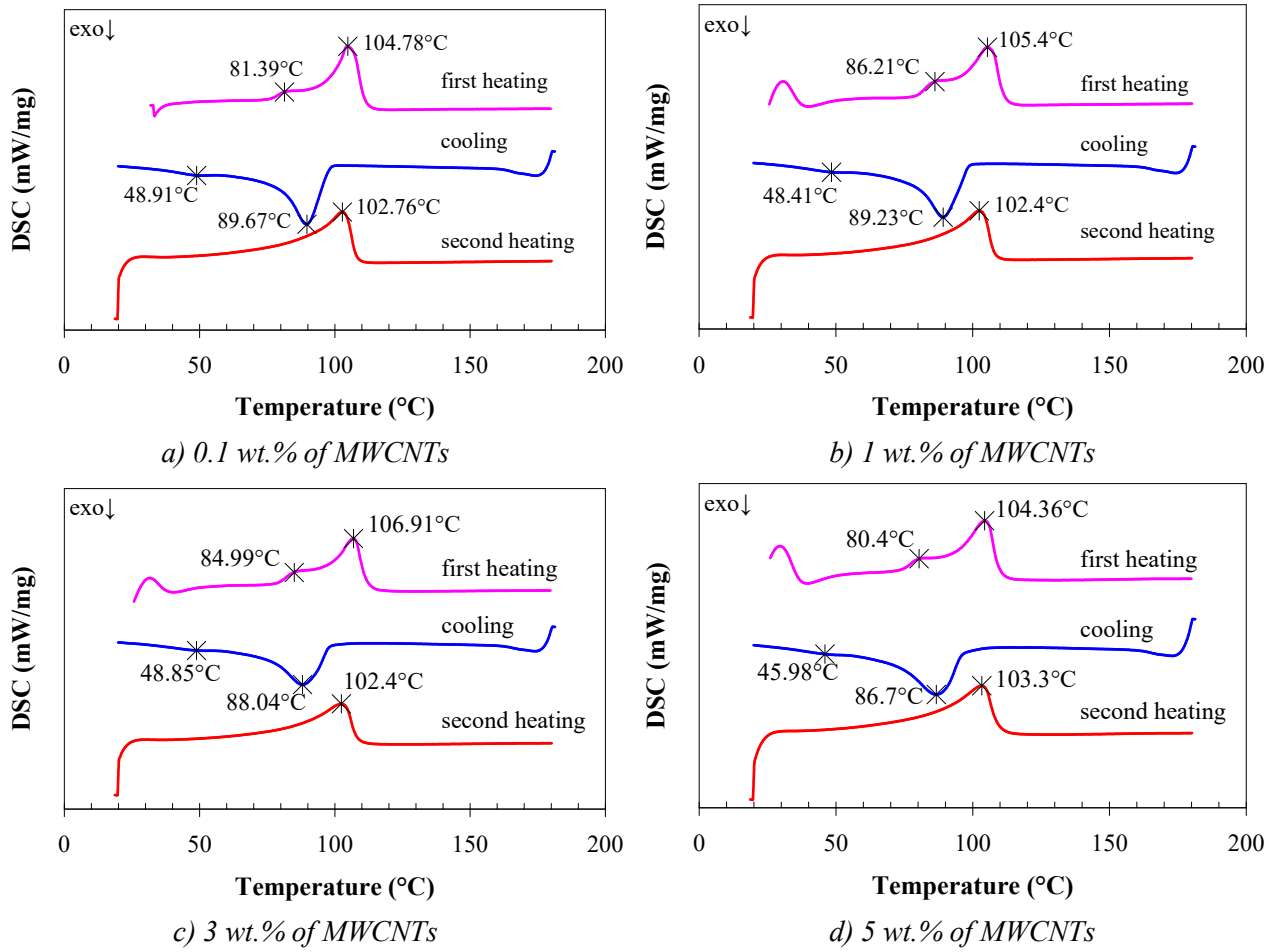


**Figure 3.1.** *DSC curves for LDPE/MWCNT nanocomposites*

Table 3.1 summarizes the melt enthalpy ($\Delta H_p$), the melting and crystallization temperatures ($T_m$, $T_c$) of the LDPE/MWCNT nanocomposites determined by the *DSC* analysis software. The LDPE/MWCNT nanocomposites show a significant change in the melt enthalpy with values from 60 to 89 J/g for MWCNT loadings ranging from 0.1 to 5 wt.% (Table 3.1), but without a clear trend. For the determination of the crystallinity degree ($\chi$), the equation (2.1) was used, where the value of the melt

enthalpy of fully crystalline LDPE ($\Delta H_c$) was selected to be 293.6 J/g [151]. The results of the second heating scan show that the % crystallinity of the LDPE/MWCNT nanocomposites has an increasing tendency compared with the first heating scan. The highest % crystallinity was obtained for the LDPE/5 wt.% of MWCNTs nanocomposite while the lowest % crystallinity was observed for the nanocomposite with 3 wt.%.

**Table 3.1.** *DSC results for the LDPE/MWCNT nanocomposites*

| MWNCTs | 1st heating scan | | | cooling scan | | 2nd heating scan | | |
|---|---|---|---|---|---|---|---|---|
| (wt.%) | $T_m$ (°C) | $\Delta H_p$ (J/g) | $\chi$ (%) | $T_c$ (°C) | $\Delta H_p$ (J/g) | $T_m$ (°C) | $\Delta H_p$ (J/g) | $\chi$ (%) |
| 0.1 | 104.78 | 66.25 | 22.59 | 89.67 | -87.00 | 102.76 | 78.94 | 26.91 |
| 0.3 | 104.71 | 71.63 | 24.47 | 89.87 | -83.24 | 102.00 | 82.44 | 28.16 |
| 0.5 | 103.80 | 84.72 | 29.00 | 89.70 | -91.65 | 101.76 | 88.78 | 30.39 |
| 1 | 105.40 | 68.77 | 23.66 | 89.23 | -82.23 | 102.40 | 80.29 | 27.62 |
| 3 | 106.91 | 60.08 | 21.10 | 88.04 | -67.65 | 102.40 | 67.65 | 23.75 |
| 5 | 104.36 | 72.73 | 26.08 | 86.70 | -85.18 | 103.30 | 86.34 | 30.96 |

## 3.2. Discussions

The cooling scans of the semi-crystalline polymers/MWCNT nanocomposites displayed a single crystallization peak. The *DSC* measured crystallization temperatures are presented in Figure 3.2 as a function of MWCNT loading. A linear trendline function on the graphs was performed in order to asses the results. An increase of the crystallization temperature was observed when the MWCNT loading increased for the PP/MWCNT nanocomposites. The gradual shift to higher temperatures indicates that the crystallization process is facilitated in the presence of MWCNTs (i.e., the nucleation starts around CNTs). When the MWCNT loading increased on the nanocomposites that have a LDPE, HDPE and EVA matrix, a small decrease of the crystallization temperature was observed.

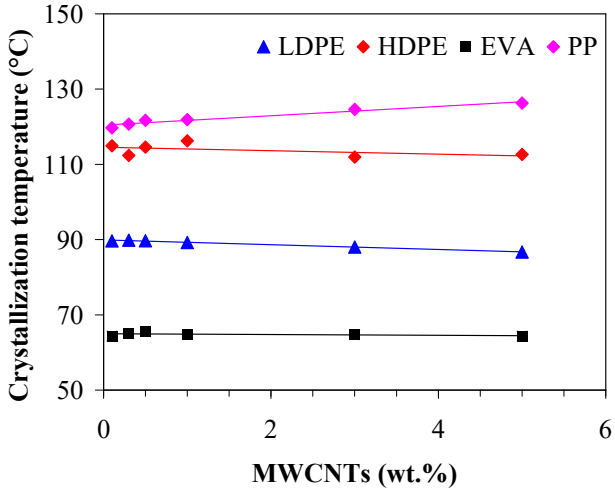


**Figure 3.2.** *Crystallization temperature of the polymer/MWCNT nanocomposites as a function of MWCNT loading (cooling scan)*

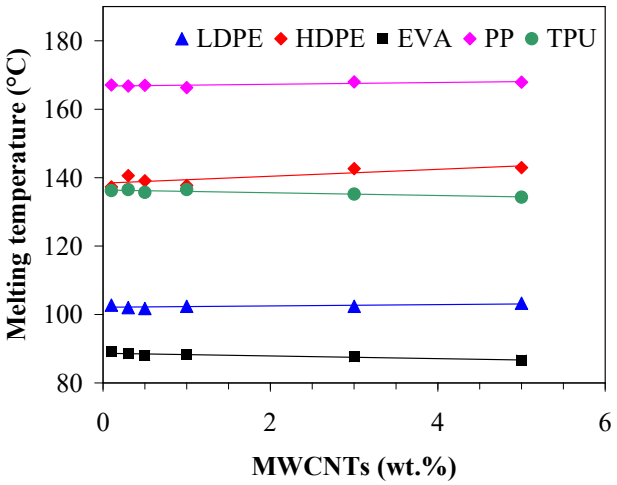


**Figure 3.3.** *Melting temperature of the polymer/MWCNT nanocomposites as a function of MWCNT loading (second heating scan)*

Figure 3.3 shows the MWCNTs influence on the melting temperature from the second heating scan (after removal of the thermal history due to processing–melt mixing conditions) for the polymer/MWCNT nanocomposites. A linear trendline function on the graphs was performed in order to asses the results. A small increase of the melting temperature was observed when the MWCNT loading increased for the nanocomposites that have a LDPE, HDPE, and PP matrix. The melting temperature slightly decreased with increasing MWCNT loading for the EVA and TPU/MWCNT nanocomposites.

# 4. VISCOSITY AND RHEOLOGICAL BEHAVIOR OF POLYMER/MWCNT NANOCOMPOSITES

## 4.1. Experimental results

### 4.1.1. Melt flow curves of LDPE/MWCNT nanocomposites

The rheological measurements on LDPE/MWCNT nanocomposites were performed at shear rates ranging from 50 to 5000 $s^{-1}$ and at temperatures ranging from 110 to 150 °C. The apparent shear stress increased with increasing shear rate due to the shear-thinning behavior (i.e., non-Newtonian behavior) of the nanocomposites, meaning that the shear stress/viscosity is dependent on the shear rate (Figure 4.1). The non-Newtonian behavior can be attributed to the chain alignment that results in an increase of the shear stress (i.e., decreased viscosity).

The apparent shear stress decreased with increasing temperature, more significantly at low shear rates. Therefore, the shear stress is dependent on temperature since the molecules disentangle and align, which increase the mobility of polymer molecules [182]. For example, at 1000 $s^{-1}$, the apparent shear stress of LDPE/MWCNT nanocomposites decreased by 45.24% to 38.40% when the temperature increased from 110 to 140 °C. The change in shear stress decreased when the MWCNT loading increased (i.e., the 45.24% and 38.40% decrease is attributed to the nanocomposites with 0.1 and 5 wt.% of MWCNTs, respectively). By further increasing the shear rate to 5000 $s^{-1}$, the temperature dependency on the shear stress decreased (i.e., 33.36% and 29.68% decrease for the 0.1 and 5 wt.%, respectively).

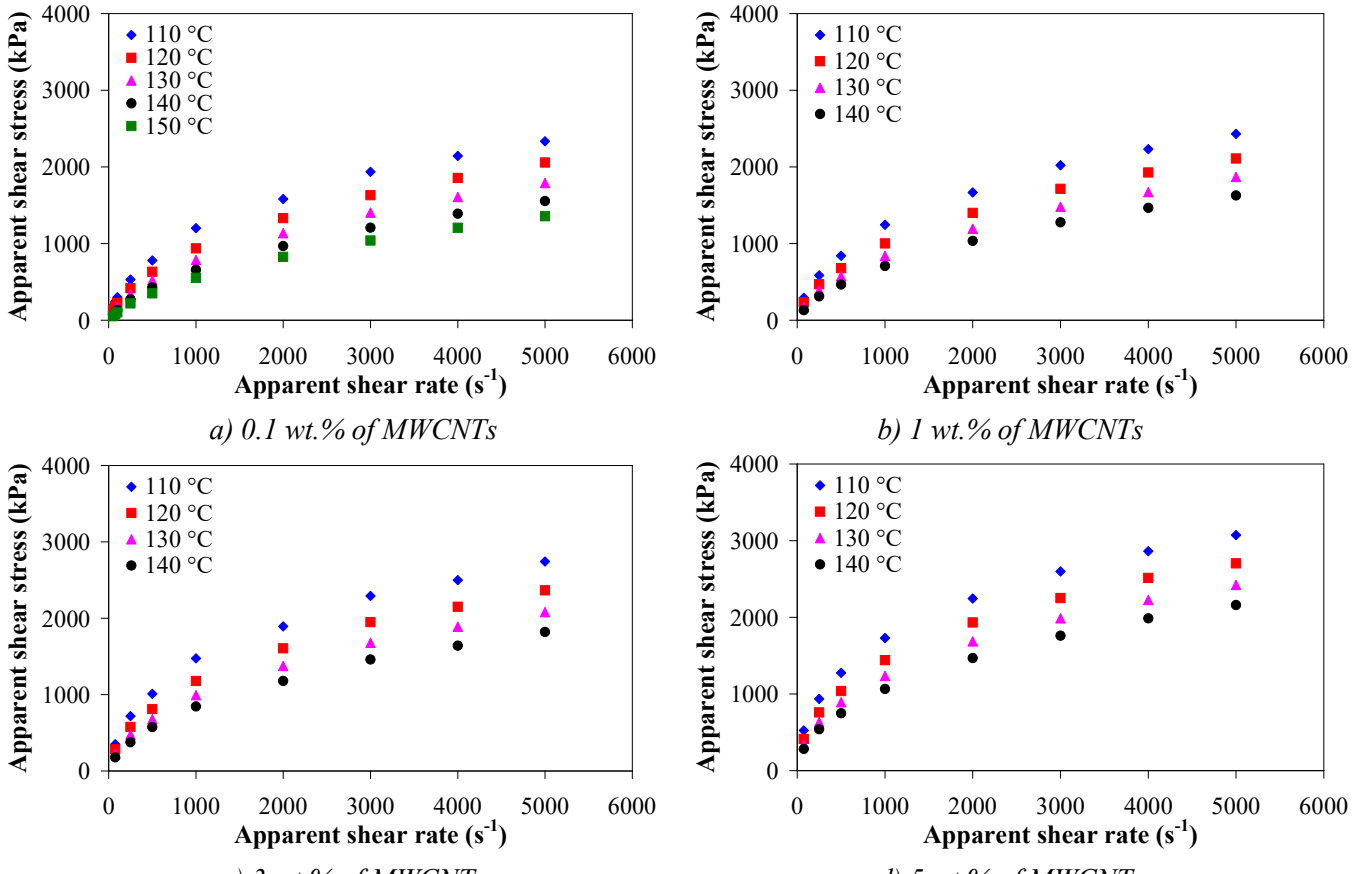


*a) 0.1 wt.% of MWCNTs*

*b) 1 wt.% of MWCNTs*

*c) 3 wt.% of MWCNTs*

*d) 5 wt.% of MWCNTs*

**Figure 4.1.** *Apparent shear stress vs apparent shear rate for LDPE/MWCNT nanocomposites (L/D = 30/1)*

## 4.2. Discussions

### 4.2.1. Shear rate dependency of melt shear stress

The apparent shear stress versus apparent shear rate plots for polymer/MWCNT nanocomposites at different temperatures, *L/D = 30/1* capillary die and MWCNT loadings are presented in Figure 4.2, in a log-log scale. The symbols represent the experimental data and the continuous lines represent the trendline analysis (linear or logarithmic fit). The shear stress clearly increases with increasing shear rate, showing the shear rate dependency for all polymer/MWCNT nanocomposites.

In the case of LDPE/MWCNT nanocomposites, at low nanotube loadings (0.1 to 0.5 wt.%) and shear rates up to 100 $s^{-1}$, as shown in Figure 4.2.a, the logarithm of the apparent shear stress deviates from a linear shape, indicating that the nanocomposites exhibit Newtonian flow behavior. However, at higher nanotube loadings, as shown in Figures 4.2.b-d, the LDPE/MWCNT nanocomposites exhibit non-Newtonian behavior even at low shear rates (50 to 100 $s^{-1}$). At higher shear rates, the shear-thinning behavior is present since the rigid MWCNT bundles in the polymer matrix tend to orient under shear force, thus disturbing the formation of the polymer chain entanglements [56].

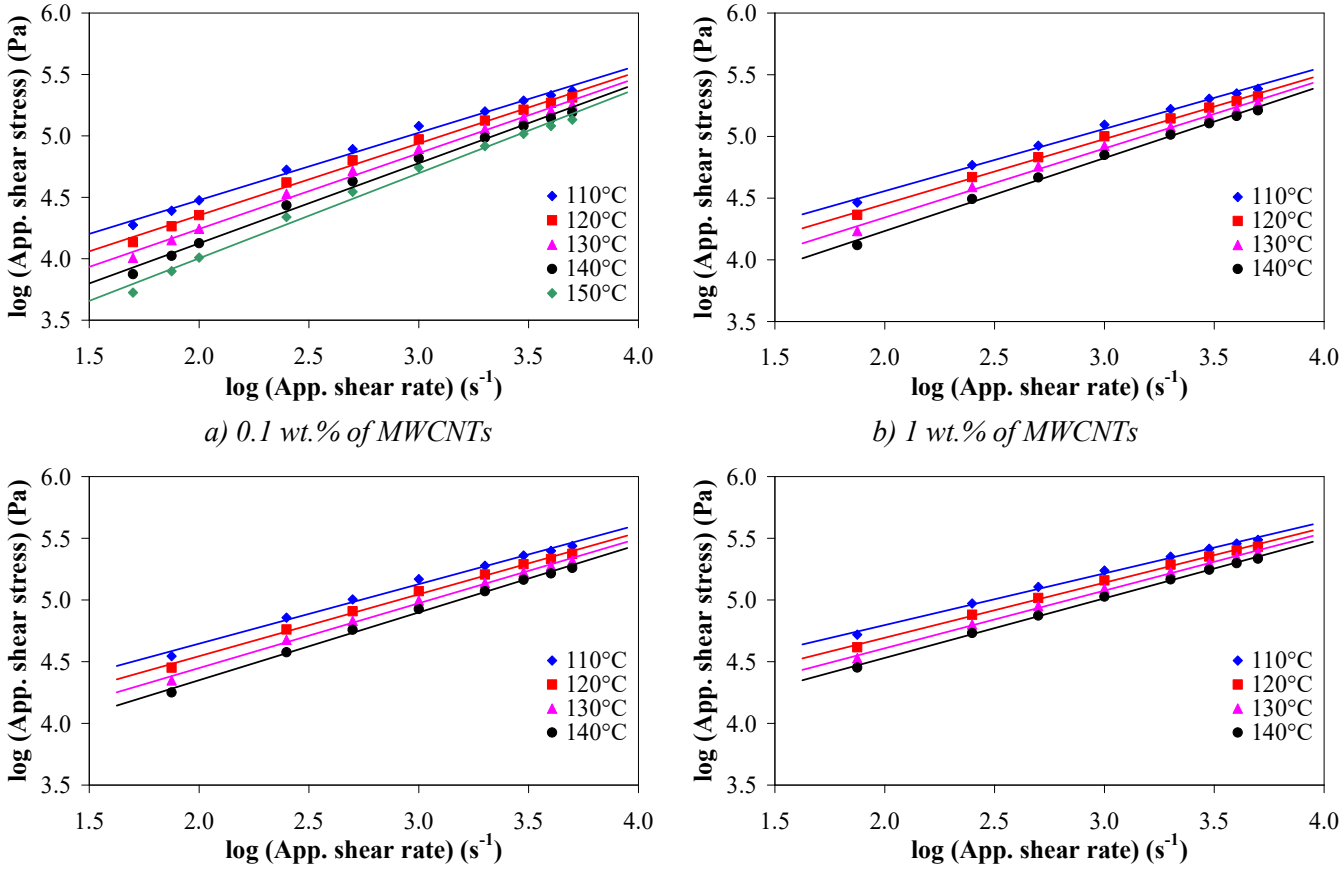


*a) 0.1 wt.% of MWCNTs* *b) 1 wt.% of MWCNTs*

*c) 3 wt.% of MWCNTs* *d) 5 wt.% of MWCNTs*

**Figure 4.2.** *Apparent shear stress vs apparent shear rate (log-log) for LDPE/MWCNT nanocomposites (L/D = 30/1)*

For all polymer/MWCNT nanocomposites, the shear stress decreases with increasing temperature, indicating an increase of the free volume [56]. Particularly, the decrease of shear stress with the temperature was significantly higher for the nanocomposites with the LDPE, EVA, and TPU matrix. Meanwhile, the apparent shear stress slightly decreases with increasing melt temperature for the HDPE and PP/MWCNT nanocomposites. Meanwhile, the shear stress increases with increasing MWCNT

loading, which indicates a transition from a liquid-like to a solid-like behavior due to the formation of a percolated nanotube network that impedes the motion of polymer chains [63].

The relationship between the apparent shear stress, $\tau_a$, and shear rate, $\dot{\gamma}_a$, can be described by the power-law equation [45,82]

$$\tau_a = K \cdot \dot{\gamma}_a^n \text{ (Pa·s)}, \tag{4.1}$$

where *K* represents the consistency of the polymer melt and *n* is the shear-thinning index. An exponent of $n = 1$ is associated with a Newtonian behavior, while $n < 1$ counts for shear-thinning [45,49]. Table 4.1 shows that both temperature and MWCNT loading have a significant effect on the *K* and *n* parameters for the polymer/MWCNT nanocomposites.

In the case of LDPE/MWCNT nanocomposites, the values of the *K* parameter was found to increase with increasing MWCNT loading and to decrease with increasing temperature, while the shear-thinning index (0.22–0.38) was found to decrease with increasing MWCNT loading, indicating shear-thinning behavior over the investigated shear rates. The values of *K* are lower for LDPE/MWCNT nanocomposites with 0.1 wt.% than for composites containing 5 wt.% (Table 4.1). On the other hand, the values of *n* are found to be higher for composites with lower MWCNT loading than for the nanocomposites with higher MWCNT loading.

**Table 4.1.** *Parameters of the power-law model for the LDPE/MWCNT nanocomposites*

| **Parameter** | **Temperature** (°C) | **MWCNTs** (wt.%) | | | | | |
|---|---|---|---|---|---|---|---|
| | | **0.1** | **0.3** | **0.5** | **1** | **3** | **5** |
| *K* | 110 | 3.646 | 3.690 | 3.680 | 3.741 | 3.852 | 4.093 |
| | 120 | 3.482 | 3.530 | 3.513 | 3.613 | 3.732 | 3.955 |
| | 130 | 3.336 | 3.372 | 3.361 | 3.459 | 3.607 | 3.843 |
| | 140 | 3.180 | 3.202 | 3.187 | 3.315 | 3.481 | 3.747 |
| *n* | 110 | 0.297 | 0.288 | 0.291 | 0.279 | 0.264 | 0.224 |
| | 120 | 0.324 | 0.313 | 0.318 | 0.296 | 0.279 | 0.242 |
| | 130 | 0.348 | 0.340 | 0.344 | 0.322 | 0.297 | 0.257 |
| | 140 | 0.376 | 0.372 | 0.376 | 0.346 | 0.316 | 0.269 |
| $R^2$ | 110 | 0.999 | 1.000 | 1.000 | 0.999 | 0.999 | 1.000 |
| | 120 | 1.000 | 0.999 | 1.000 | 0.999 | 1.000 | 0.999 |
| | 130 | 1.000 | 1.000 | 1.000 | 1.000 | 1.000 | 0.999 |
| | 140 | 1.000 | 1.000 | 1.000 | 1.000 | 1.000 | 0.999 |

Figure 4.3 presents the shear-thinning index as a function of temperature and polymer matrix. It clearly shows that, as the MWCNT loading increases, the temperature dependency of the *n* index decreases. For example, when the temperature increased from 180 to 210 °C, the shear-thinning index increased by 58.68% and 7.17%, for TPU/MWCNT nanocomposites with 0.1 and 5 wt.%, respectively.

### 4.2.2. Temperature dependency of melt shear viscosity

Temperature influences the rheological properties of the polymer matrix, but it can also affect the state of dispersion of the nanocomposites via changes in the nanotube–nanotube interactions and in the wettability of the CNTs with the matrix [183]. The temperature dependence of the melt shear viscosity of the LDPE/MWCNT nanocomposite is governed by the Arrhenius law and is depicted in Figure 4.4 for different apparent shear rates. The slopes of the graphs ($E_a / R_g$) define the flow activation energy, $E_a$, where $R_g$ is the gas constant, $R_g = 8.314$ J/(mol·K). The values of the activation energy of LDPE/MWCNT nanocomposites are presented in Table 4.2.

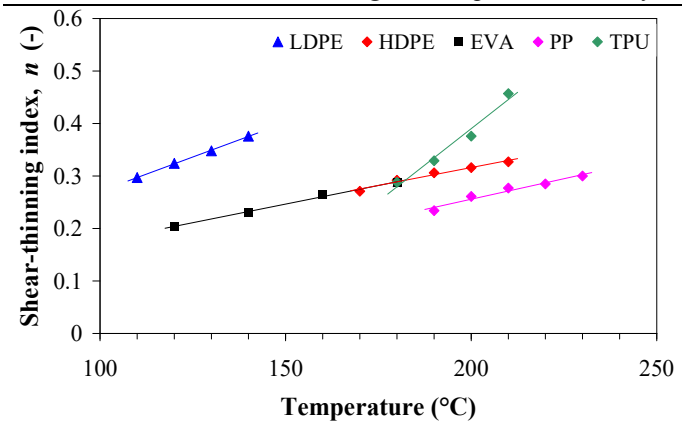


*a) 0.1 wt.% of MWCNTs*

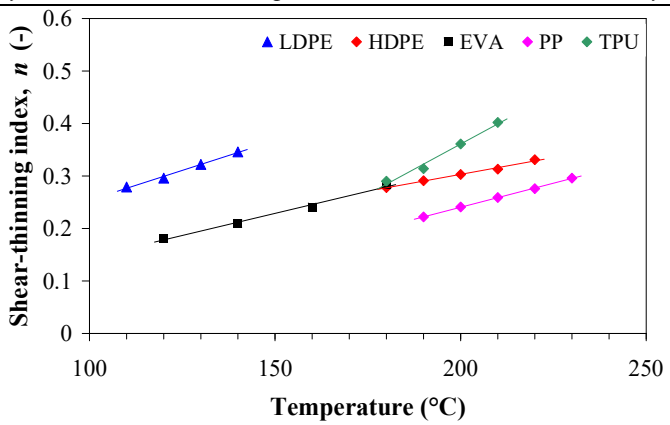


*b) 1 wt.% of MWCNTs*

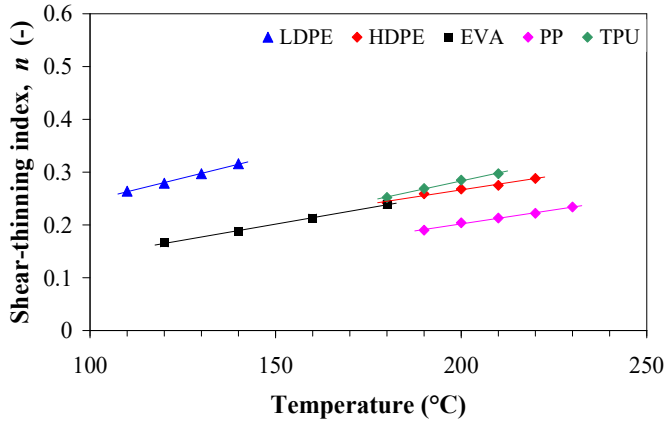


*c) 3 wt.% of MWCNTs*

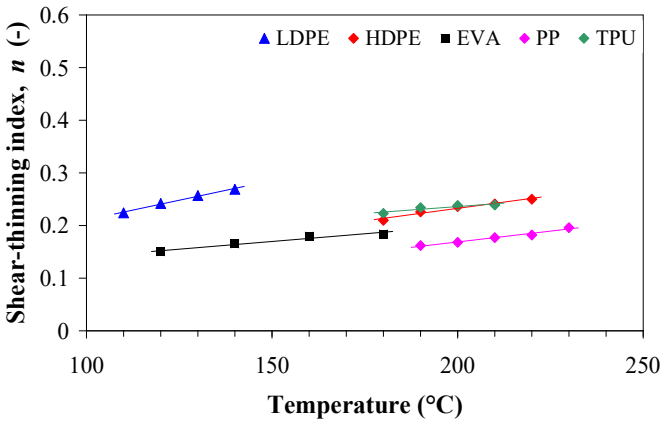


*d) 5 wt.% of MWCNTs*

**Figure 4.3.** *Shear-thinning index of the polymer/MWCNT nanocomposites (L/D = 30/1)*

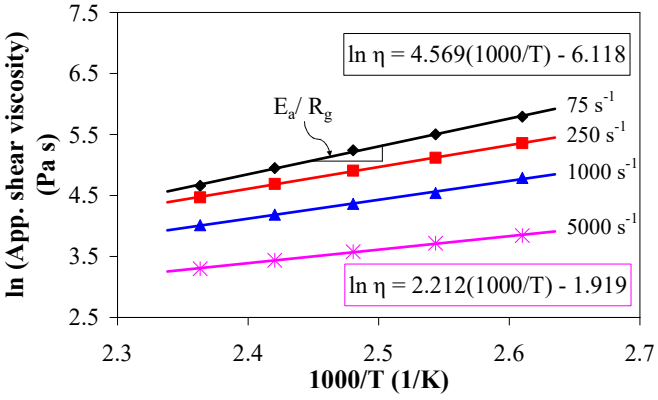


*a) 0.1 wt.% of MWCNTs*

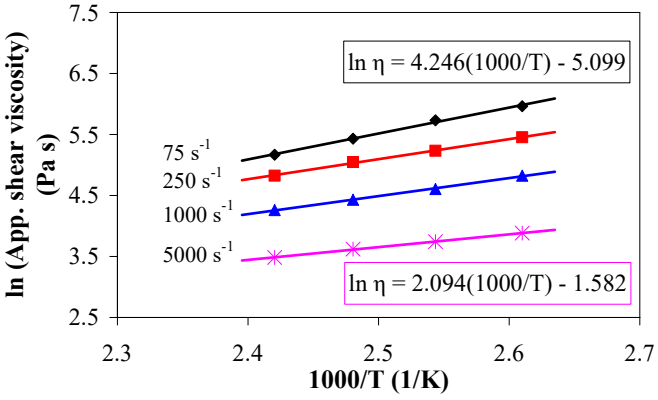


*b)1 wt.% of MWCNTs*

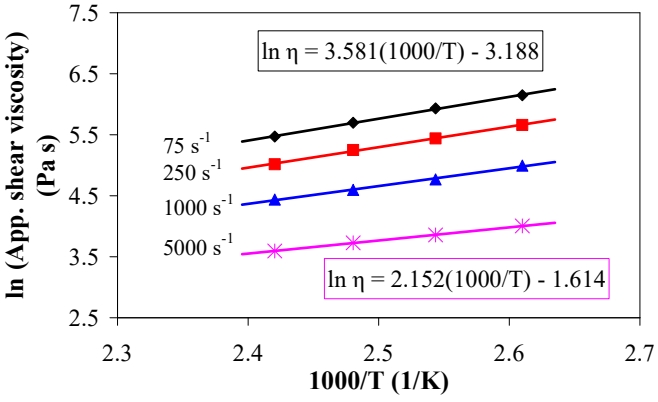


*c) 3 wt.% of MWCNTs*

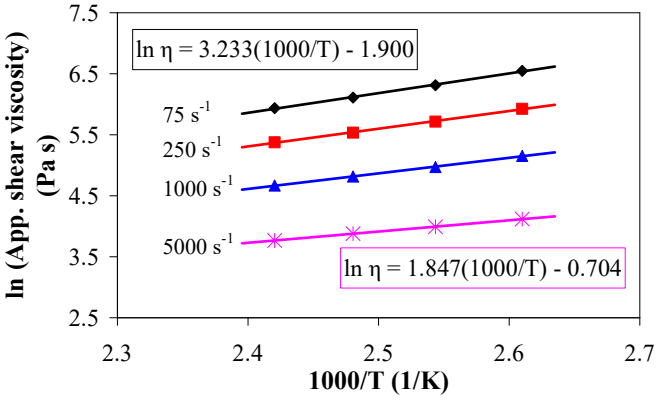


*d) 5 wt.% of MWCNTs*

**Figure 4.4.** *Dependence of shear viscosity of LDPE/MWCNT nanocomposites on temperature and apparent shear rate*

**Table 4.2.** *Activation energy of LDPE/MWCNT nanocomposites, based on Arrhenius equation*

| App. shear rate, $\dot{\gamma}$ (1/s) | Activation energy, $E_a$ (kJ/mol) | | | | | |
|---|---|---|---|---|---|---|
| | **0.1 wt.%** | **0.3 wt.%** | **0.5 wt.%** | **1 wt.%** | **3 wt.%** | **5 wt.%** |
| 75 | 37.986 | 39.880 | 39.584 | 35.303 | 29.769 | 26.880 |
| 250 | 29.722 | 30.432 | 30.183 | 27.297 | 27.928 | 24.134 |
| 500 | 26.806 | 27.163 | 27.125 | 25.670 | 24.639 | 23.061 |
| 1000 | 25.723 | 24.564 | 24.457 | 24.603 | 24.236 | 21.168 |
| 2000 | 21.816 | 21.936 | 21.997 | 20.905 | 20.742 | 18.555 |
| 3000 | 20.839 | 20.778 | 20.677 | 20.048 | 19.793 | 17.025 |
| 4000 | 19.407 | 19.407 | 19.286 | 18.504 | 18.308 | 16.014 |
| 5000 | 18.391 | 18.380 | 18.302 | 17.413 | 17.893 | 15.355 |

For all polymer/MWCNT nanocomposites, the $E_a$ decreases with increasing shear rate and with increasing MWCNT loading from 0.1 to 5 wt.%, indicating that the nanotubes are less restricted and have less interactions with the polymer chains, meaning that more nanotube–nanotube interactions exist [183,184]. The sensitivity of the viscosity to the nanotube loading weakens at high shear rates and temperature since the motion ability of polymer chains is enhanced, thus significantly decreases the resistance between the melt layers, reducing the melt viscosity [184-187].

### 4.2.3. Effect of MWCNTs of melt shear viscosity

The variation of the apparent shear viscosity with apparent shear rate during the capillary flow of the LDPE/MWCNT nanocomposites at two temperatures is presented in Figure 4.5, in a bi-logarithmic scale. The melt shear viscosity of all polymer/MWCNT nanocomposites increases with increasing MWCNT loading at the shear rates investigated. With the increase of nanotube loading, nanotube–nanotube interactions increase and the polymer chains are generally more restrained. As a result, the apparent viscosities of the nanocomposites melt increases.

At a constant shear rate, the viscosity curves of LDPE/MWCNT nanocomposites with low loadings (0.1, 0.3, and 0.5 wt.%) are overlapped with each other, as illustrated in Figure 4.5, indicating that the effect of low MWCNT loadings on the shear viscosity is less pronounced. It is evident that the apparent shear viscosity almost decreases linearly with increasing the shear rate, especially for the LDPE filled with 1, 3, and 5 wt.% of MWCNTs. At a given MWCNT loading and *L/D* ratio, the apparent shear viscosity decreases with increasing temperature, indicating an increase of the free volume [56]. Same tendancies were present for the HDPE, EVA, PP, and TPU/MWCNT nanocomposites.

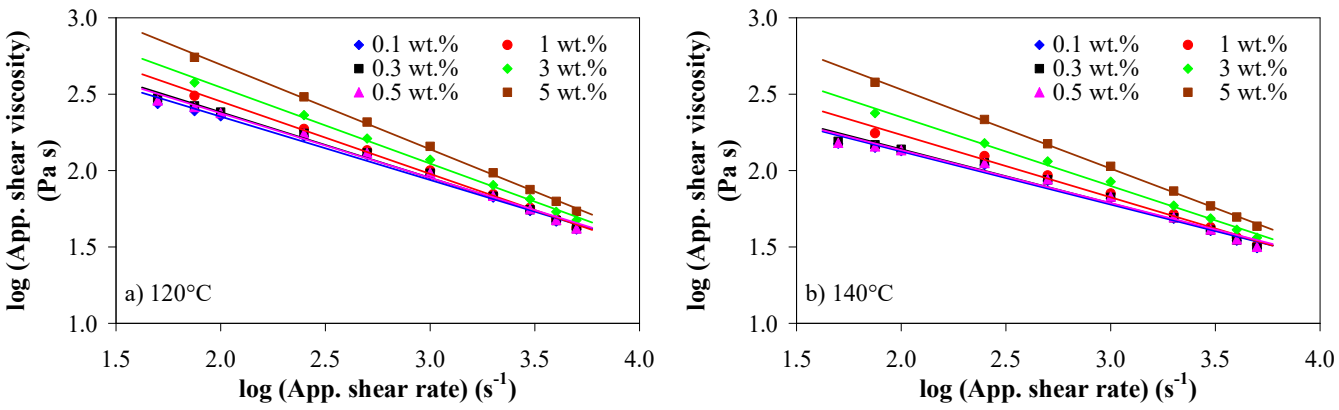


**Figure 4.5.** *Apparent shear viscosity vs apparent shear rate (log-log) of LDPE/MWCNT nanocomposites at (a) 120 °C and (b) 140 °C melt temperatures (L/D = 30/1)*

To further present the effect of MWCNT loading the shear viscosity, the apparent melt shear viscosity is plotted versus MWCNT loading in Figure 4.6 for different apparent shear rates and two melt temperatures. It was observed that the apparent shear viscosity linearly increases with increasing MWCNT loading.

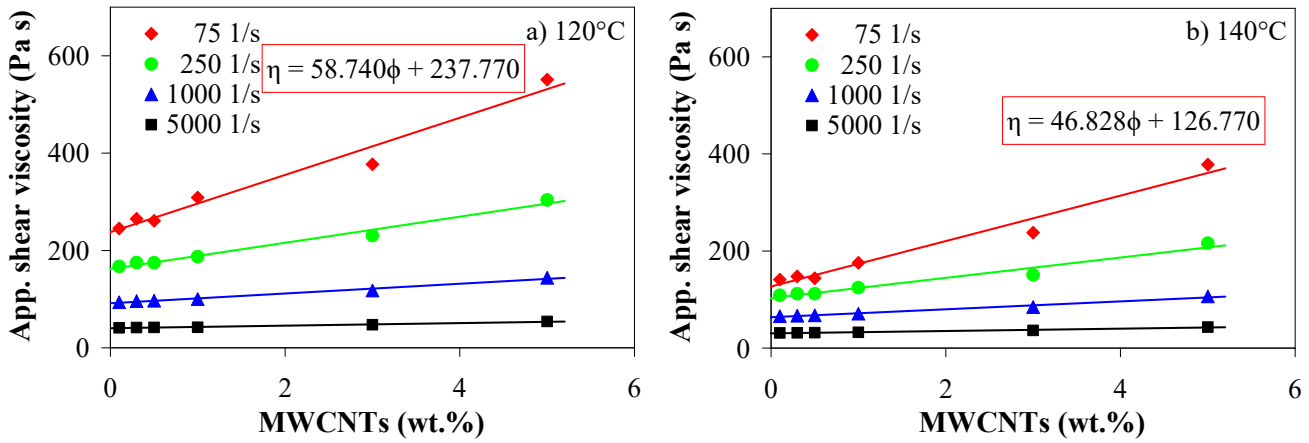


**Figure 4.6.** *Linear relationship between apparent viscosity and MWCNT loading for LDPE/MWCNT nanocomposites at (a) 120 °C and (b) 140 °C melt temperatures (L/D = 30/1)*

In the case of LDPE/MWCNT nanocomposites, at a temperature of 120 °C (Figure 4.6.a) and a shear rate of 75 $s^{-1}$, the apparent shear viscosity increased from 245.22 Pa·s to 551.19 Pa·s when nanotube loading increased from 0.1 to 5 wt.% (apparent shear viscosity increased with 125%). At a shear rate of 5000 $s^{-1}$, the apparent shear viscosity increased from 41.13 Pa·s to 54.08 Pa·s when nanotube loading increased from 0.1 to 5 wt.% (apparent shear viscosity increased by 31.49%).

The solid lines in Figure 4.6 represent the best fit of apparent shear viscosity assuming a linear relationship between viscosity and MWCNT loading is formed by

$$\eta = \alpha \cdot \phi + \beta \text{ (Pa·s)}, \tag{4.2}$$

where $\phi$ is the MWCNT loading (wt.%) and $\alpha$ and $\beta$ are constants. The best-fit parameters for the LDPE/MWCNT nanocomposites are given in Table 4.3, at different shear rates and melt temperatures.

**Table 4.3.** *Values of α and β parameters for the LDPE/MWCNT nanocomposites*

| **Melt temperature** (°C) | **App. shear rate,** $\dot{\gamma}$ (1/s) | $\alpha$ | $\beta$ (Pa·s) |
|---|---|---|---|
| 110 | 75 | 70.358 | 313.550 |
| | 250 | 32.112 | 205.250 |
| | 1000 | 11.540 | 114.110 |
| | 5000 | 3.038 | 46.021 |
| 120 | 75 | 58.740 | 237.770 |
| | 250 | 26.836 | 162.170 |
| | 1000 | 9.998 | 91.591 |
| | 5000 | 2.604 | 40.402 |
| 130 | 75 | 51.102 | 176.170 |
| | 250 | 23.485 | 130.310 |
| | 1000 | 8.943 | 76.301 |
| | 5000 | 2.514 | 35.174 |
| 140 | 75 | 46.828 | 126.770 |
| | 250 | 20.925 | 102.840 |
| | 1000 | 8.166 | 63.556 |
| | 5000 | 2.398 | 30.450 |

The values of $\alpha$ and $\beta$ parameters decrease with increasing apparent shear rate or temperature, indicating that the sensibility of the apparent shear viscosity on the nanotube loading is weakened by increasing apparent shear rate and temperature. At low shear rates, the movements of the macromolecule chains of the polymer matrix melt are blocked by the presence of MWCNTs, which eventually form nanotube–nanotube networks. This results to an increase in flow resistance during capillary extrusion, which increases with increasing MWCNT loading [150]. Whereas, at high shear rates, the nanotubes align along the shearing direction, which leads to a decrease in melt flow resistance through the capillary (i.e., a decrease in viscosity) [150].

### 4.2.4. Effect of pressure on capillary flow

The Bagley correction was performed to correct the entrance and exit effects on the capillary rheological data and to determine the true wall shear stress, $\tau_w$, [49-51]. The linear Bagley (i.e., pressure loss) and Weißenberg-Rabinowitsch (i.e., pseudo-plastic behavior) corrections were applied using the WinRheo II software (Göttfert, Germany) [181] from capillaries with the *L/D* ratios of 30/1, 20/1 and 10/1, to determine the true shear viscosity.

Figure 4.7 shows the Bagley plots for the LDPE/MWCNT nanocomposites with 0.1 to 5 wt.% of MWCNTs at 140 °C for apparent shear rates ranging from 75 to 5000 $s^{-1}$. The pressure drop increases with increasing shear rate and is influenced by the MWCNT loading, more observed at higher loadings. The determination coefficients ($R^2$) of the regression lines were used to assess the linearity of the Bagley plots [150].

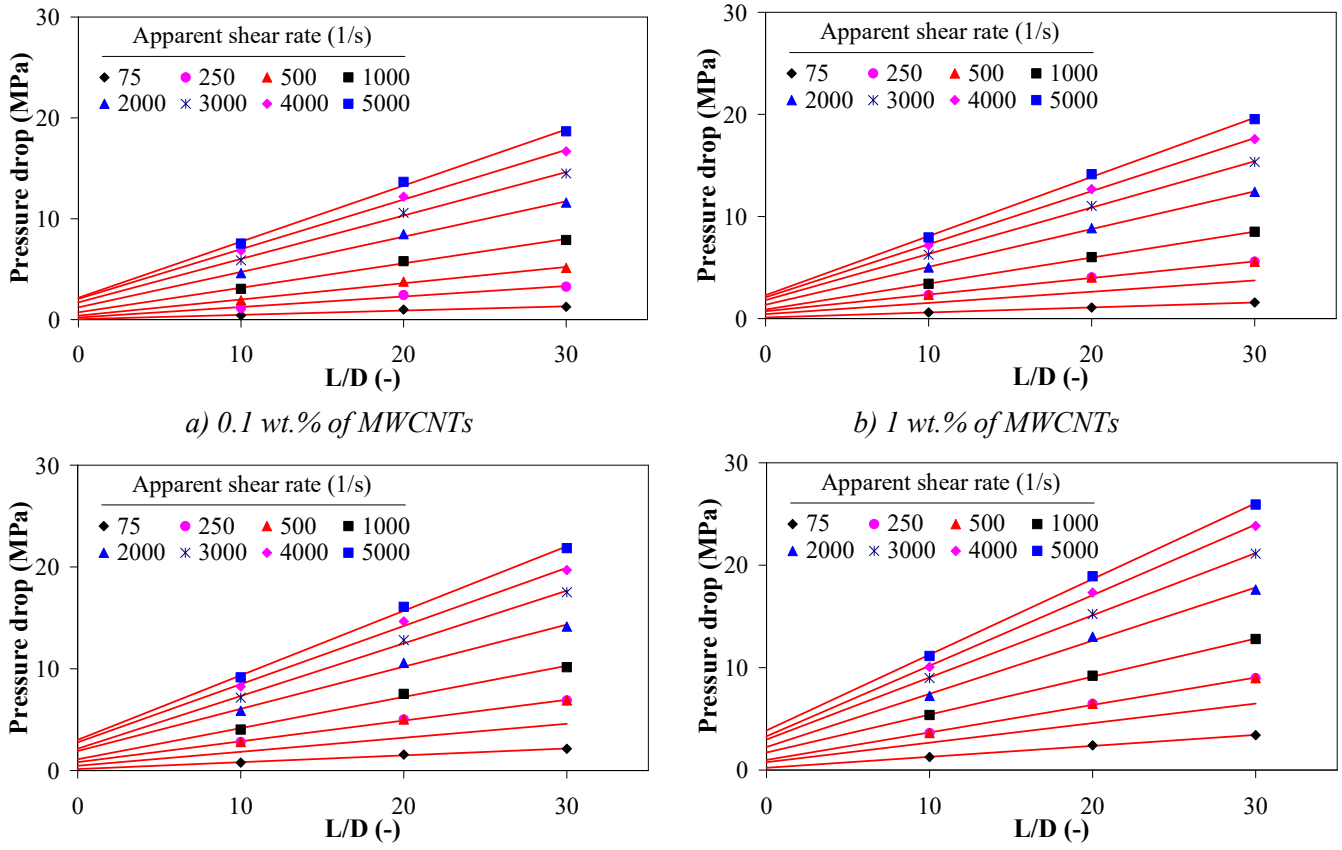


*a) 0.1 wt.% of MWCNTs* *b) 1 wt.% of MWCNTs*

*c) 3 wt.% of MWCNTs* *d) 5 wt.% of MWCNTs*

**Figure 4.7.** *Bagley plots for LDPE/MWCNT nanocomposites at 140 °C*

Figure 4.8 clearly displays a high degree of linearity between the pressure drop and *L/D* ratio even at low shear rates, and, in general, the values of $R^2$ were higher than 0.994, indicating that, with

short durations, the pressure effect is not significant [150]. By examining the pressure drop across the capillary from different sets of results, it could be determined that the short-term effect of pressure on the shear viscosity is not significant [150]. The pressure drop also increases with increasing MWCNT loading and the increase is more evident at higher shear rates (Figure 4.8). For example, at a shear rate of 5000 $s^{-1}$ and a temperature of 140 °C, the pressure drop increased from about 2.14 to 3.87 MPa as the nanotube loading increased from 0.1 to 5 wt.% of MWCNTs.

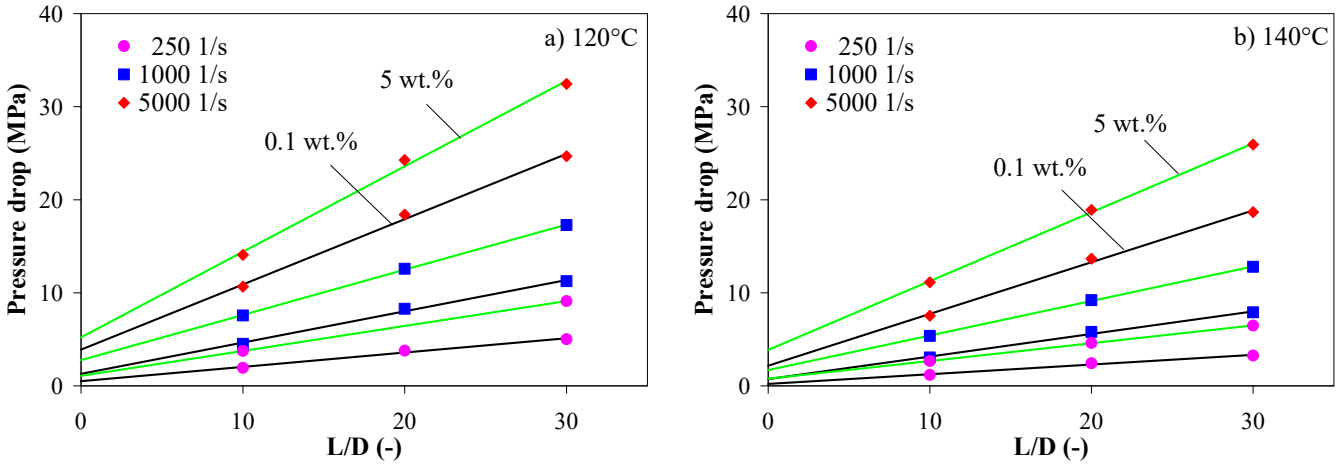


**Figure 4.8.** *Bagley plots for LDPE with 0.1 and 5 wt.% of MWCNTs at (a) 120 °C and (b) 140 °C temperatures*

The tendancy of pressure drop to increase with increasing shear rate and MWCNT loading is also found for the polymer/MWCNT nanocomposites with the HDPE, EVA, PP, and TPU matrix. When the MWCNT loading increased from 0.1 to 5 wt.% of MWCNTs, the pressure drop of the polymer/MWCNT nanocomposites increased, regardless of temperature and shear rate.

Figure 4.9 shows the dependence of the pressure drop on the melt temperature for the LDPE/MWCNT nanocomposites with 0.1 and 5 wt.% at three apparent shear rates. The pressure drop decreases almost linearly when the melt temperature increases due to the fact that, at higher temperatures, the mobility of the molecular chains is enhanced and the melt through the capillary die shows a lower viscosity. The pressure drop dependency on temperature is significantly lower at higher shear rates, regardless of the polymer matrix, as shown in Figure 4.9.

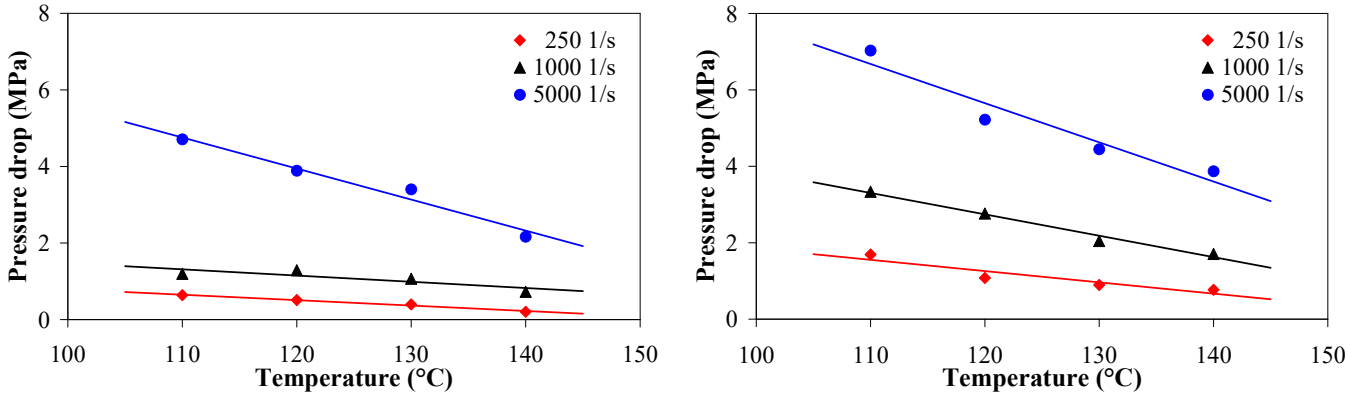


*a) 0.1 wt.% of MWCNTs* *b) 5 wt.% of MWCNTs*

**Figure 4.9.** *Dependence of pressure drop on temperature for LDPE/MWCNT nanocomposites under various apparent shear rates*

# 5. PRESSURE-VOLUME-TEMPERATURE DIAGRAMS OF POLYMER/MWCNT NANOCOMPOSITES

## 5.1. Experimental results

### 5.1.1. *pVT* diagrams of LDPE/MWCNT nanocomposites

The *pVT* behavior of LDPE/MWCNT nanocomposites was investigated at increasing pressures ranging from 10 to 1500 bar and at decreasing temperatures ranging from 160 to 30 °C (isothermal mode). The *pVT* diagrams of LDPE/MWCNT nanocomposites are shown in Figure 5.1 and display three distinct regions: the solid, transition, and melting region, respectively. The step decrease in the specific volume indicates the crystallization transition of the composite.

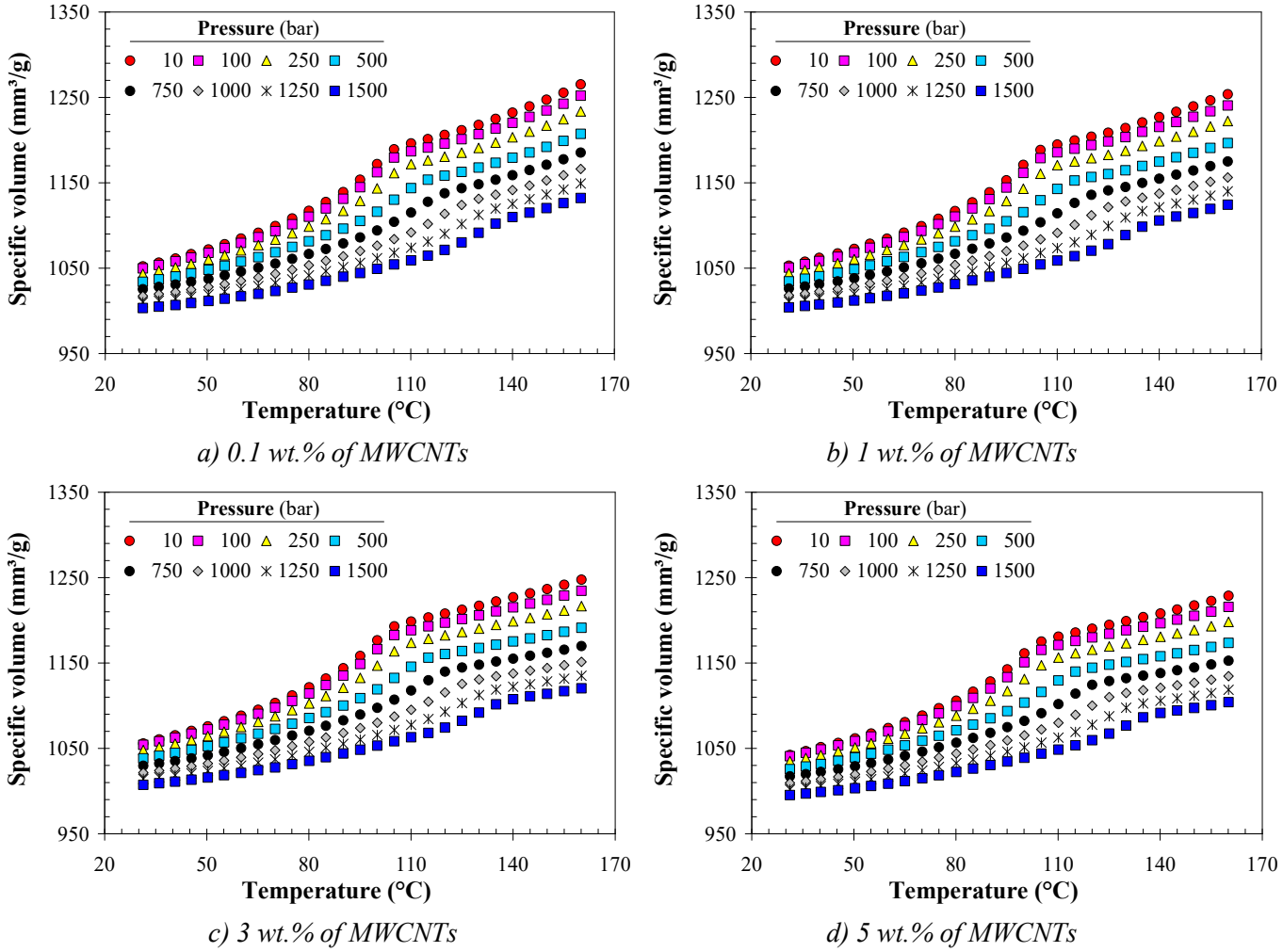


*a) 0.1 wt.% of MWCNTs* *b) 1 wt.% of MWCNTs*

*c) 3 wt.% of MWCNTs* *d) 5 wt.% of MWCNTs*

**Figure 5.1.** *pVT data for LDPE/MWCNT nanocomposites*

As expected from the literature review, the specific volume decreased with increasing pressure and decreasing temperature due to reducing the free volume available to molecules which resulted in an increase in the intermolecular interactions [29]. Also, the decrease in the specific volume is associated with the crystallization process. With increasing pressure, the specific volume change gets smaller and

smaller, corresponding to a decrease in compressibility [150]. In the solid state, the specific volume change (the solid compressibility) is much smaller than that in the melt state (the melt compressibility) [150].

At 10 bar, the specific volume of the LDPE nanocomposite with 5 wt.% of MWCNTs (Figure 5.1.d) varies between 1041.23 $mm^3/g$ at 30 °C and 1227.55 $mm^3/g$ at 160 °C, an increase of 18%. At 1500 bar, the specific volume variation is only 11% and has values of 994.39 $mm^3/g$ and 1103.09 $mm^3/g$ at temperatures of 30 °C and 160 °C, respectively.

## 5.2. Discussions

### 5.2.1. Pressure and temperature dependencies of specific volume

Based on the *pVT* diagrams of LDPE/MWCNT nanocomposites (Figure 5.1), the change in specific volume within the pressure-temperature (*p-T*) window is about 5 to 20%, depending on the MWCNT loading. The specific volume of the LDPE/MWCNT nanocomposites decreases with increasing pressure and the decrease is the same for every MWCNT loading, about 11%–12% and 5% in the melt and solid state, respectively. Meanwhile, the specific volume increases with increasing temperature with changes of 11%–13% and 18%–21% at pressures of 10 and 1500 bar, respectively. The effect of the temperature on the *pVT* data of the LDPE/MWCNT nanocomposites is apparently more significant than the effect of the pressure due to the phase change that occurs in the investigated temperature range, regardless of the MWCNT loading [150].

From the *pVT* data of all polymer/MWCNT nanocomposites, the effect of temperature on the specific volume is shown to decrease with increasing pressure, which corresponds to a decrease in compressibility. Meanwhile, the pressure dependency on the specific volume increases with increasing temperature with a peak in values that can be observed in the transition region.

### 5.2.2. Effect of MWCNTs on specific volume

The *pVT* data for the LDPE filled with 0.1, 1, 3, and 5 wt.% of MWCNTs are compared in Figure 5.2 to illustrate the effect of MWCNT loading on the specific volume at the lowest and highest pressure. It can be seen that, for the nanocomposites with the LDPE (Figure 5.2), HDPE, and PP matrix, the specific volume is nearly constant with increasing nanotube loading up to 1 wt.%, where a further increase of MWCNT loading results in a decrease in the specific volume. However, the specific volume of the EVA/MWCNT nanocomposites has similar values only at the low MWCNT loadings (0.1, 0.3, and 0.5 wt.%) with a decreasing trend with increasing the MWCNT loading. Regarding the *pVT* data of the TPU/MWCNT nanocomposites, the specific volume in the solid state has lower values at 1 wt.% than the ones found at low MWCNT loadings.

The reduction of the specific volume with the addition of MWCNTs can be explained by the nanotubes that do not expand or contract as the temperature changes and that counteract shrinkage effects due to molecular orientation [155]. Also, the effect of MWCNTs on the specific volume slightly decreases by increasing pressure.

### 5.2.3. Effect of MWCNTs on specific density

The specific density calculated from the *pVT* data as a function of temperature and pressure is presented in Table 5.1. At a constant pressure, the specific density of the polymer/MWCNT nanocomposites decreases with increasing temperature and increases with increasing MWCNT loading.

In addition to the temperature dependence, the density is also dependent on the pressure, i.e., the specific density shifted to lower values with increasing pressure [155].

The bulk density of the LDPE/MWCNT nanocomposites calculated using equation (2.2) was also listed in Table 5.1 and represented in Figure 5.3. As expected, the densities of the HDPE/MWCNT nanocomposites are higher than the nanocomposites with the LDPE matrix due to the side chains that allow the HDPE polymer backbone to align and pack together to form a crystalline, high-density material [123]. Also, the density of the PP/MWCNT nanocomposites are lower than LDPE and HDPE, as expected [125], by 6 to 8%. Compared with the density mentioned in the technical data sheets of the polymer matrix (dashed lines in Figure 5.3, the density of the TPU matrix was not available), the bulk densities of the polymer/MWCNT nanocomposites are lower by up to 4%, which can be caused by the density measurement procedures used in the TDS.

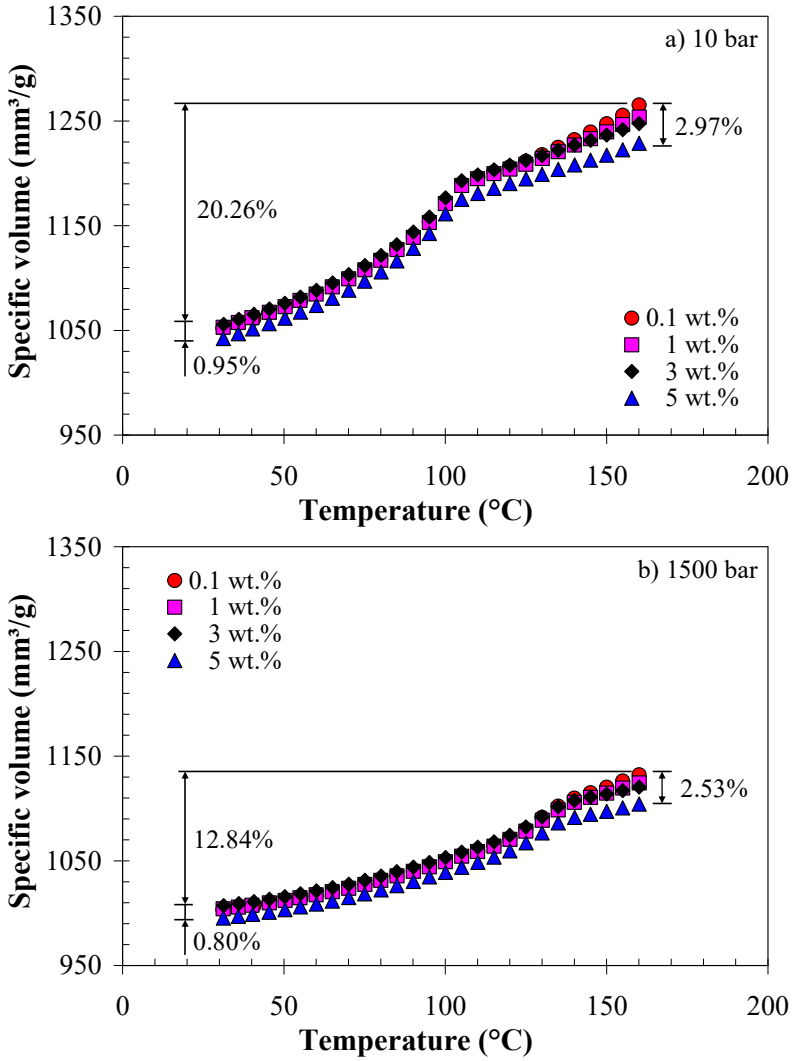


**Figure 5.2.** *Effect of melt temperature and MWCNT loading on the specific volume of the LDPE/MWCNT nanocomposites at (a) 10 bar and (b) 1500 bar*

Figure 5.4 presents the *pVT* density of the polymer/MWCNT nanocomposites at the lowest temperature and at the lowest pressure of 10 bar. It can be observed that the *pVT* density has higher values than the bulk density since the measurements were done under pressure. The effect of MWCNTs on the bulk density is similar to that of the *pVT* density – the density is independent of MWCNTs at MWCNT loadings up to 1 wt.% and it increases with further wt.% increase [155].

**Table 5.1.** *Density of LDPE/MWCNT nanocomposites as a function of temperature and pressure*

| **MWCNTs** (wt.%) | **Temperature** (°C) | ***pVT* density** (g/cm$^3$) | | **Bulk density** (g/cm$^3$) |
|---|---|---|---|---|
| | | **10 bar** | **1500 bar** | |
| 0.1 | 30 | 0.9505 | 0.9967 | 0.8940±0.0012 |
| | 160 | 0.7903 | 0.8833 | |
| 0.3 | 30 | 0.9537 | 1.0004 | 0.8960±0.0008 |
| | 160 | 0.7904 | 0.8840 | |
| 0.5 | 30 | 0.9382 | 0.9836 | 0.8976±0.0012 |
| | 160 | 0.7840 | 0.7975 | |
| 1 | 30 | 0.9497 | 0.9959 | 0.8969±0.0036 |
| | 160 | 0.7976 | 0.8894 | |
| 3 | 30 | 0.9472 | 0.9928 | 0.9026±0.0036 |
| | 160 | 0.8016 | 0.8926 | |
| 5 | 30 | 0.9595 | 1.0047 | 0.9162±0.0015 |
| | 160 | 0.8138 | 0.9057 | |

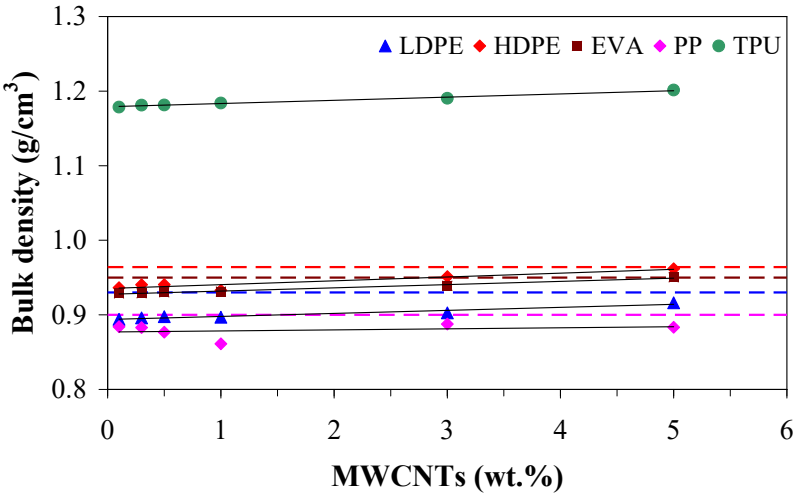


**Figure 5.3.** *Bulk densities of polymer/MWCNT nanocomposites as a function of MWCNT loading*

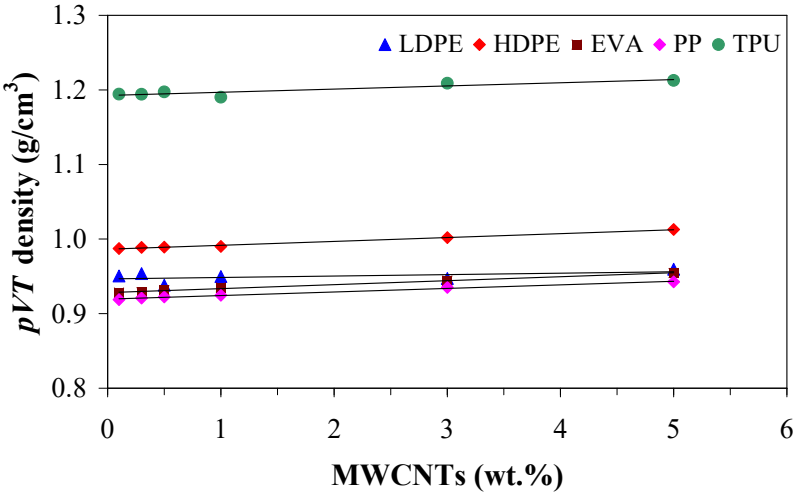


**Figure 5.4.** *pVT densities of polymer/MWCNT nanocomposites at 10 bar as a function of MWCNT loading*

# 6. THERMAL CONDUCTIVITY OF POLYMER/MWCNT NANOCOMPOSITES

## 6.1. Experimental results

### 6.1.1. Thermal conductivity of LDPE/MWCNT nanocomposites

The thermal conductivity of LDPE/MWCNT nanocomposites was measured at increasing pressures ranging from 100 to 500 bar and at decreasing temperatures ranging from 140 to 50 °C (isothermal mode). The *TC* of LDPE/MWCNT nanocomposites as a function of temperature and pressure are shown in Figure 6.1 and three distinct regions can be distinguished: the solid, transition, and melting region, respectively.

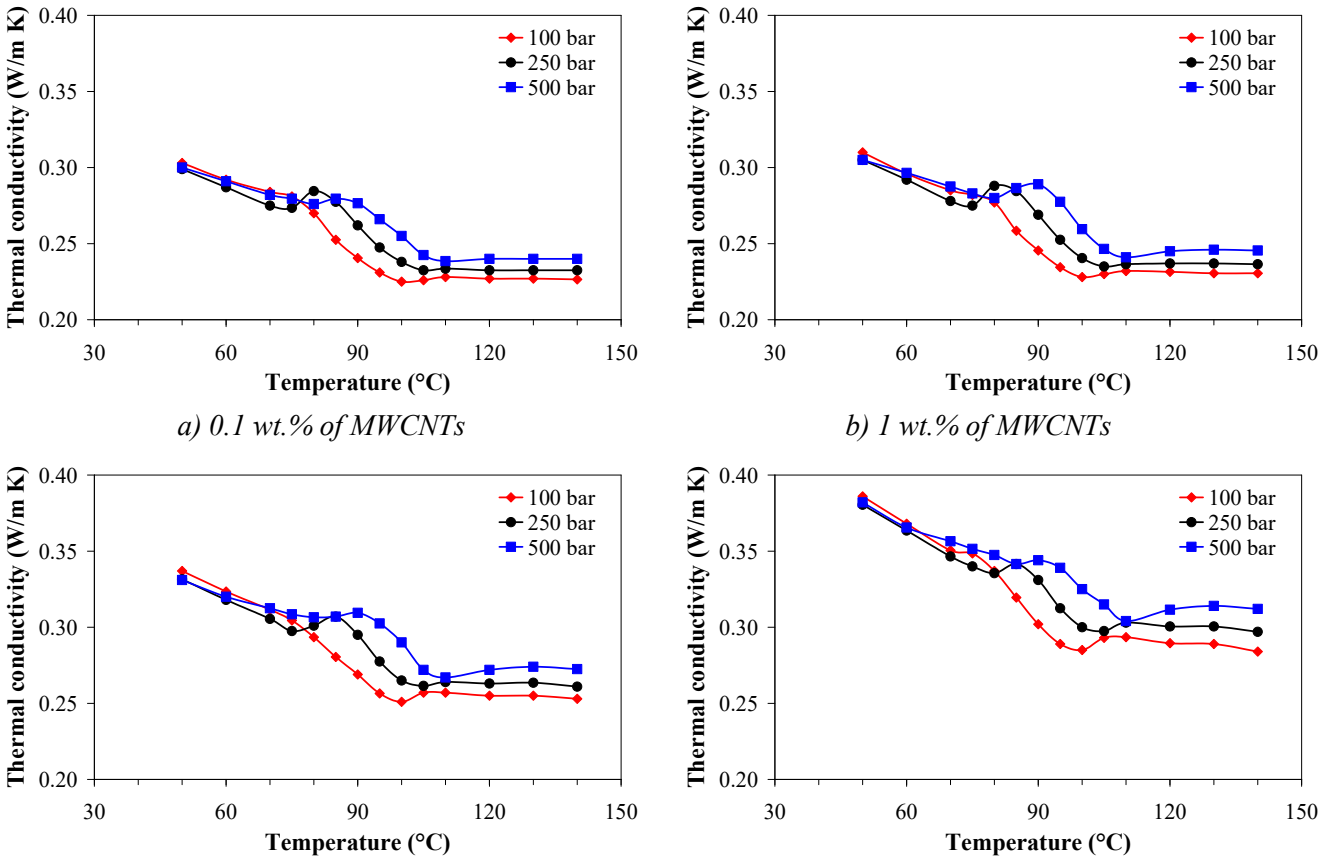


*a) 0.1 wt.% of MWCNTs*

*b) 1 wt.% of MWCNTs*

*c) 3 wt.% of MWCNTs*

*d) 5 wt.% of MWCNTs*

**Figure 6.1.** *Thermal conductivity of the LDPE/MWCNT nanocomposites as a function of temperature and pressure*

In the solid state, *TC* decreases with increasing temperature up to 70 °C, which is the complete crystallization of the melt, whereas, in the melt state, the *TC* is nearly independent of temperature from 100 °C. With increasing pressure, the *TC* values increase in the melt state due to the melt compressibility; therefore the MWCNTs are more close together. However, in the solid state, the effect of pressure is less significant due to the low solid compressibility (see Chapter 5). For example, in the melt state, when the pressure increased from 100 to 500 bar the *TC* increased by up to 5% to 10%, depending on the MWCNT loading.

Based on the *pVT* diagrams (Figure 5.1), at 500 bar, the LDPE/MWCNT nanocomposites can be considered that are in solid state up to 70 °C and in melt state starting with 110 °C. In the solid state, the *TC* of the LDPE/MWCNT nanocomposites with low MWCNT loadings (0.1 to 0.5 wt.%) can be approximated to a value of 0.286 W/m K, regardless of the applied pressure. With further increasing the MWCNT loading to 5 wt.%, the *TC* increases up to 0.362 W/m K, a 26.62% change. Meanwhile, in the melt state, the *TC* of the LDPE/MWCNT nanocomposites with low MWCNT loadings increases with increasing pressure from 100 to 500 bar with values from 0.227 to 0.239 W/m K, respectively. At 5 wt.% of MWCNTs, the thermal conductivity varies between 0.289 and 0.310 W/m K in the pressure range of 100 and 500 bar.

## 6.2. Discussions

### 6.2.1. Pressure and temperature dependencies of thermal conductivity

The thermal conductivity is influenced by the temperature and pressure, regardless of the MWCNT loading, which reflects the morphological changes during the cooling of the composite melts. The thermal conductivity of the semi-crystalline polymer/MWCNT nanocomposites as a function of temperature displays three distinct regions: the solid, transition, and melting region, respectively. Due to the low crystallinity of EVA matrix and the amorphous TPU matrix, the transition region is not present.

The effect of pressure is very important for the injection molding process; the experimental results indicate that the *TC* increases with increasing pressure, especially in the melt state, due to the fact that the pressure significantly reduces the inter-tube distance, therefore reducing the contact between adjacent nanotubes, enhancing the photon transport [150]. In the melt state, the effect of pressure on the thermal conductivity is more significant than in the solid state due to the MWCNTs that are able to move and align, which allows phonon transport [110,163,191,192].

Figure 6.2 represents the thermal conductivity of the polymer/MWCNT nanocomposites with 5 wt.% in order to compare the effect of temperature on the analysed nanocomposites at a pressure of 100 bar. In the solid state, the *TC* decreases with increasing temperature, whereas, in the melt state, the *TC* is nearly independent of temperature. Also observed in the solid state, the *TC* has higher values than in the melt state, especially for the semi-crystalline polymers, due to the formation of crystals that enhance the heat transport mechanism [107,150,193]. Between the solid and melt states, the *TC* changes are of 20.45%, 51.54%, and 36.28% for the 5 wt.% nanocomposites with the LDPE, HDPE, and PP matrix, respectively. However, for the nanocomposites with the EVA and TPU matrix, the changes were only of 2.85% and 1.29%, respectively.

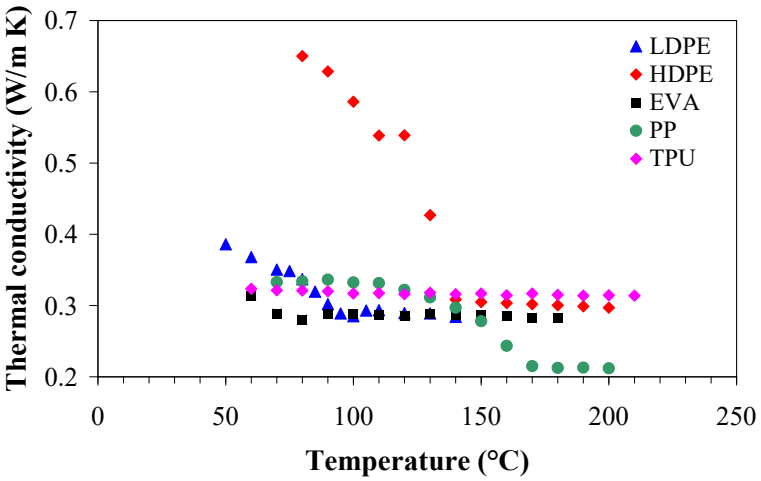


**Figure 6.2.** *Thermal conductivity of the polymer/MWCNT nanocomposites with 5 wt.% as a function of temperature at a pressure of 100 bar*

The *TC* of the nanocomposites with 5 wt.% of MWCNTs is presented in Figure 6.3 as a function of pressure for the solid and melt states. When the pressure increased from 100 to 500 bar, the *TC* in the solid state increased for the nanocomposites with the EVA and TPU matrix by only 6.86% and 5.49%, respectively. This behavior can be attributed to their low or no crystallinity, where the CNTs are able to interact under applied pressure since the nanotubes are not encapsulated into the crystallizing matrix [60,160,163]. Comparing the nanocomposites with the LDPE and HDPE matrix, the *TC* values of the HDPE/MWCNT nanocomposites are higher, especially in the solid state, which can be attributed to its higher crystallinity [15,103] (i.e., crystallinity degree values of 30.96% and 65.04% for the 5 wt.% nanocomposites with the LDPE and HDPE matrix, respectively).

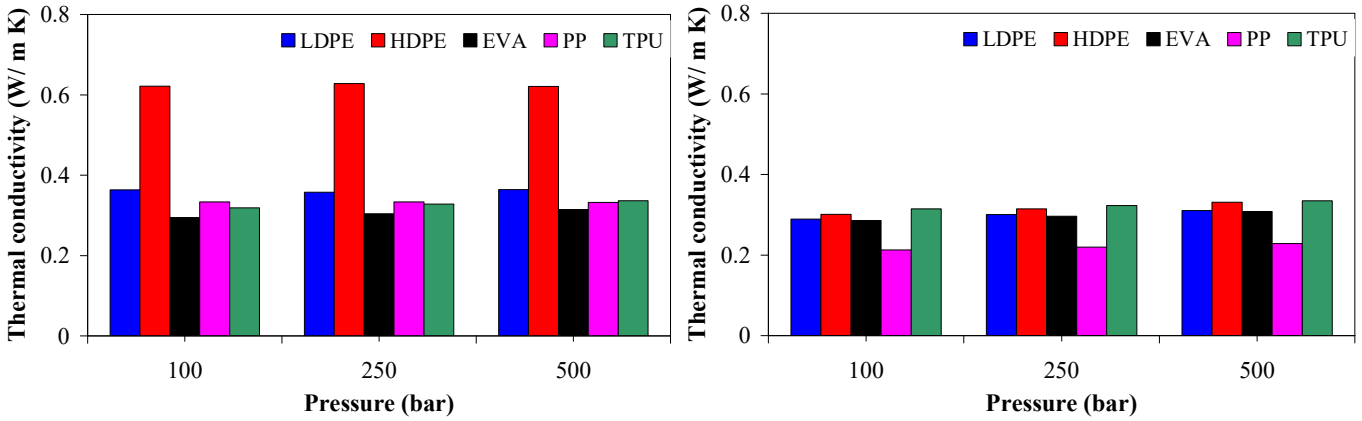


*a) solid state* *b) melt state*

**Figure 6.3.** *Thermal conductivity of the polymer/MWCNT nanocomposites with 5 wt.% as a function of pressure in the (a) solid state and (b) melt state*

### 6.2.2. Effect of MWCNTs on thermal conductivity

When the effects of temperature and pressure were separated from that of the MWCNTs, the results indicated a moderate enhancement in the thermal conductivity of the polymer/MWCNT nanocomposite (24–46%) with increasing MWCNT loading from 0.1 to 5 wt.% (Table 6.1), although MWCNTs can exhibit thermal conductivity as high as 3000 W/m·K [194,195]. In the solid state, at 500 bar, the *TC* increased with increasing MWCNT loading from 0.1 to 5 wt.% for the nanocomposites with the LDPE, HDPE, EVA, and PP matrix by approx. 26%, 32%, 24%, and 32%, respectively, whereas the highest change was found for the nanocomposites with the TPU matrix by 46%.

**Table 6.1.** *Thermal conductivity of polymer/MWCNT nanocomposites in the solid state*

| **Pressure** (bar) | **MWCNTs** (wt.%) | **Thermal conductivity** (W/m K) | | | | |
|---|---|---|---|---|---|---|
| | | **LDPE** | **HDPE** | **EVA** | **PP** | **TPU** |
| 100 | 0.1 | 0.290 | 0.465 | 0.231 | 0.252 | 0.225 |
| | 5 | 0.363 | 0.622 | 0.294 | 0.334 | 0.319 |
| 250 | 0.1 | 0.284 | 0.469 | 0.243 | 0.250 | 0.227 |
| | 5 | 0.358 | 0.628 | 0.304 | 0.333 | 0.328 |
| 500 | 0.1 | 0.288 | 0.469 | 0.254 | 0.252 | 0.231 |
| | 5 | 0.364 | 0.621 | 0.315 | 0.332 | 0.336 |

The increase in *TC* with increasing MWCNT loading is mainly due to a denser nanotube network that is formed as the MWCNT loading increases, which allows phonon transport [110,150,163,191,192] and in part due to the effect of CNTs on the crystallization of the polymer. In the solid state, the *TC* of semi-crystalline polymers is affected by the crystallinity due to the phonon scattering at the interface

between the amorphous and crystalline phases [15,37,150,196], which successively is affected by the MWCNT loading that contributes nucleation sites for polymer crystallization and accelerates the crystal growth rate, as well as modifying the crystal size [63,150,156,158,160,161,180].

Figure 6.4 shows the effect of MWCNT loading on the *TC* of the polymer/MWCNT nanocomposites at a pressure of 500 bar. The variation in thermal conductivity suggests two distinct zones for the semi-crystalline polymers, which hold for both the solid and melt states [150]. Below 1 wt.% of MWCNTs, the *TC* of the semi-crystalline polymer/MWCNT nanocomposites was nearly constant with nanotube loading, especially in the melt state. Meanwhile, the *TC* of the TPU/MWCNT nanocomposites increased linearly with increasing MWCNT loading from 0.1 to 5 wt.%.

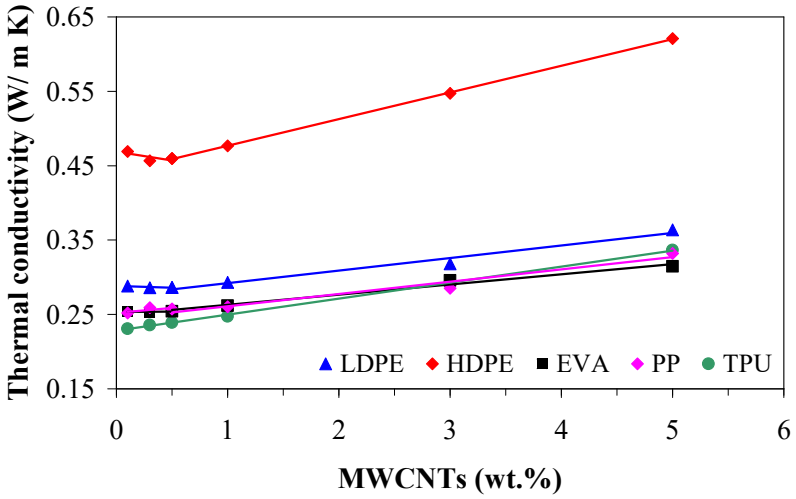


*a) solid state*

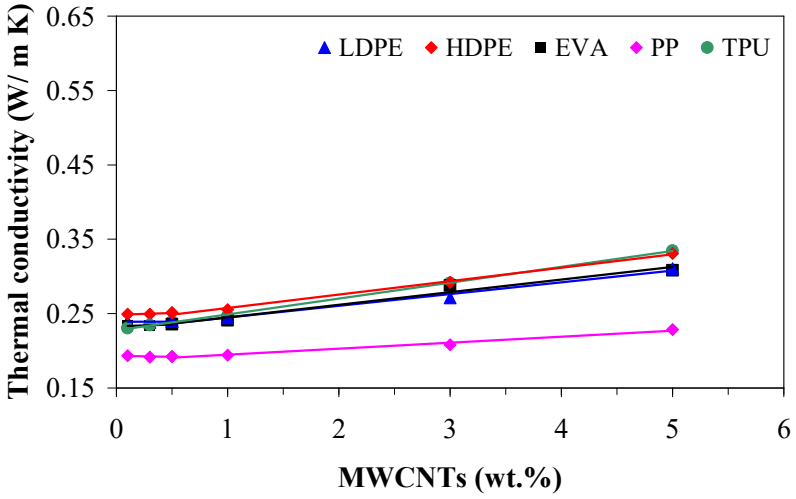


*b) melt state*

**Figure 6.4.** *Thermal conductivity of the polymer/MWCNT nanocomposites as a function of MWCNT loading in the (a) solid state and (b) melt state at 500 bar*

In the nanocomposites with semi-crystalline matrix and lower wt.%, an insulating trans-crystalline layer around MWCNTs may form since MWCNTs act as nuclei for crystallization [197]. Therefore, the interface thermal resistance between the MWCNTs and semi-crystalline matrix is larger than the critical value [107,193,196] and there are too few nanotubes for photons to move effectively. In the semi-crystalline polymer/MWCNT nanocomposites with higher wt.%, the thermal conductivity is steadily increasing with increasing MWCNT loading (Figure 6.4). The increase in *TC* could be mainly related to the formation of a heat transport pathway between MWCNTs, which significantly facilitates the photons' movement through the nanocomposites [150]. Based on these considerations, it was concluded that 1 wt.% loading is in the region of the thermal percolation in the case of the nanocomposites with semi-crystalline matrix [150].

# 7. ANALYTICAL MODELING OF MATERIAL PROPERTIES

## 7.1. Introduction

### 7.1.1. Cross–WLF model

The Cross–WLF viscosity model is the most common model used by injection molding simulation software, offering the best fit to most rheological data [51]. The seven parameter Cross–WLF model describes the viscosity dependency on shear rate, temperature and pressure, $\eta(\dot{\gamma}, T, p)$, for a shear-thinning melt [51,200,201,204]. If the melt viscosity at infinite shear rate is negligible (Figure 7.1), the Cross–WLF model can be written as

$$\eta(\dot{\gamma}, T, p) = \frac{\eta_0}{1 + \left(\frac{\eta_0 \cdot \dot{\gamma}}{\tau^*}\right)^{1-n}} \text{ (Pa·s)}, \tag{7.6}$$

where $\eta_0$ is the zero-shear rate viscosity, $\tau^*$ is the critical shear stress at which the onset of shear-thinning behavior occurs and $n$ is the shear-thinning index.

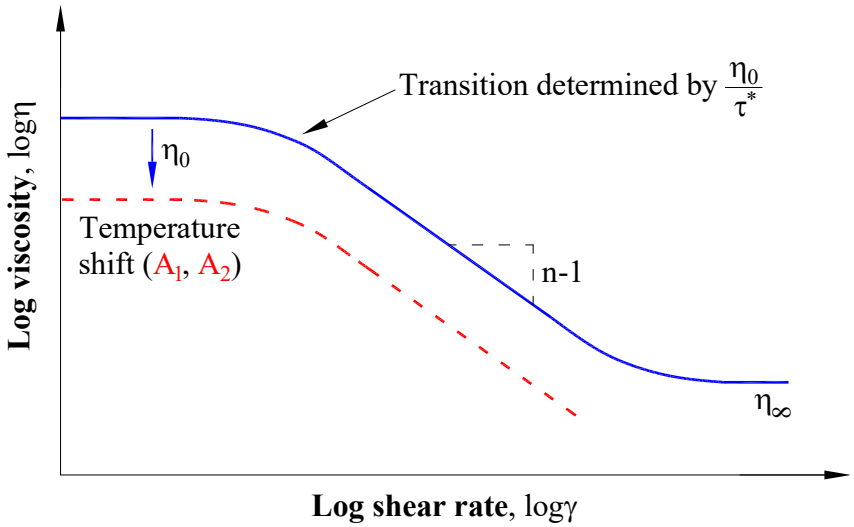


**Figure 7.1.** *Schematic of the viscosity approximation using the Cross–WLF model*
Recreated from [51]

Beside the temperature dependence, pressure dependence is known. With increasing pressure, the viscosity is increased [44] and the free volume is reduced, thus reducing molecular mobility [1]. An increase in viscosity is reflected from the fact that high pressure raises $T_g$ and $T_m$ [1]. The combination of high pressure and low temperature tends to promote crystallization, orientation and structural changes [1].

### 7.1.2. The modified 2-domain Tait model

According to the modified 2-domain Tait model equation, the relationship between the specific volume and the pressure and temperature represents the $pVT$ data of polymer solids and melts with an accuracy of $1\times10^{-6}$ to $2\times10^{-6}$ $m^3/kg$ [31]. The Tait equation is valid only for extremely low cooling

rates and it fails to accurately predict *pVT* behavior at high cooling rates found in normal processing conditions [31].

$$V(T,p) = V_0(T) \cdot \left[1 - C \cdot \ln\left(1 + \frac{p}{B(T)}\right)\right] + V_t(T,p), \tag{7.7}$$

where $C$ is a universal constant, $C = 0.0894$ [92,94,205],

$$V_0(T) = \begin{cases} b_{1s} + b_{2s} \cdot \overline{T}, & T \le T_t(p); \\ b_{1m} + b_{2m} \cdot \overline{T}, & T > T_t(p); \end{cases} \tag{7.8}$$

$$B(T) = \begin{cases} b_{3s} \cdot \exp(-b_{4s} \cdot \overline{T}), & T \le T_t(p); \\ b_{3m} \cdot \exp(-b_{4m} \cdot \overline{T}), & T > T_t(p); \end{cases} \tag{7.9}$$

$$V_t(T,p) = \begin{cases} b_7 \cdot \exp(b_8 \cdot \overline{T} - b_9 \cdot p), & T \le T_t(p); \\ 0, & T > T_t(p); \end{cases} \tag{7.10}$$

in which

$$\overline{T} = T - b_5, \tag{7.11}$$

$$T_t = b_5 + b_6 \cdot p, \tag{7.12}$$

where $b_1$ to $b_9$ are material constants, $T_t$ is the *pVT* transition temperature between melt and solid state (subscript *m* and *s*) was found to be a linear function of pressure [205].

By inserting zero pressure, $p = 0$, in equation (7.12), the $b_5$ parameter represents the transition temperature at zero pressure, $T_t(p=0) = b_5$ [31].

From equation

$$\frac{dT_g}{dP} = \frac{T_g V_g \Delta\alpha}{\Delta C_p}, \tag{7.13}$$

the transition temperature increases almost linearly with pressure [31]. Differentiation of equation (7.12) yields

$$\frac{dT_g(P)}{dP} = b_6, \tag{7.14}$$

where $V_g$ is the specific volume at glass transition temperature, $\Delta\alpha$, $\Delta C_p$ are the volume expansion coefficient difference and the excess heat capacity, respectively, between polymer melt and solid, $b_6$ is the rate of change of $T_g$ and $T_t$ with pressure for amorphous and semi-crystalline polymer, respectively.

## 7.2. Modeling of the shear viscosity

### 7.2.1. Master curves of LDPE/MWCNT nanocomposites

Based on the corrected melt shear viscosity, master curves were constructed by employing the Time-Temperature-Superposition (*TTS*) principle at a reference temperature of 130 °C. Figure 7.2 compares the melt shear viscosity master curves obtained for LDPE nanocomposites with 0.1, 1, 3, and 5 wt.% of MWCNTs, with the coefficients listed in Table 7.1. With increasing MWCNT loading, the zero viscosity increases due to the addition of MWCNTs that blocks the movement and extensional activities of the macromolecular chains.

All the LDPE/MWCNT nanocomposites exhibited solid-like behavior and the shear-thinning exponent *n* decreased with increasing MWCNT loading (Table 7.1) [150]. This behavior is an indication

that MWCNT–MWCNT interactions are dominant as the MWCNT loading increases and the shear rate affects both the CNT network and the polymer entangled network [150].

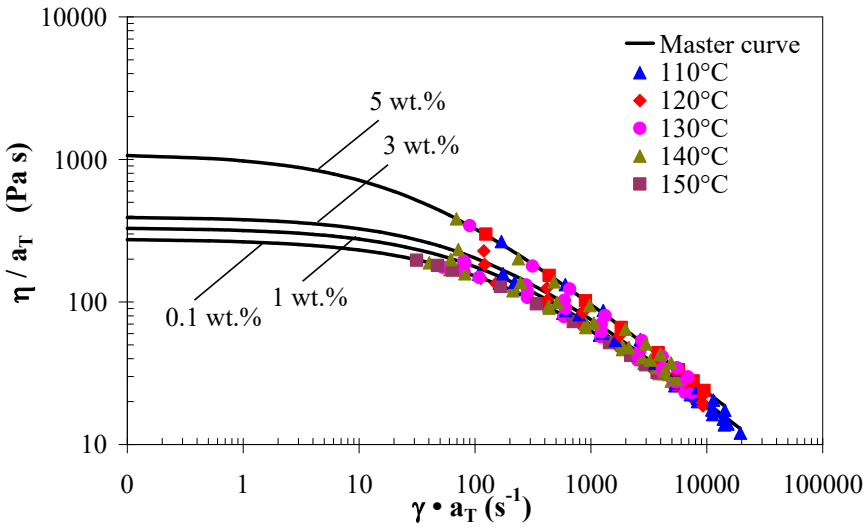


**Figure 7.2.** *Master curves of the LDPE/MWCNT nanocomposites for the corrected rheological data*

**Table 7.1.** *Cross-WLF parameters for the master curves of the LDPE/MWCNT nanocomposites at a 130 °C reference temperature*

| **Parameters** | **MWCNTs** (wt.%) | | | | | |
|---|---|---|---|---|---|---|
| | **0.1** | **0.3** | **0.5** | **1** | **3** | **5** |
| $\eta_0$ (Pa s) | 276.546 | 381.761 | 380.719 | 332.029 | 395.089 | 1093.517 |
| $\tau^*$ (kPa) | 38.365 | 28.161 | 28.595 | 40.465 | 42.938 | 29.113 |
| $\lambda$ (s) | 0.007 | 0.014 | 0.013 | 0.008 | 0.009 | 0.038 |
| $n$ | 0.379 | 0.398 | 0.400 | 0.362 | 0.347 | 0.354 |
| $R^2$ | 0.999 | 0.998 | 0.999 | 0.996 | 0.989 | 0.999 |

## 7.3. Modeling of the specific volume

### 7.3.1. Specific volume prediction for LDPE/MWCNT nanocomposites

Figure 7.3 shows the *pVT* diagrams for LDPE/MWCNT nanocomposites and the corresponding *DSC* cooling scans since the *pVT* measurements were performed in cooling mode. Generally, at temperatures above $T_m$, the composites must be treated as a melt mixture of polymer and MWCNTs. For temperatures between $T_g$ and $T_m$, a combination of crystals, MWCNTs and melt polymer exists while, for temperatures lower than $T_g$, the composite solidifies and can be regarded as solid.

The *pVT* diagrams display three distinct regions: the solid, transition, and melting regions, respectively. The step decrease in the specific volume indicates the crystallization transition. Therefore, the solid curve $T_t = T(p)$ indicates the onset of the transition associated with the crystallization (below this curve the melt starts to crystallize), which is clearly dependent on the pressure [150].

At the lowest pressure, i.e., 10 bar, and 110 °C, the nanocomposite is well above the $T_t$ curve (i.e., melting temperature) and is highly expanded, typical of a polymer melt. As the pressure increases, the nanocomposite crystallizes as can be seen by following down the line at 110 °C and the crystallization shifts to higher temperatures with increasing pressure. The LDPE/MWCNT nanocomposites are able to crystallize at a higher temperature than that found by *DSC* only through increasing the applied pressure. However, the crystallization process occurs over a temperature range and the onset transition temperature

at low pressure (10 bar, for example) is in good agreement with the *DSC* onset crystallization temperature [150].

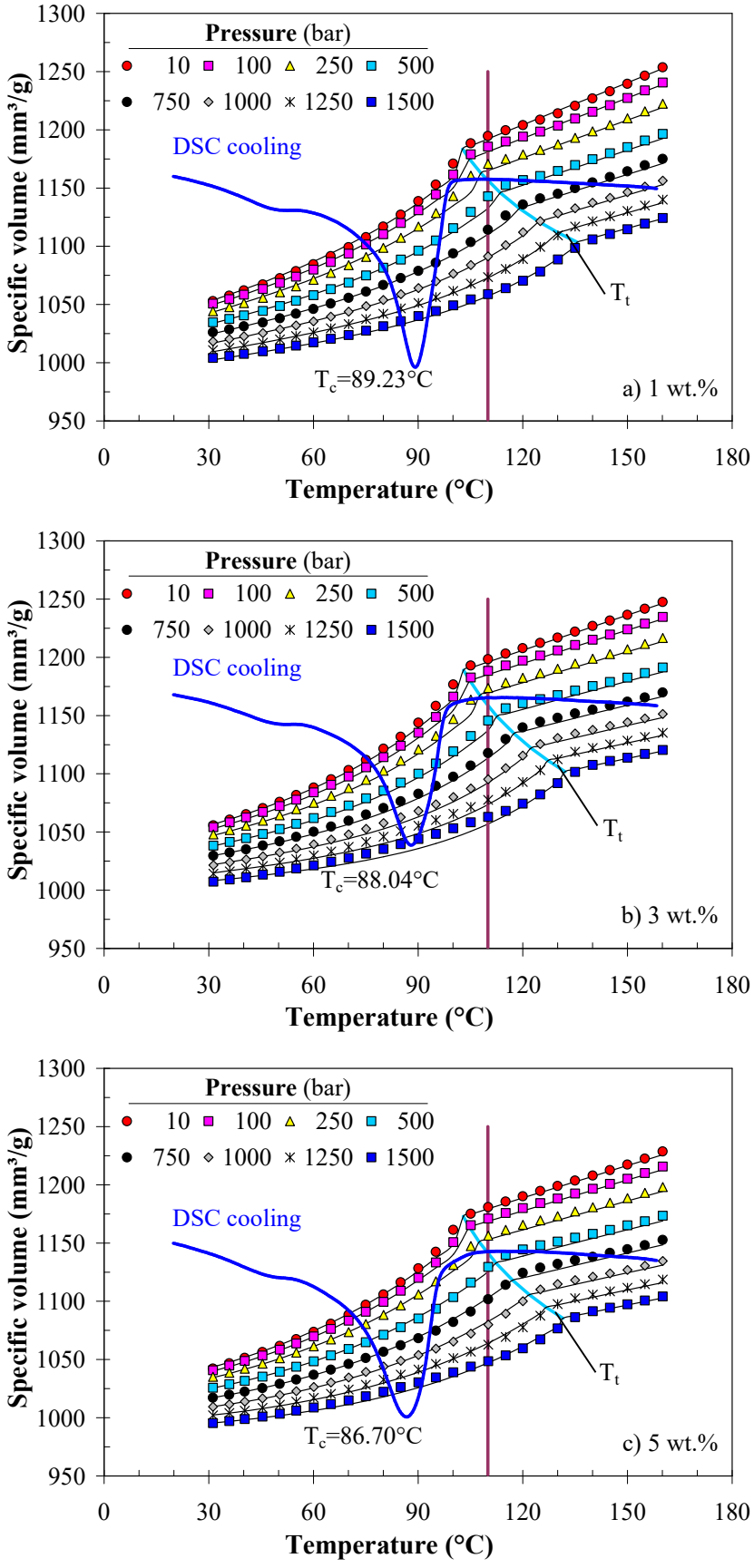


**Figure 7.3.** *pVT diagrams of the LDPE nanocomposites with (a) 1 wt.%, (b) 3 wt.%, and (c) 5 wt.% of MWCNTs. The solid lines show data fitting to the Tait model*

The Tait model coefficients of LDPE/MWCNT nanocomposites are presented in Table 7.2 with respect to the MWCNT loading. In the experimental window, the parameter $b_5$ turns to be nearly independent of MWCNT loading. The average value for $b_5$ was found to be 102.42±0.42 °C.

**Table 7.2.** *Parameters estimated by 2-domain Tait model for LDPE/MWCNT nanocomposites*

| **Parameters** | **MWCNTs** (wt.%) | | | | | |
|---|---|---|---|---|---|---|
| | **0.1** | **0.3** | **0.5** | **1** | **3** | **5** |
| $b_{1s}$ ($mm^3/g$) | $1.1018\times10^3$ | $1.0968\times10^3$ | $1.0976\times10^3$ | $1.0969\times10^3$ | $1.0815\times10^3$ | $1.0060\times10^3$ |
| $b_{2s}$ ($mm^3/g$ °C) | 0.7860 | 0.7615 | 0.6290 | 0.7156 | 0.5372 | 0.1017 |
| $b_{3s}$ (bar) | $1.0294\times10^3$ | $1.0945\times10^3$ | $1.0742\times10^3$ | $1.1483\times10^3$ | $1.1377\times10^3$ | $1.8648\times10^3$ |
| $b_{4s}$ (1/°C) | 0.0120 | 0.0109 | 0.0121 | 0.0101 | 0.0118 | 0.0105 |
| $b_{1m}$ ($mm^3/g$) | $1.1863\times10^3$ | $1.1782\times10^3$ | $1.2029\times10^3$ | $1.1844\times10^3$ | $1.1899\times10^3$ | $1.1739\times10^3$ |
| $b_{2m}$ ($mm^3/g$ °C) | 1.2794 | 1.3516 | 1.1170 | 1.2138 | 1.0137 | 0.9333 |
| $b_{3m}$ (bar) | $7.1798\times10^2$ | $7.2243\times10^2$ | $7.5580\times10^2$ | $8.3479\times10^2$ | $8.6149\times10^2$ | $8.5315\times10^2$ |
| $b_{4m}$ (1/°C) | 0.0005 | 0.0005 | 0.0016 | 0.0035 | 0.0038 | 0.0032 |
| $b_5$ (°C) | 102.5101 | 101.5450 | 102.4029 | 102.5101 | 102.8318 | 102.7245 |
| $b_6$ (°C/bar) | 0.0204 | 0.0211 | 0.0203 | 0.0220 | 0.0195 | 0.0192 |
| $b_7$ ($mm^3/g$) | 71.1385 | 66.1666 | 90.4323 | 73.9621 | 92.7879 | 151.1069 |
| $b_8$ (1/°C) | 0.0337 | 0.0351 | 0.0264 | 0.0264 | 0.0266 | 0.0169 |
| $b_9$ (1/bar) | 0.0006 | 0.0006 | 0.0004 | 0.0005 | 0.0004 | 0.0004 |

Figure 7.4 shows the transition temperature as a function of pressure and MWCNTs, calculated by the Tait model (equation (7.12)). The transition temperature of the LDPE/MWCNT nanocomposites increased linearly with increasing pressure [150]. The shift of the transition temperature to higher value indicates that, under pressure, the LDPE/MWCNT nanocomposites crystallizes at higher temperatures as compared with the *DSC* transition temperature [150], which varies between 88 to 90 °C (Table 3.1). No significant effect of the MWCNTs addition on the transition temperature of the LDPE/MWCNT nanocomposites was observed.

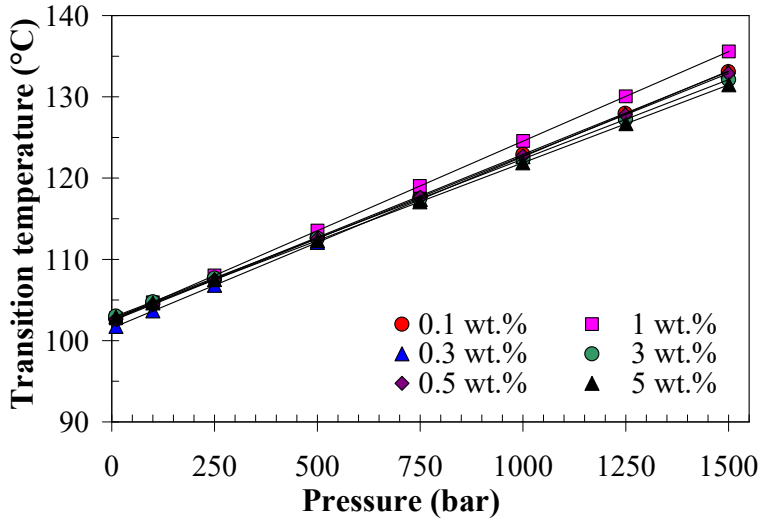


**Figure 7.4.** *pVT transition temperature of LDPE/MWCNT nanocomposites as a function of pressure and MWCNT loading*

From manufacturing point of view, the dependence of crystallization temperature on the pressure is very important [150]. For example, during the packing stage of the injection molding process, the melt is held constant under high pressure [89,150,190,206-208], which can induce changes in crystallinity and, consequently, in the final properties of the parts. This effect is even more important in the presence of nanotubes, which provides sites for nucleation process [150,156,207]. As illustrated in Figure 7.3, the crystallization temperature of the LDPE/MWCNT nanocomposites may be increased by about 29–33 °C if the nanocomposite is cooled under pressure, which leads to a better mechanical performance when subjected to various stresses in a relatively high temperature environment [190,206].

## 7.4. Discussions

### 7.4.1. Effect of MWCNTs on the shear-thinning index

Figure 7.5 presents the shear-thinning index from the Cross–WLF model as a function of MWCNT loading and polymer matrix. The shear-thinning index indicates that the polymer/MWCNT nanocomposites are suitable for injection molding. Furthermore, the values of shear-thinning index indicate that the nanotubes are in a state of good dispersion and aligned in the flow direction. No trend was specifically found between the addition of MWCNTs and shear-thinning index; however, a change in the shape of the graphs is found at the nanocomposites with 1 wt.% of MWCNTs.

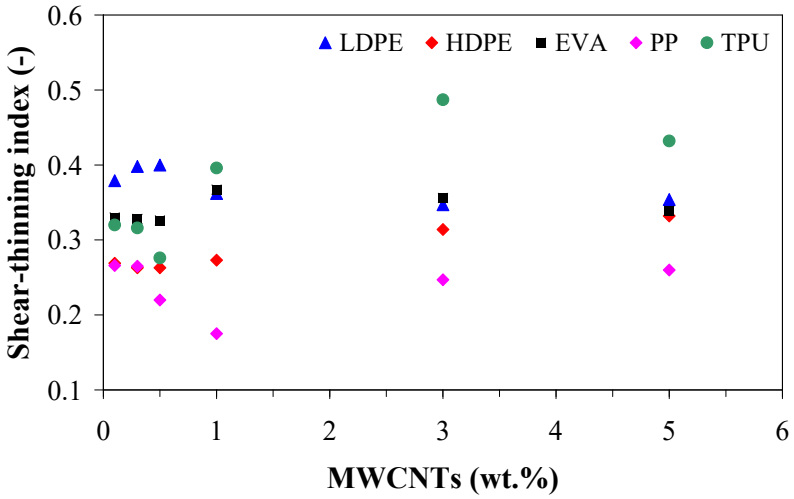


**Figure 7.5.** *Cross–WLF shear-thinning index of polymer/MWCNT nanocomposites as a function of MWCNT loading and polymer matrix*

### 7.4.2. Effect of MWCNTs on the activation energy

Based on the corrected melt shear viscosity, the master curves were constructed by employing the *TTS* principle and the shift factors required for the numerical simulation were determined using the WinRheo II software (Göttfert, Germany). In the process, the activation energy, $E_a$ (J/mol), was also calculated and is presented in Table 7.3 and Figure 7.6.

A significant change in the activation energy with increasing MWCNT loading from 0.1 to 5 wt.% was present for the nanocomposites with TPU matrix, where between 0.1 and 5 wt.%, the change was approx. 80%, indicating that the nanotubes are less restricted and have less interactions with the polymer chains [183,184]. In the case of the HDPE/MWCNT nanocomposites, the $E_a$ decreases when the MWCNT loading increases up to 3 wt.% of MWCNTs, then increases for the nanocomposites with 5 wt.% of MWCNTs, a difference of 223% between the 3 and 5 wt.%. For the nanocomposites with the

LDPE, EVA, and PP matrix, average values for the activation energy of 41.936±2.119, 40.616±1.044, and 43.290±3.925 kJ/mol, respectively, were found.

**Table 7.3.** *Activation energy of polymer/MWCNT nanocomposites from the TTS principle*

| Polymer matrix | MWCNTs (wt.%) | | | | | |
|---|---|---|---|---|---|---|
| | **0.1** | **0.3** | **0.5** | **1** | **3** | **5** |
| **LDPE** | 40354.812 | 40956.957 | 40833.899 | 43616.272 | 45881.551 | 39967.547 |
| **HDPE** | 21409.548 | 21819.211 | 18735.487 | 26724.060 | 15537.272 | 50135.320 |
| **EVA** | 39495.236 | 40354.859 | 39894.527 | 41990.554 | 42106.898 | 39855.811 |
| **PP** | 40151.755 | 37191.234 | 44717.904 | 45230.321 | 42880.345 | 49569.519 |
| **TPU** | 85329.345 | 83796.367 | 83927.385 | 82808.937 | 76611.782 | 16216.425 |

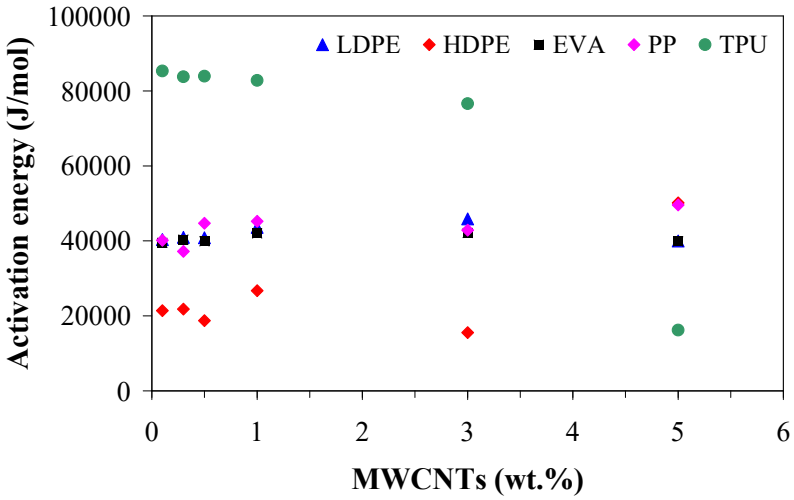


**Figure 7.6.** *The activation energy of polymer/MWCNT nanocomposites as a function of MWCNT loading and polymer matrix*

### 7.4.3. Effect of MWCNTs on the specific volume and density at zero pressure

The specific volume at the zero pressure, $V_0(T)$, represented in Figure 7.7, was obtained by extrapolating the $pVT$ data using the 2-domain Tait model. It can be seen that, for the nanocomposites with the LDPE (Figure 7.7.a), HDPE (Figure 7.7.b), and PP (Figure 7.7.d) matrix, the specific volume is nearly constant with increasing nanotube loading up to 1 wt.%, where a further increase of MWCNT loading results in a decrease in the specific volume. However, the specific volume of the EVA/MWCNT nanocomposites (Figure 7.7.c) has similar values only at the low MWCNT loadings (0.1, 0.3, and 0.5 wt.%) with a decreasing trend with increasing the MWCNT loading. Regarding the TPU/MWCNT nanocomposites (Figure 7.7.e), the specific volume at 1 wt.% do not follow the normal tendency. The reduction of the specific volume with the addition of MWCNTs can be explained by the nanotubes that do not expand or contract as the temperature changes and that counteract shrinkage effects due to molecular orientation.

The specific density, $\rho_{sp}$, was determined from the inverse relationship that exists between the volume and density. Table 7.4 clearly shows the effect of MWCNT on the specific density, which increases with MWCNT loading, regardless of temperature. With increasing temperature, the specific density decreases due to the expansion in volume of the polymer melt without an increase in weight.

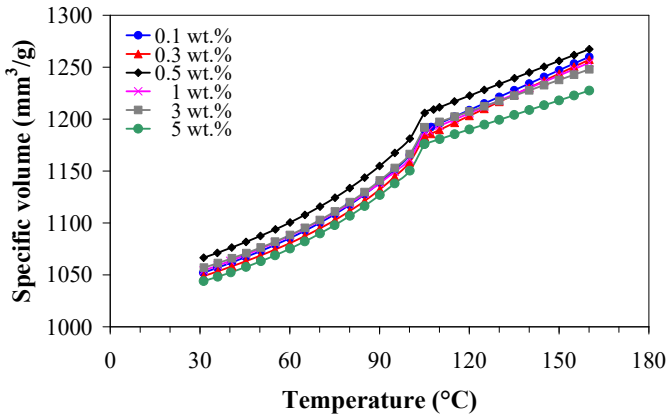


*a) LDPE/MWCNT nanocomposites*

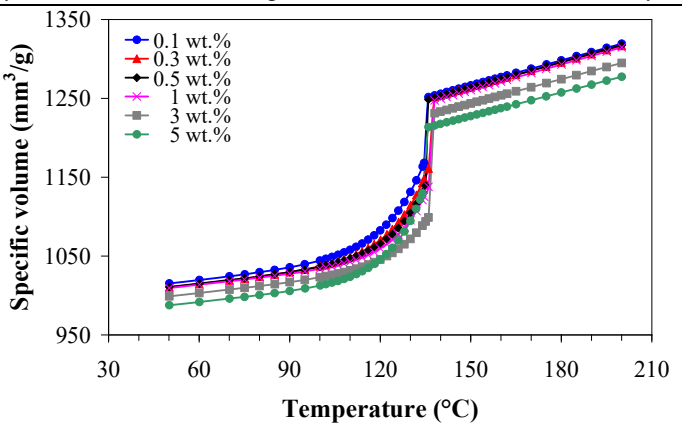


*b) HDPE/MWCNT nanocomposites*

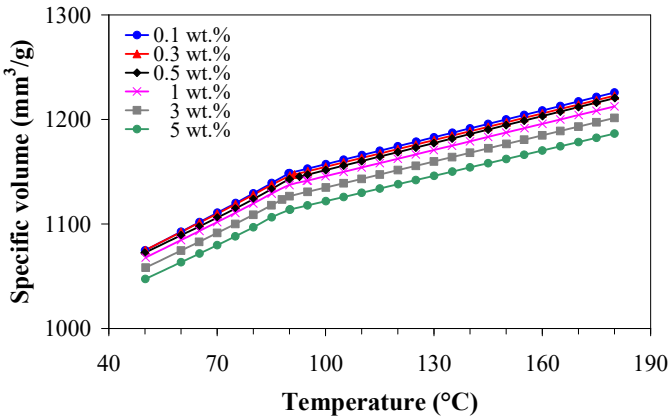


*c) EVA/MWCNT nanocomposites*

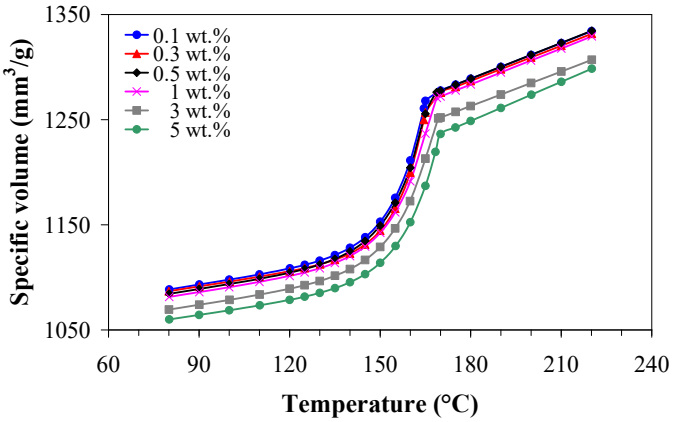


*d) PP/MWCNT nanocomposites*

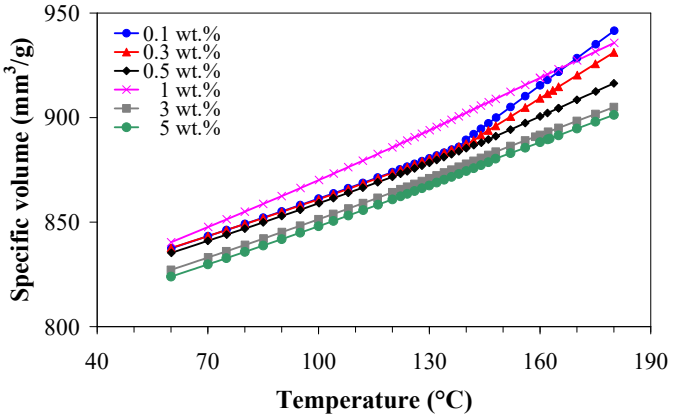


*e) TPU/MWCNT nanocomposites*

**Figure 7.7.** *The specific volume at the zero pressure as a function of temperature and MWCNT loading*

**Table 7.4.** *Specific density of polymer/MWCNT nanocomposites at zero pressure*

| Polymer matrix | Temperature (°C) | MWCNTs (wt.%) | | | | | |
|---|---|---|---|---|---|---|---|
| | | **0.1** | **0.3** | **0.5** | **1** | **3** | **5** |
| **LDPE** | 30 | 0.951 | 0.953 | 0.938 | 0.949 | 0.946 | 0.958 |
| | 160 | 0.794 | 0.795 | 0.789 | 0.797 | 0.801 | 0.815 |
| **HDPE** | 50 | 0.985 | 0.990 | 0.989 | 0.991 | 1.001 | 1.013 |
| | 200 | 0.758 | 0.760 | 0.759 | 0.761 | 0.772 | 0.783 |
| **EVA** | 50 | 0.930 | 0.930 | 0.933 | 0.936 | 0.945 | 0.955 |
| | 180 | 0.816 | 0.818 | 0.819 | 0.825 | 0.832 | 0.843 |
| **PP** | 80 | 0.919 | 0.920 | 0.922 | 0.925 | 0.935 | 0.943 |
| | 220 | 0.750 | 0.751 | 0.749 | 0.752 | 0.765 | 0.770 |
| **TPU** | 60 | 1.194 | 1.194 | 1.197 | 1.190 | 1.209 | 1.214 |
| | 180 | 1.062 | 1.074 | 1.091 | 1.069 | 1.105 | 1.109 |

Figure 7.8 represents the specific density for the polymer/MWCNT nanocomposites and clearly shows that the addition of MWCNT influenced the specific densities. A linear relationship can be used to show the effect of MWCNT loading on the specific density, such as $\rho_{sp}^{LDPE} = 0.008 \cdot wt.\% + 0.955$, $\rho_{sp}^{HDPE} = 0.005 \cdot wt.\% + 0.997$, $\rho_{sp}^{EVA} = 0.005 \cdot wt.\% + 0.969$, $\rho_{sp}^{PP} = 0.005 \cdot wt.\% + 0.941$, and $\rho_{sp}^{TPU} = 0.005 \cdot wt.\% + 1.224$ for the nanocomposites with the LDPE, HDPE, EVA, PP, and TPU matrix, respectively.

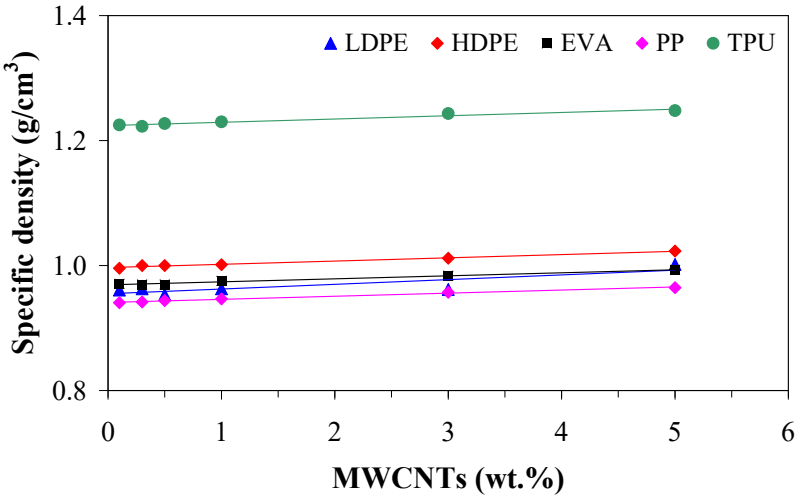


**Figure 7.8.** *The specific density at zero pressure of polymer/MWCNT nanocomposites as a function of MWCNT loading and polymer matrix*

### 7.4.4. Effect of MWCNTs on the *pVT* transition temperature

At zero pressure, the *pVT* transition temperature from equation (7.12) is equal to the $b_5$ parameter. Table 7.5 and Figure 7.9 show the transition temperatures as a function of polymer matrix and MWCNTs. No significant effect of the MWCNTs addition on the transition temperature of the nanocomposites with the LDPE, HDPE matrix was observed. Therefore, the $T_t$ of the polymer/MWCNT nanocomposites can be approximated by the average values of 102.421±0.417, 135.734±0.739, and 87.731±1.095 °C for the LDPE, HDPE, and EVA matrix, respectively. However, the effect of the MWCNTs addition was significant for the nanocomposites with the PP and TPU matrix and the following linear relationships can be drawn: $T_t^{PP} = 0.493 \cdot wt.\% + 166.22$ and $T_t^{TPU} = 1.223 \cdot wt.\% + 142.08$.

**Table 7.5.** *pVT transition temperature of polymer/MWCNT nanocomposites at zero pressure*

| **Polymer matrix** | **MWCNTs** (wt.%) | | | | | |
|---|---|---|---|---|---|---|
| | **0.1** | **0.3** | **0.5** | **1** | **3** | **5** |
| **LDPE** | 102.510 | 101.545 | 102.403 | 102.510 | 102.832 | 102.725 |
| **HDPE** | 135.218 | 136.025 | 135.756 | 136.564 | 136.429 | 134.411 |
| **EVA** | 87.205 | 87.475 | 87.385 | 88.648 | 89.550 | 86.123 |
| **PP** | 139.755 | 142.560 | 143.220 | 145.200 | 146.520 | 147.345 |
| **TPU** | 165.964 | 166.129 | 166.293 | 167.445 | 167.938 | 168.431 |

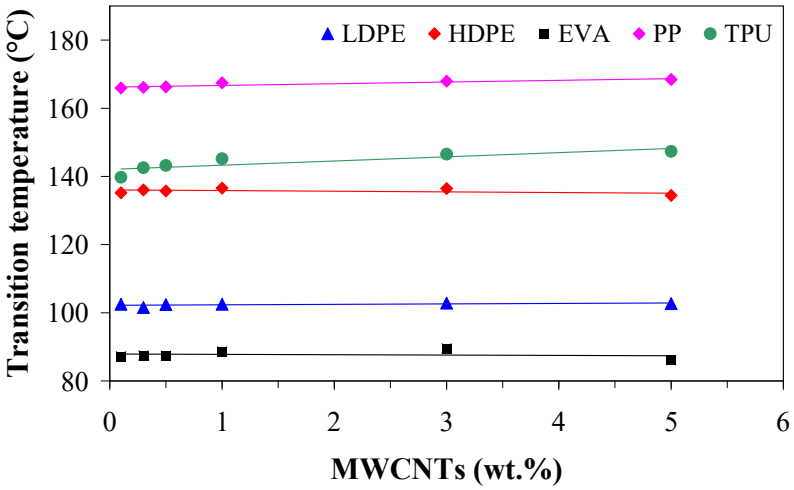


**Figure 7.9.** *The pVT transition temperature of polymer/MWCNT nanocomposites as a function of MWCNT loading and polymer matrix*

# 8. CONCLUDING REMARKS, PERSONAL CONTRIBUTIONS AND FUTURE RESEARCH DIRECTIONS

This research aimed to determine the material properties of polymer/MWCNTs nanocomposites as analytical models that can be used in processing simulation of the injection molding process and material properties prediction. The effect of MWCNTs on the rheological behavior, specific volume and thermal conductivity of polymer/MWCNT nanocomposites was also investigated. As reported in the previous chapters and sub-chapters, the objectives of this thesis have been achieved. The structure in Figure 8.1 shows the main tasks performed during the whole thesis work procedures.

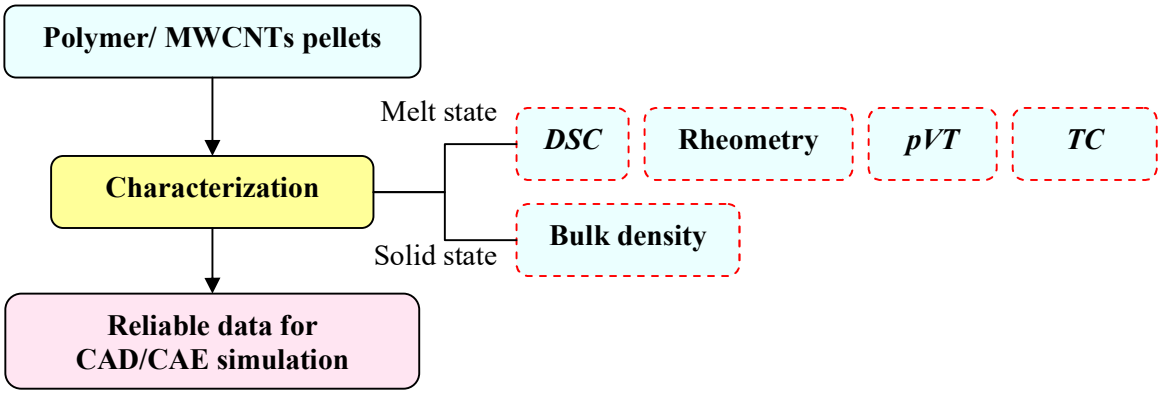


**Figure 8.1.** *Summary of the measurements performed*

In **Chapter one**, the state-of-the-art was presented for better understanding the three types of measurements for determining the physical properties: viscosity, specific volume and thermal conductivity. The rheological behavior of the polymer/carbon nanotube nanocomposites was reviewed to asses the influence of CNTs, temperature and shear rate on the viscosity. Mainly, the rheological properties were characterized using rotational viscometers, which are restricted in their use only to low shear rates for unidirectional shear and low-frequency oscillations during oscillatory shear. The second review presents the available articles that studied the influence of pressure and temperature on the specific volume. Lastly, the third part of the state-of-the-art shows the various types of methods to determine the thermal conductivity of conductive materials, such as polymer/MWCNT nanocomposites.

The nanocomposites analyzed in this thesis (**Chapter two**) are thermoplastics, such as low-density polyethylene (LDPE), high-density polyethylene (HDPE), ethylene vinyl acetate (EVA), polypropylene (PP) and thermoplastic polyurethane (TPU) filled with 0.1, 0.3, 0.5, 1, 3, and 5 wt.% of MWCNTs. The five types of measurements performed on the polymer/MWCNT nanocomposites were *DSC*, bulk density, capillary rheometry, specific volume and thermal conductivity.

**Chapter three** presents the thermal properties of the polymer/MWCNT nanocomposites analyzed. The addition of carbon nanotubes influenced the crystallization behavior of semi-crystalline polymers since they act as nucleating agents. The crystal growth, a stage of the crystallization process, can be accelerated by the CNTs presence as a result of the heterogeneous nucleation process. Also, the CNT networks can restrict the diffusion of polymer chains, which slows the crystallization rate and/or block the crystal growth by forming an external barrier (i.e., the barrier effect of CNTs).

The rheological behavior of the polymer/MWCNT nanocomposites analyzed is presented and discussed in **Chapter four**. Several findings were discussed in this chapter. First, the shear stress clearly increased with increasing shear rate, showing the shear rate dependency for all polymer/MWCNT

nanocomposites. The nanocomposites exhibited non-Newtonian behavior at low shear rates, while, at higher shear rates, the Newtonian behavior was present since the rigid MWCNT bundles in the polymer matrix tend to orient under shear force, thus disturbing the formation of the polymer chain entanglements. Second, the temperature dependence of the melt shear viscosity of the polymer/MWCNT nanocomposite was governed by the Arrhenius law, where the activation energy decreases with increasing shear rate and with increasing MWCNT loading from 0.1 to 5 wt.%. Lastly, the sensibility of the shear viscosity on the nanotube loading was found to be weakened by increasing apparent shear rate and temperature.

The *pVT* diagrams in **Chapter five** showed that the specific volume of all polymer/MWCNT nanocomposites was found to decrease with increasing MWCNT loading and pressure, while it increased with increasing temperature. The reduction of the specific volume with the addition of MWCNTs can be explained by the nanotubes that do not expand or contract as the temperature changes and that counteract shrinkage effects due to molecular orientation.

The experimental data in **Chapter six** showed that the thermal conductivity increased with increasing pressure, especially in the melt state, due to the fact that the pressure significantly reduces the inter-tube distance, therefore reducing the contact between adjacent nanotubes, enhancing the photon transport. In the melt state, the effect of pressure on the thermal conductivity was more significant than in the solid state due to the MWCNTs are able to move and align, which allows phonon transport. A moderate enhancement (24–46%) in the thermal conductivity of the polymer/MWCNT nanocomposites was found with increasing MWCNT loading from 0.1 to 5 wt.%, although MWCNTs can exhibit thermal conductivity as high as 3000 W/m·K. The increase in thermal conductivity with increasing MWCNT loading was mostly due to the fact that a denser nanotube network is formed, which allows phonon transport.

**Chapter seven** presents the analytical modeling of material properties of the polymer-CNT based composites, i.e., the rheological and specific volume behavior using the Cross–WLF and 2-domain Tait models, respectively, in order to perform numerical simulations of the injection molding process. First, based on the corrected melt shear viscosity, the master curves were constructed by employing the *TTS* principle and the shift factors required for the numerical simulation were determined. The shear-thinning index indicated that the polymer/MWCNT nanocomposites are suitable for injection molding and the nanotubes are in a state of good dispersion and aligned in the flow direction. No trend was found between the MWCNT loading and shear-thinning index. Second, the specific volume at the zero pressure was obtained by extrapolating the *pVT* data using the Tait model. The specific volume was nearly constant with increasing nanotube loading up to 1 wt.%, where a further increase of MWCNT loading resulted in a decrease in the specific volume.

**Personal contributions**. Over the doctoral research and development period, the main personal contributions presented below were made.

- The state-of-the-art on the rheological behavior and thermal conductivity of the polymer/CNT nanocomposites and the specific volume of polymer-based composites;
- The experimental characterization (bulk density, rheometry, *pVT* diagrams, thermal conductivity) of thermoplastics such as LDPE, HDPE, EVA, PP and TPU filled with 0.1 – 5 wt.% of MWCNTs was perfomed;
- The effect of MWCNT loading on the rheological behavior, specific volume and thermal conductivity of the polymer-based CNT composites was assessed;
- The effect of shear rate and temperature on the rheological behavior of the polymer-based CNT composites was assessed;
- The effect of pressure and temperature on the specific volume and thermal conductivity of the polymer-based CNT composites was assessed;

- Based on the experimental measurements, the analytical models of the rheological behavior (Cross-WLF), *pVT* (Tait model) and *TC* of the polymer-based CNT composites were determined.

The **future research directions** are related to the limitations of the current thesis.

- The characterization of other types of polymer-based composites. This thesis presents only the thermal, rheological, *pVT*, and *TC* behaviors of only 5 polymers filled with 0.1–5 wt.% of MWCNTs;
- The rheological behavior of the polymer/CNT nanocomposites at lower shear rates (<100 $s^{-1}$), which could be performed only using a rotational viscometer;
- The influence of the cooling rate on the *DSC* and *pVT* diagrams of the polymer/CNT nanocomposites;
- The numerical simulation of manufacturing processes using polymer/CNT nanocomposites, which require the physical, thermal, and mechanical properties.

# REFERENCES

[1] Shenoy, A.V. (1999). „Rheology of filled polymer systems". *Springer Science+Business Media*, ISBN 9789401592130;

[2] Zhao, J., Wu, L., Zhan, C., Shao, Q., Guo, Z., Zhang, L. (2017). „Overview of polymer nanocomposites: Computer simulation understanding of physical properties". *Polymer*, **133**, 272–287;

[3] Paul, D.R., Robeson, L.M. (2008). „Polymer nanotechnology: Nanocomposites". *Polymer*, **49**, 3187–3204;

[4] Young, R.J., Eichhorn, S.J. (2007). „Deformation mechanisms in polymer fibres and nanocomposites". *Polymer*, **48**, 2–18;

[5] Sahraeian, R., Esfandeh, M., Hashemi, S.A. (2013). „Rheological, thermal and dynamic mechanical studies of the LDPE/perlite nanocomposites". *Polymers & Polymer Composites*, **21**(4), 243–249;

[6] Weon, J.I., Sue, H.J. (2005). „Effects of clay orientation and aspect ratio on mechanical behavior of nylon-6 nanocomposite". *Polymer*, **46**, 6325–6334;

[7] Coleman, J.N., Khan, U., Gun'ko, Y.K. (2006). „Mechanical reinforcement of polymers using carbon nanotubes". *Advanced Materials*, **18**, 689–706;

[8] Coleman, J.N., Khan, U., Blau, W.J., Gun'ko, Y.K. (2006). „Small but strong: A review of the mechanical properties of carbon nanotube–polymer composites". *Carbon*, **44**, 1624–1652;

[9] Fernandez, M., Landa, M., Munoz, M.E., Santamaria, A. (2011). „Electrical conductivity of PUR/MWCNT nanocomposites in the molten state, during crystallization and in the solid state". *European Polymer Journal*, **47**, 2078–2086;

[10] Grossiord, N., Kivit, P.J.J., Loos, J., Meuldijk, J., Kyrylyuk, A.V., van der Schoot, P., Koning, C.E. (2008). „On the influence of the processing conditions on the performance of electrically conductive carbon nanotube/polymer nanocomposites". *Polymer*, **49**, 2866–2872;

[11] Liang, G.D., Tjong, S.C. (2006). „Electrical properties of low-density polyethylene/ multiwalled carbon nanotube nanocomposites". *Materials Chemistry and Physics*, **100**, 132–137;

[12] Sharma, A., Vijay, Y.K. (2012). „Effect of electric field variation in alignment of SWNT/PC nanocomposites". *International Journal of Hydrogen Energy*, **37**, 3945–3948;

[13] Huang, S., Wang, M., Liu, T., Zhang, W.D., Tjiu, W.C., He, C., Lu, X. (2009). „Morphology, thermal, and rheological behavior of nylon 11/multi-walled carbon nanotube nanocomposites prepared by melt compounding". *Polymer Engineering and Science*, **49**, 1063–1068;

[14] Babaahmadi, M., Sabzi, M., Mahdavinia, G.R., Keramati, M. (2017). „Preparation of amorphous nanocomposites with quick heat triggered shape memory behavior". *Polymer*, **112**, 26–34;

[15] Han, Z., Fina, A. (2011). „Thermal conductivity of carbon nanotubes and their polymer nanocomposites: A review". *Progress in Polymer Science*, **36**, 914–944;

[16] Kumar, S., Sarita, Nehra, M., Dilbaghi, N., Tankeshwar, Kim, K.H. (2018). „Recent advances and remaining challenges for polymeric nanocomposites in healthcare applications". *Progress in Polymer Science*, 80, 1–38;

[17] Thakur, V.K., Kessler, M.R. (2015). „Self-healing nanocomposites materials: A review". *Polymer*, **69**, 369–383;

[18] Iijima, S. (1991). „Helical microtubules of graphitic carbon". *Nature*, **354**, 56–58;

[19] Harris, P.J.F. (2001). „Carbon nanotubes and related structures: new materials for the twenty-first century". *Cambridge University Press*, ISBN 9780521005333;

[20] Lee, S.H., Cho, E., Jeon, S.H., Youn, J.R. (2007). „Rheological and electrical properties of polypropylene composites containing functionalized multi-walled carbon nanotubes and compatibilizers". *Carbon*, **45**, 2810–2822;

[21] Abdalla, M., Dean, D., Robinson, P., Nyairo, E. (2008). „Cure behavior of epoxy/ MWCNT nanocomposites: The effect of nanotube surface modification". *Polymer*, **49**, 3310–3317;

[22] Hong, J., Park, D.W., Shim, S.E. (2012). „Electrical, thermal, and rheological properties of carbon black and carbon nanotube dual filler-incorporated poly(dimethylsiloxane) nanocomposites". *Macromolecular Research*, **20**, 465–472;

[23] Arrigo, R., Malucelli, G. (2020). „Rheological behavior of polymer/carbon nanotube composites: An overview". *Materials*, **13**, 2771;

[24] Chaurasia, A., Suzhu, Y., Henry, C.K.F., Mogal, V.T., Saha, S. (2015). „Properties and applications of polymer nanocomposite". In *Handbook of manufacturing engineering and technology*; Nee, A., Ed.; *Springer*, ISBN 9781447146711;

[25] Murat, A., Aysegul, A.E., Bulent, E. (2017). „Carbon nanotube-based nanocomposites and their applications". *Journal of Adhesion Science and Technology*, **31**, 1977–1997;

[26] Rajan, K.P. (2016). „Studies on nanocomposites of polypropylene and polylactic acid blends reinforced with halloysite nanotubes". Thesis, *Vignan's Foundation For Science*, Technology and Research, India;

[27] Penu, C., Hu, G.H., Fernandez, A., Marchal, P., Choplin, L. (2012). „Rheological and electrical percolation thresholds of carbon nanotube/polymer nanocomposites". *Polymer Engineering and Science*, **52**, 2173–2181;

[28] Sharma, R., Maiti, S.N. (2015). „Melt rheological properties of PBT/SEBS and reactively compatibilized PBT/SEBS/SEBS-g-MA polymer blends". *Journal of Applied Polymer Science*, **132**(5), 41402;

[29] Fernandez, M., Munoz, M.E., Santamaria, A., Syrjala, S., Aho, J. (2009). „Determining the pressure dependency of the viscosity using PVT data: A practical alternative for thermoplastics". *Polymer Testing*, **28**, 109–113;

[30] Aho, J. (2011). „Rheological characterization of polymer melts in shear and extension: Measurement reliability and data for practical processing". Thesis, *University of Technology*;

[31] Chang, R.Y., Chen, C.H., Su, K.S. (1996). „Modifying the Tait equation with cooling-rate effects to predict the pressure-volume-temperature behaviors of amorphous polymers: Modeling and experiments". *Polymer Engineering and Science*, **36**(13), 1789–1795;

[32] Wang, J. (2012). „Some critical issues for injection molding". *InTech*, ISBN 9789535102977;

[33] Hess, M. (2004). „The use of pressure-volume-temperature measurements in polymer science". *Macromolecular Symposia*, **241**, 361–379;

[34] Thermal Conductivity Measurement – Operating Manual, Gottfert, Germany;

[35] Zhai, S., Zhang, P., Xian, Y., Zeng, J., Shi, B. (2018). „Effective thermal conductivity of polymer composites: Theoretical models and simulation models". *International Journal of Heat and Mass Transfer*, **117**, 358–374;

[36] Chen, H., Ginzburg, V.V., Yang, J., Yang, Y., Liu, W., Huang, Y., Du, L., Chen, B. (2016). „Thermal conductivity of polymer-based composites: Fundamentals and applications". *Progress in Polymer Science*, **59**, 41–85;

[37] Burger, N., Laachachi, A., Ferriol, M., Lutz, M., Toniazzo, V., Ruch, D. (2016). „Review of thermal conductivity in composites: Mechanisms, parameters and theory". *Progress in Polymer Science*, **61**, 1–28;

[38] Hussain, A.R.J., Alahyari, A.A., Eastman, S.A., Thibaud-Erkey, C., Johnston, S., Sobkowicz, M.J. (2017). „Review of polymers for heat exchanger applications: Factors concerning thermal conductivity". *Applied Thermal Engineering*, **113**, 1118–1127;

[39] Moldflow Plastics Insight® Manual, Flow Training Theory and Concepts, Release 6.0, March 2006, Moldflow Corporation;

[40] Gupta, R.K. (2000). „Polymer and composite rheology". 2nd edition, revised and expanded, *Marcel Dekker* Inc., New York; ISBN 9780367398484;

[41] Kutz, M. (2002). „Handbook of materials selection". *John Wiley & Sons* Inc., ISBN 9780471359241;

[42] College Physics for AP Courses, (2015). *OpenStax, Rice University*, https://openstax.org/details/books/college-physics-ap-courses;

[43] Mezger, T.G. (2014). „The rheology handbook". 4th edition, *Vincentz Network*, ISBN 9783866308428;

[44] Deshpande, A.P., Krishnan, J.M., Kumar, P.B.S. (2010). „Rheology of complex fluids". *Springer Science+Business Media*, ISBN 9781441964946;

[45] Morrison, F.A. (2001). „Understanding rheology". *Oxford University Press*, ISBN 9780195141665;

[46] https://www.ptonline.com/articles/a-new-look-at-evaluating-fill-times-for-injection-molding

[47] Lakkanna, M., Mohan Kumar, G.C., Kadoli, R. (2016). „Computational design of mould sprue for injection moulding thermoplastics". *Journal of Computational Design and Engineering*, **3**(1), 37–52;

[48] Rheograph 75 Operating manual, Gottfert, Germany;

[49] Lima, P., Magalhaes da Silva, S P., Oliveira, J., Costa, V. (2015). „Rheological properties of ground tyre rubber based thermoplastic elastomeric blends". *Polymer Testing*, **45**, 58–67;

[50] Mitsoulis, E., Hatzikiriakos, S.G., Christodoulou, K., Vlassopoulos, D. (1998). „Sensitivity analysis of the Bagley correction to shear and extensional rheology". *Rheologica Acta*, **37**, 438–448;

[51] Osswald, T.A., Rudolph, N. (2014). „Polymer rheology. Fundamentals and applications". *Hanser Publishers*, ISBN: 9781569905173;

[52] Dealy, J.M., Wissbrun, K.F. (1990). „Melt rheology and its role in plastics processing". *Van Nostrand Reinhold*, ISBN 9789400921634;

[53] Zonder, L., Ophir, A., Kenig, S., McCarthy, S. (2011). „The effect of carbon nanotubes on the rheology and electrical resistivity of polyamide 12/high density polyethylene blends". *Polymer*, **52**, 5085–5091;

[54] Bai, J., Goodridge, R.D., Hague, R.J.M., Song, M., Okamoto, M. (2014). „Influence of carbon nanotubes on the rheology and dynamic mechanical properties of polyamide-12 for laser sintering". *Polymer Testing*, **36**, 95–100;

[55] Versavaud, S., Regnier, G., Gouadec, G., Vincent, M. (2014). „Influence of injection molding on the electrical properties of polyamide 12 filled with multi-walled carbon nanotubes". *Polymer*, **55**, 6811–6818;

[56] Wang, M., Wang, W., Liu, T., Zhang, W.D. (2008). „Melt rheological properties of nylon 6/multi-walled carbon nanotube composites". *Composites Science and Technology*, **68**, 2498–2502;

[57] Latko-Durałek, P., Kozera, R., Boczkowska, A. (2017). „Effect of functionalized carbon nanotubes on properties of hot melt copolyamide". *Composites theory and practice*, **17**(4), 226–231;

[58] Sung, Y.T., Han, M.S., Song, K.H., Jung, J.W., Lee, H.S., Kum, C.K., Joo, J., Kim, W.N. (2006). „Rheological and electrical properties of polycarbonate/multi-walled carbon nanotube composites". *Polymer*, **47**, 4434–4439;

[59] Kim, J., Son, Y. (2016). „Effects of matrix viscosity, mixing method and annealing on the electrical conductivity of injection molded polycarbonate/MWCNT nanocomposites". *Polymer*, **88**, 29–35;

[60] McNally, T., Potschke, P., Halley, P., Murphy, M., Martin, D., Bell, S.E.J., Brennan, G.P., Bein, D., Lemoine, P., Quinn, J.P. (2005). „Polyethylene multiwalled carbon nanotube composites". *Polymer*, **46**, 8222–8232;

[61] Zhang, Q., Lippits, D.R., Vaidya, S.N., Rastogi, S. (2006). „Dispersion and rheological aspects of SWNTs in ultra high molecular weight polyethylene". *NSTI Nanotech*, **1**;

[62] Xiao, K.Q., Zhang, L.C., Zarudi, I. (2007). „Mechanical and rheological properties of carbon nanotube-reinforced polyethylene composites". *Composites Science and Technology*, **67**, 177–182;

[63] Aalaie, J., Rahmatpour, A., Maghami, S. (2007). „Preparation and characterization of linear low density polyethylene/carbon nanotube nanocomposites". *Journal of Macromolecular Science B Physics*, **46**(5), 877–889;

[64] Valentino, O., Sarno, M., Rainone, N.G., Nobile, M.R., Ciambelli, P., Neitzert, H.C., Simon, G.P. (2008). „Influence of the polymer structure and nanotube concentration on the conductivity and rheological properties of polyethylene/CNT composites". *Physica E*, **40**, 2440–2445;

[65] Thomas, S.P., Rahaman, M., Hussein, I.A. (2014). „Impact of aspect ratio and CNT loading on the dynamic mechanical and flammability properties of polyethylene nanocomposites". *e-Polymers*, **14**, 57–63;

[66] Sabet, M., Soleimani, H., Mohammadian, E. (2019). „Effect of graphene and carbon nanotube on low-density polyethylene nanocomposites". *Journal of Vinyl and Additive Technology*, **25**, 35–40;

[67] Vega, J.F., Martinez-Salazar, J. (2009). „Rheology, processing, tensile properties, and crystallization of polyethylene/ carbon nanotube nanocomposites". *Macromolecules*, **42**, 4719–4727;

[68] Han, M.S., Lee, Y.K., Lee, H.S., Yun, C.H., Kim, W.N. (2009). „Electrical, morphological and rheological properties of carbon nanotube composites with polyethylene and poly(phenylene sulfide) by melt mixing". *Chemical Engineering Science*, **64**, 4649–4656;

[69] Palza, H., Reznik, B., Kappes, M., Hennrich, F., Naue, I.F.C., Wilhelm, M. (2010). „Characterization of melt flow instabilities in polyethylene/carbon nanotubes composites". *Polymer*, **51**, 3753–3761;

[70] Bangarusampath, D.S., Ruckdaschel, H., Altstadt, V., Sandler, J.K.W., Garray, D., Shaffer, M.S.P. (2009). „Rheology and properties of melt-processed poly(ether ether ketone)/multi-wall carbon nanotube composites". *Polymer*, **50**, 5803–5811;

[71] Isayev, A.I., Kumar, R., Lewis, T.M. (2009). „Ultrasound assisted twin screw extrusion of polymer–nanocomposites containing carbon nanotubes". *Polymer*, **50**, 250–260;

[72] Hu, G., Zhao, C., Zhang, S., Yang, M., Wang, Z. (2006). „Low percolation thresholds of electrical conductivity and rheology in poly(ethylene terephthalate) through the networks of multi-walled carbon nanotubes". *Polymer*, **47**, 480–488;

[73] McClory, C., McNally, T., Baxendale, M., Potschke, P., Blau, W., Ruether, M. (2010). „Electrical and rheological percolation of PMMA/MWCNT nanocomposites as a function of CNT geometry and functionality". *European Polymer Journal*, **46**, 854–868;

[74] Seo, M.K., Park, S.J. (2004). „Electrical resistivity and rheological behaviors of carbon nanotubes-filled polypropylene composites". *Chemical Physics Letters*, **395**, 44–48;

[75] Lee, S.H., Kim, M.W., Kim, S.H., Youn, J.R. (2008). „Rheological and electrical properties of polypropylene/MWCNT composites prepared with MWCNT masterbatch chips". *European Polymer Journal*, **44**, 1620–1630;

[76] Xu, D., Wang, Z. (2008). „Role of multi-wall carbon nanotube network in composites to crystallization of isotactic polypropylene matrix". *Polymer*, **49**, 330–338;

[77] Prashantha, K., Soulestin, J., Lacrampe, M.F., Krawczak, P., Dupin, G., Claes, M. (2009). „Masterbatch-based multi-walled carbon nanotube filled polypropylene: Assessment of rheological and mechanical properties". *Composites Science and Technology*, **69**, 1756–1763;

[78] Thiebaud, F., Gelin, J.C. (2010). „Characterization of rheological behaviors of polypropylene/carbon nanotubes composites and modeling their flow in a twin-screw mixer". *Composites Science and Technology*, **70**, 647–656;

[79] Huegun, A., Fernandez, M., Munoz, M.E., Santamaría, A. (2012). „Rheological properties and electrical conductivity of irradiated MWCNT/PP nanocomposites". *Composites Science and Technology*, **72**, 1602–1607;

[80] Steinmann, W., Vad, T., Weise, B., Wulfhorst, J., Seide, G., Gries, T., Heidelmann, M., Weirich, T. (2013). „Extrusion of CNT-modified polymers with low viscosity – influence of crystallization and CNT orientation on the electrical properties". *Polymers & Polymer Composites*, **21**(8), 473–482;

[81] Narimani, A., Hemmati, M. (2014). „Electrical and steady shear rheological behaviour of polypropylene composites reinforced with single-walled carbon nanotubes". *Polymer & Polymer Composites*, **22**(6), 533–540;

[82] Liang, J.Z., Chen, C.Y., Zou, S.Y., Tsui, C.P., Tang, C.Y., Zhang, S.D. (2015). „Melt flow behavior of polypropylene composites filled with multi-walled carbon nanotubes during extrusion". *Polymer Testing*, **45**, 41–46;

[83] Verma, P., Verma, M., Gupta, A., Chauhan, S.S., Malik, R.S., Choudhary, V. (2016). „Multi walled carbon nanotubes induced viscoelastic response of polypropylene copolymer nanocomposites: Effect of filler loading on rheological percolation". *Polymer Testing*, **55**, 1–9;

[84] Yetgin, S.H. (2019). „Effect of multi walled carbon nanotube on mechanical, thermal and rheological properties of polypropylene". *Journal of Materials Research and Technology*, **8**(5), 4725–4735;

[85] Park, J.U., Cho, S., Cho, K.S., Ahn, K.H., Lee, S.J., Lee, S.J. (2005). „Effective in-situ preparation and characteristics of polystyrene-grafted carbon nanotube composites". *Korea-Australia Rheology Journal*, **17**(2), 41–45;

[86] Park, S.D., Han, D., Teng, D., Kwon, Y. (2008). „Rheological properties and dispersion of multi-walled carbon nanotube (MWCNT) in polystyrene matrix". *Current Applied Physics*, **8**, 482–485;

[87] Gracia-Fernandez, C., Gomez-Barreiro, S., Lopez-Beceiro, J., Naya, S., Artiaga, R. (2014). „Characterization of MWCNT/TPU systems by large amplitude oscillation shear". *Journal of Thermal Analysis and Calorimetry*, **115**, 1727–1731;

[88] Hassanabadi, H.M., Wilhelm, M., Rodrigue, D. (2014). „A rheological criterion to determine the percolation threshold in polymer nano-composites". *Rheologica Acta*, **53**, 869–882;

[89] Zuidema, H., Peters, G.W.M., Meijer, H.E.H. (2001). „Influence of cooling rate on pVT-data of semi-crystalline polymers". *Journal of Applied Polymer Science*, **82**(5), 1170–1186;

[90] Osswald, T., Hernandez-Ortiz, J.P. (2006). „Polymer processing. Modeling and Simulation". *Hanser Publishers*, Munich;

[91] Oehmke, F., Wiegmann, T. (1992). „pvT Behavior of Polymers-Measurement Technique, Recent Results". In *Theoretical and applied rheology*; Moldenaers, P., Keunings, R., Eds.; *Elsevier Science Publishers B.V.*, ISBN 9780444890078;

[92] Wang, J., Hopmann, C., Schmitz, M., Hohlweck, T., Wipperfurth, J. (2019). „Modeling of pvT behavior of semi-crystalline polymer based on the two-domain Tait equation of state for injection molding". *Materials & Design*, **183**, 108149;

[93] Park, H.P., Cha, B.S., Park, S.B., Choi, J.H., Kim, D.H., Rhee, B.O., Lee, K.H. (2014). „A study on the void formation in residual wall thickness of fluid-assisted injection molding parts". *Advances in Materials Science and Engineering*, **2014**, 1–6;

[94] Zoller, P. (1979). „Pressure-volume-temperature relationship of solid and molten polypropylene and poly(butene-1)". *Journal of Applied Polymer Science*, **23**, 1057–1061;

[95] Sato, Y., Yamasaki, Y., Takishima, S., Masuoka, H. (1997). „Precise measurement of the PVT of polypropylene and polycarbonate up to 330 °C and 200 MPa". *Journal of Applied Polymer Science*, **66**, 141–150;

[96] Schmidt, M., Maurer, F.H.J. (1998). „Pressure–volume–temperature properties and free volume parameters of PEO/PMMA blends". *Journal of Polymer Science. Part B, Polymer physics*, **36**(6), 1061–1080;

[97] Utracki, L.A. (2005). „Pressure–volume–temperature dependencies of polystyrenes". *Polymer*, **46**, 11548–11556;

[98] Utracki, L.A., Sedlacek, T. (2007). „Free volume dependence of polymer viscosity". *Rheologica Acta*, **46**, 479–494;

[99] Utracki, L.A. (2009). „Compressibility and thermal expansion coefficients of nanocomposites with amorphous and crystalline polymer matrix". *European Polymer Journal*, **45**, 1891–1903;

[100] Utracki, L.A. (2010). „PVT of amorphous and crystalline polymers and their nanocomposites". *Polymer Degradation and Stability*, **95**, 411–421;

[101] Greco, A., Maffezzoli, A., Gennaro, R., Rizzo, M. (2012). „Analysis of ageing of amorphous thermoplastic polymers by PVT analysis". *AIP Conference Proceedings*, **1459**, 39–41;

[102] Heidari, B.S., Davachi, S.M., Moghaddam, A.H., Seyfi, J., Hejazi, I., Sahraeian, R., Rashedi, H. (2018). „Optimization simulated injection molding process for ultrahigh molecular weight polyethylene nanocomposite hip liner using response surface methodology and simulation of mechanical behavior". *Journal of the Mechanical Behavior of Biomedical Materials*, **81**, 95–105;

[103] Ebadi-Dehaghani, H., Nazempour, M. (2012). „Thermal conductivity of nanoparticles filled polymers". In *Smart nanoparticles technology*; Hashim, A.A., Ed.; *IntechOpen*, ISBN 9789535105008;

[104] Toberer, E.S., Baranowski, L.L., Dames, C. (2012). „Advances in Thermal Conductivity". *Annual Review of Materials Research*, **42**, 179–209;

[105] Teaching course, „Chapter 16 – Determination of thermal conductivity". *Institute of Chemical Technology*;

[106] Zhao, D., Qian, X., Gu, X., Jajja, A.A., Yang, R. (2016). „Measurement techniques for thermal conductivity and interfacial thermal conductance of bulk and thin film materials". *Journal of Electronic Packaging*, **138**(4), EP-16-1067.

[107] Kumanek, B., Janas, D. (2019). „Thermal conductivity of carbon nanotube networks: A review". *J. Materi. Sci*., **54**, 7397–7427;

[108] Kashiwagi, T., Grulke, E., Hilding, J., Groth, K., Harris, R., Butler, K., Shields, J., Kharchenko, S., Douglas, J. (2004). „Thermal and flammability properties of polypropylene/carbon nanotube nanocomposites". *Polymer*, **45**, 4227–4239;

[109] Haggenmueller, R., Guthy, C., Lukes, J.R., Fischer, J.E., Winey, K.I. (2007). „Single wall carbon nanotube/ polyethylene nanocomposites: Thermal and electrical conductivity". *Macromolecules*, **40**, 2417–2421;

[110] Kalakonda, P., Cabrera, Y., Judith, R., Georgiev, G.Y., Cebe, P., Iannacchione, G.S. (2015). „Studies of electrical and thermal conductivities of sheared multi-walled carbon nanotube with isotactic polypropylene polymer composites". *Nanomaterials and Nanotechnology*, **5**, 2.

[111] Mertens, J., Senthilvelan, S. (2018). „Mechanical and tribological properties of carbon nanotube reinforced polypropylene composites". *Proceedings of the Institution of Mechanical Engineers, Part L: Journal of Materials: Design and Applications*, **232**(8), 669–680;

[112] Ali, A.M., Ahmad, S.H., Tarawneh, M.A. (2016). „Effect of multi walled carbon nanotubes on thermal conductivity of polylactic acid nanocomposites". *Malaysian Journal of Analytical Sciences*, **20**(5), 1084–1089;

[113] Nanocyl Technical Data Sheet: NC7000™, Edited 12th July 2016;

[114] Nanocyl Technical Data Sheet: Plasticyl™ LDPE2001, Edited 26th January 2016;

[115] Nanocyl Technical Data Sheet: Plasticyl ™ HDPE1501, Edited 8th November 2016;

[116] Nanocyl Technical Data Sheet: Plasticyl ™ EVA2001, Edited 26th January 2016;

[117] Nanocyl Technical Data Sheet: Plasticyl ™ PP2001, Edited 8th November 2016;

[118] Nanocyl Technical Data Sheet: Plasticyl ™ TPU1001, Edited 8th November 2016;

[119] Yusupov, K., Zakhidov, A., You, S., Stumpf, S., Martinez, P.M., Ishteev, A., Vomiero, A., Khovaylo, V., Schubert, U. (2018). „Influence of oriented CNT forest on thermoelectric properties of polymer-based materials". *Journal of Alloys and Compounds*, **741**, 392–397;
[120] Prusty R.K., Rathore, D.K., Ray, B.C. (2017). „CNT/polymer interface in polymeric composites and its sensitivity study at different environments". *Advances in Colloid and Interface Science*, **240**, 77–106;
[121] Punetha V.D., Rana, S., Yoo, H.J., Chaurasia, A., McLeskey Jr., J.T., Ramasamy, M.S., Sahoo, N.G., Cho, J.W. (2017). „Functionalization of carbon nanomaterials for advanced polymer nanocomposites: A comparison study between CNT and graphene". *Progress in Polymer Science*, **67**, 1–47;
[122] Wang, S. (2009). „Optimum degree of functionalization for carbon nanotubes". *Current Applied Physics*, **9**, 1146–1150;
[123] Sastri, V.R. (2014). „Commodity thermoplastics: Polyvinyl chloride, polyolefins, and polystyrene". In *Plastics in medical devices*, 2nd edition; Sastri, V.R. Ed.; *William Andrew Publishing*, ISBN 9781455732012;
[124] Sadiku, E.R., Reddy, A.B., Gnanasekarana, D., Oboirien, B., Aderibigbe, B.A., Varaprasad, K., Goddeti, S.M.R. (2016). „Chapter 12 – Nanostructured polymer blends for gas/vapor barrier and dielectric applications". In *Design and applications of nanostructured polymer blends and nanocomposite* systems; Thomas, S., Shanks, R., Chandrasekharakurup, S., Eds.; *Elsevier*, ISBN 9780323394086;
[125] Cooper, T.A. (2013). „Developments in plastic materials and recycling systems for packaging food, beverages and other fast-moving consumer goods". In *Trends in packaging of food, beverages and other fast-moving consumer goods (FMCG)*; Farmer, N. Ed.; *Woodhead Publishing*, ISBN 9780857095039;
[126] Li, D., Zhou, L., Wang, X., He, L., Yang, X. (2019). „Effect of crystallinity of polyethylene with different densities on breakdown strength and conductance property". *Materials (Basel)*, **12**, 1746;
[127] Fellows, P.J. (2017). „Food processing technology. Principles and practice", 4th edition. *Woodhead Publishing*, ISBN 9780081019078;
[128] Paszkiewicz, S., Szymczyk, A., Zubkiewicz, A., Subocz, J., Stanik, R., Szczepaniak, J. (2020). „Enhanced functional properties of low-density polyethylene nanocomposites containing hybrid fillers of multi-walled carbon nanotubes and nano carbon black". *Polymers*, **12**, 1356;
[129] ExxonMobil™ LDPE LD 655 Product Data Sheet;
[130] Bormed™ HE9621-PH Product Data Sheet;
[131] Emblem, A. (2012). „Plastics properties for packaging materials". In *Packaging technology. Fundamentals, materials and processes*; Emblem, A., Emblem, H., Eds.; *Woodhead Publishing*, ISBN 9781845696658;
[132] Izdebska, J. (2016). „Corona treatment". In *Printing on polymers. Fundamentals and applications*; Izdebska, J., Thomas, S., Eds.; Elsevier, ISBN 9780323374682;
[133] McKeen, L.W. (2017). „Polyolefins, polyvinyls, and acrylics". In *Permeability properties of plastics and elastomers*; McKeen, L.W., Ed.; Elsevier, ISBN 9780323508599;
[134] Paul C.W. (2002). „Chapter 15 - Hot melt adhesives". In *Adhesion science and engineering*, Volume 2: Surfaces, chemistry and applications; Dillard, D.A., Pocius, A.V., Chaudhury, M., Eds.; *Elsevier*, ISBN 9780444511409;
[135] EVATANE® 20-20 Product Data Sheet;
[136] Moplen HP400R Product Data Sheet;
[137] Yue, M., Chian, K. S. (1996). „Chapter 29 - Properties and applications of thermoplastic polyurethane blends". In *Advances in engineering fluid mechanics: Multiphase reactor and polymerization system hydrodynamics*; Cheremisinoff, N.P., Ed.; *Elsevier*, ISBN 9780884154976;
[138] Khalifa, M., Anandhan, S., Wuzella, G., Lammer, H., Mahendran, A.R. (2020). „Thermoplastic polyurethane composites reinforced with renewable and sustainable fillers – a review". *Polymer-Plastics Technology and Materials*, **59**, 1751–1769;
[139] Estane® 54610 Product Data Sheet;
[140] Hatakeyama, T., Quinn, F.X. (1999). „Thermal analysis: Fundamentals and applications to polymer science", *New York John Wiley & Sons*, Ltd., U.K.;
[141] DSC 200 F3 Maia Operating manual, Netzsch;
[142] Mohammed, N.A. (2014). „Rheology, processing and properties of polymer nanocomposites based on POSS and Boehmite. A thesis", *Technical University of Berlin*;
[143] Barton, J.M. (2004). „The application of differential scanning calorimetry (DSC) to the study of epoxy resins curing reactions". *Epoxy Resins and Composites*, **72**, 111–154;

[144] Russo, P., Acierno, D., Marletta, G., Destri G.L. (2013). „Tensile properties, thermal and morphological analysis of thermoplastic polyurethane films reinforced with multiwalled carbon nanotubes". *European Polymer Journal*, **49**, 3155–3164;
[145] Mariappan, B., Rajappa, V., Jaisankar, S.N. (2014). „Morphology and electrical conductivity of compatilized thermoplastic polyurethane/single-walled carbon nanotube composites". *Procedia Engineering*, **93**, 59–65;
[146] Jaruga, T. Bociaga, E. (2008). „Crystallinity of parts from multicavity injection mould". *Archives of Materials Science and Engineering*, **30**, 53–56;
[147] Abu-Zahra, N.H., Seth, A. (2002). „In-process density control of extruded foam PVC using wavelet packet analysis of ultrasound waves". *Mechatronics*, 12, 1083–1095;
[148] Operating instructions for the Density Kit, Mettler Toledo, Switzerland;
[149] Operating manual for the Thermal Conductivity Measurement, Gottfert;
[150] Stanciu, N.V., Stan, F., Fetecău, C. (2020). „Experimental investigation of the melt shear viscosity, specific volume and thermal conductivity of low-density polyethylene/multi-walled carbon nanotube composites using capillary flow". *Polymers*, **12**(6), 1230;
[151] Rojas A., Torres, A., Anazco, A., Villegas, C., Galotto, M.J., Guarda, A., Romero, J. (2018). „Effect of pressure and time on scCO2-assisted incorporation of thymol into LDPE-based nanocomposites for active food packaging". *Journal of $CO_2$ Utilization*, **26**, 434–444;
[152] Chen, W., Chu, J., Wu, G., Zhang, Y., Yang, M. (2019). „Rheology control of HDPE/PP binary system forming a multilayer structure: Effects of MWD and shear rate". *Polymer Testing*, **73**, 60–71;
[153] Bao, S.P., Tjong, S.C. (2008). „Mechanical behaviors of polypropylene/carbon nanotube nanocomposites: The effects of loading rate and temperature". *Materials Science and Engineering: A*, **485**, 508–516;
[154] Soitong, T., Pumchusak, J. (2011). „The relationship of crystallization behavior, mechanical properties, and morphology of polypropylene nanocomposite fibers". *Journal of Material Science*, **46**, 1697–1704.
[155] Stanciu, N.V., Stan, F., Sandu, I.L., Fetecău, C., Ţurcanu, A.M. (2021). „Thermal, rheological, mechanical, and electrical properties of polypropylene/multi-walled carbon nanotube nanocomposites". *Polymers*, **13**, 187;
[156] Seo, M.K., Lee, J.-R., Park, S.-J. (2005). „Crystallization kinetics and interfacial behaviors of polypropylene composites reinforced with multi-walled carbon nanotubes". *Materials Science and Engineering: A*, **404**, 79–84.
[157] Aalaie, J., Rahmatpour, A., Maghami, S. (2007). „Preparation and characterization of linear low density polyethylene-carbon nanotube nanocomposites". *Journal of Macromolecular Science*, **46**, 877–889;
[158] Liu, T.X., Huang, S. (2010). „Morphology and thermal behavior of polymer/carbon nanotube composites". In *Physical properties and applications of polymer nanocomposites*; Tjong, S.C., Mai, Y.W., Eds.; *Woodhead Publishing*, ISBN 9781845696726;
[159] Bikiaris, D. (2010). "Microstructure and properties of polypropylene/ carbon nanotube nanocomposites". *Materials*, **3**, 2884–2946;
[160] Singh, B.P., Prabha; Saini, P., Gupta, T., Garg, P., Kumar, G., Pande, I., Pande, S., Seth, R.K., Dhawan, S.K., Mathur, R.B. (2011). „Designing of multiwalled carbon nanotubes reinforced low density polyethylene nanocomposites for suppression of electromagnetic radiation". *Journal of Nanoparticle Research*, **13**, 7065–7074;
[161] Avalos-Belmontes, F., Ramos-deValle, L.F., Ramirez-Vargas, E., Sanchez-Valdes, S., Mendez-Nonel, J., Zitzumbo-Guzman, R. (2012). „Nucleating effect of carbon nanoparticles and their influence on the thermal and chemical stability of polypropylene". *Journal of Nanomaterials*, **2012**, 406214;
[162] Sinha Ray, S. (2013). „Crystallization behavior, kinetics and morphology of environmentally friendly polymer nanocomposites using biodegradable polymer matrices and clay/carbon nanotube (CNT) reinforcements". In *Environmentally friendly polymer nanocomposites*; Sinha Ray, S., Ed.; *Woodhead Publishing*, ISBN 9780857097774;
[163] Gumede, T.P., Luyt, A.S., Perez-Camargo, R.A., Tercjak, A., Muller, A.J. (2018). „Morphology, nucleation, and isothermal crystallization kinetics of poly(butylenes succinate) mixed with a polycarbonate/MWCNT masterbatch". *Polymers*, **10**, 424;
[164] Riley, A. (2012). „Basics of polymer chemistry for packaging materials". In *Packaging technology. Fundamentals, materials and processes*; Emblem, A., Emblem, H., Eds.; *Woodhead Publishing*, ISBN 9781845696658;
[165] Swallowe, G.M. (1999). „Crystallinity". In *Mechanical properties and testing of polymers. Polymer science and technology series*; Swallowe, G.M., Ed.; *Springer*, ISBN 9789048140244;

[166] Gleadall, A. (2015). „Mechanical properties of biodegradable polymers for medical applications". In *Modelling degradation of bioresorbable polymeric medical devices*; Pan, J., Ed.; Elsevier, ISBN 9781782420163;
[167] Cheng, S.Z.D., Jin, S. (2002). „Chapter 5 - Crystalization and melting of metastable crystalline polymers". In *Handbook of thermal analysis and calorimetry*, Volume 3: Application to polymers and plastics; Cheng, S.Z.D., Ed.; *Elsevier*, ISBN 9780444512864;
[168] Assouline, E., Lustiger, A., Harber, A.H., Cooper, C.A., Klein, E., Wachtel, E., Wagner, H.D. (2003). „Nucleation ability of multiwall carbon nanotubes in polypropylene composites". *Journal of Polymer Science B*, **41**, 520–527;
[169] Ganß, M., Stapathy, B.K., Thunga, M., Weidisch, R., Potschke, P., Jehnichen, D. (2008). „Structural interpretations of deformation and fracture behavior of polypropylene/multi-walled carbon nanotube composites". *Acta Materialia*¸ **56**, 2247–2261;
[170] Stan, F., Sandu, I.L., Fetecau, C. (2014). „Effect of processing parameters and strain rate on mechanical properties of carbon nanotube–filled polypropylene nanocomposites". *Composites Part B*, **59**, 109–122;
[171] Coppola, B., Maio, L.D., Incarnato, L., Tulliani, J.M. (2020). „Preparation and characterization of polypropylene/carbon nanotubes (PP/CNTs) nanocomposites as potential strain gauges for structural health monitoring". *Nanomaterials*, **10**, 814;
[172] Zhou, Z., Wang, S., Zhang, Y., Zhang, Y.X. (2006). „Effect of different carbon fillers on the properties of PP composites: comparison of carbon black with multiwalled carbon nanotubes". *Journal of Applied Polymer Science*, **102**, 4823–4830;
[173] Yang, B.X., Shi, J.H., Pramoda, K.P., Goh, S.H. (2008). „Enhancement of the mechanical properties of polypropylene using polypropylene-grafted multiwalled carbon nanotubes". *Composites Science and Technology*, **68**, 2490–2497;
[174] Kim, J.Y., Han, S.I., Kim, D.K., Kim, S.H. (2009). „Mechanical reinforcement and crystallization behavior of poly(ethylene 2,6-naphthalate) nanocomposites induced by modified carbon nanotube". *Composites Part A*, **40**, 45–53;
[175] Stan, F., Stanciu, N.V., Fetecău, C., Sandu, I.L. (2018). „Characterization of welding attributes in friction spot stir welding of high-density polyethylene/multi-walled carbon nanotube composites". Proceedings of the 2018 Manufacturing Science and Engineering Conference MSEC2018, MSEC2018-6317, pp. V002T04A006, 10 pages;
[176] Sinha Ray, S., Maiti, P., Okamoto, M., Yamada, K., Ueda, K. (2002). „New polylactide-layered silicate nanocomposites. 1. Preparation, characterization, and properties". *Macromolecules*, **35**, 3104–3110;
[177] Grady, B.P., Pompeo, F., Shambaugh, R.L., Resasco, D.E. (2002). „Nucleation of polypropylene crystallization by single-wall carbon nanotubes". *Journal of Physical Chemistry B*, **106**, 5852–5858;
[178] Li, S.N., Li, Z.M., Yangm M.B., Hu, Z.Q., Xu, X.B., Huang, R. (2004). „Carbon nanotubes induced nonisothermal crystallization of ethylene–vinyl acetate copolymer". *Materials Letters*, **58**, 3967–3970;
[179] Kodjie, S.L., Li, L., Li, B., Cai, W., Li, C.Y., Keating, M. (2006). „Morphology and crystallization behavior of HDPE/CNT nanocomposite". *Journal of Macromolecular Science B*, **45**, 231–245;
[180] Micusik, M., Omastova, M., Pionteck, J., Pandis, C., Logakis, E., Pissis, P. (2011). „Influence of surface treatment of multiwall carbon nanotubes on the properties of polypropylene/carbon nanotubes nanocomposites". *Polymers for Advanced Technologies*, **22**, 38–47;
[181] Program documentation: WinRheo II, Gottfert, Germany;
[182] Dawson, P.C. (1999). „Flow properties of molten polymers". In *Mechanical properties and testing of polymers. Polymer science and technology series*; Swallowe, G.M., Ed.; *Springer*, ISBN 9789048140244;
[183] Abbasi, S., Carreau, P.J., Derdouri, A., Moan, M. (2009). „Rheological properties and percolation in suspensions of multiwalled carbon nanotubes in polycarbonate". *Rheological Acta*, **48**, 943–959;
[184] Stan, F., Stanciu, N.V., Fetecău, C. (2017). „Melt rheological properties of ethylene-vinyl acetate/ multi-walled carbon nanotube composites". *Composites Part B Engineering,* **110**, 20–31;
[185] Song, Y.S. (2006). „Rheological characterization of carbon nanotubes/poly (ethylene oxide) composites". *Rheological Acta,* **46**, 231–238;
[186] Hamad, K., Kaseem, M., Deri, F. (2011). „Effect of recycling on rheological and mechanical properties of poly(lactic acid)/polystyrene polymer blend". *Journal of Materials Science*, **46**, 3013–3019;
[187] Ariff, Z.M., Ariffin, A., Jikan, S.S., Rahim, N.A.A. (2012). „Rheological behaviour of polypropylene through extrusion and capillary rheometry". In *Polypropylene*; Dogan, F., Ed.; *InTech*, ISBN: 978-953-51-0636-4;

[188] Park, H.E., Lim, S.T., Laun, H.M., Dealy, J.M. (2008). „Measurement of pressure coefficient of melt viscosity: Drag flow versus capillary flow". *Rheological Acta*, **47**, 1023–1038;
[189] Moldenaers, P., Vermant, J., Mewis, J. (1996). „Origin of nonlinearities in the Bagley plots of thermotropic copolyesters". *Journal of Rheology*, **40**(2), 203–219;
[190] Fischer, J.M. (2013). „Handbook of molded part shrinkage and warpage", 2nd ed.; *Elsevier Inc.,* ISBN 9781455725977;
[191] Marconnet, A.M., Yamamoto, N., Panzer, M.A., Wardle, B.L., Goodson, K.E. (2011). „Thermal conduction in aligned carbon nanotube-polymer nanocomposites in high packing density". *ACS Nano*, **5**, 4818–4825;
[192] Huang, C., Qian, X., Yang, R. (2018). „Thermal conductivity of polymers and polymer nanocomposites". *Materials Science & Engineering R: Reports*, **132**, 1–22;
[193] Zhou, T.Y., Tsui, G.C.P., Liang, J.Z., Zou, S.Y., Tang, C.Y., Miskovic-Stankovic, V. (2016). „Thermal properties and thermal stability of PP/MWCNT composites". *Composites Part B*, **90**, 107„114;
[194] Berber, S., Kwon, Y.K., Tomanek, D. (2000). „Unusually high thermal conductivity of carbon nanotubes". *Physical Review Letters*, **84**, 4613–4616;
[195] Kim, P., Shi, L., Majumdar, A., McEuen, P.L. (2001). „Thermal transport measurements of individual multiwalled nanotubes". *Physical Review Letters*, **87**, 215502;
[196] Hida, S., Hori, T., Shiga, T., Elliott, J., Shiomi, J. (2013). „Thermal resistance and phonon scattering at the interface between carbon nanotube and amorphous polyethylene". *International Journal of Heat and Mass Transfer*, **67**, 1024–1029;
[197] Zhang, S., Minus, M.L., Zhu, L., Wong, C.-P., Kumar, S. (2008). „Polymer transcrystallinity induced by carbon nanotubes". *Polymer*, **49**, 1356–1364;
[198] Williams, M.L., Landel, R.F., Ferry, J.D. (1955). „The temperature dependence of relaxation mechanisms in amorphous polymers and other glass-forming liquids". *Journal of the American Chemical Society*, **77**, 3701–3707;
[199] Eyring, H. (1936). „Viscosity, plasticity and diffusion as examples of absolute reaction rates". *The Journal of Chemical Physics*, **4**, 283–291;
[200] Raha, S., Sharma, H., Senthilmurugan, M., Bandyopadhyay, S., Mukhopadhyay, P. (2019). „Determination of the pressure dependence of polymer melt viscosity using a combination of oscillatory and capillary rheometer". *Polymer Engineering & Science*, **60**, 517–523;
[201] Kirchberg, S. (2013). „Simulation and injection molding of ring-shaped polymer bonded nickel braze metal composite preforms based on rheological and thermal analyses". *Open Journal of Composite Materials*, **3**, 24–29;
[202] Tcharkhtchi, A., Nony, F., Khelladi, S., Fitoussi, J., Farzaneh, S. (2015). „Epoxy/amine reactive systems for composites materials and their thermomechanical properties". In *Advances in composites manufacturing and process design*; Boisse, P., Ed.; *Elsevier*, ISBN 9781782423072;
[203] Ratna, D. (2012). „Thermal properties of thermosets". In *Thermosets*; Guo, Q., Ed.; *Woodhead Publishing*, ISBN 9780857090867;
[204] Zhao, P., Yang, W., Wang, X., Li, J., Yan, B., Fu, J. (2019). „A novel method for predicting degrees of crystallinity in injection molding during packing stage". *Journal of Engineering manufacture*, **233**, 204–214;
[205] Zheng, R., Tanner, R.I., Fan, X.J. (2011). „Injection molding. Integration of theory and modeling methods". *Springer Verlag GmbH*, ISBN 9783642212635;
[206] Mekhilef, N. (2001). „Viscoelastic and pressure–volume–temperature properties of poly(vinylidene fluoride) and poly(vinylidene fluoride)–hexafluoropropylene copolymers". *Journal of Applied Polymer Science*, **80**, 230–241;
[207] Lucyshyn, T., Knapp, G.; Kipperer, M.; Holzer, C. (2012). „Determination of the transition temperature at different cooling rates and its influence on prediction of shrinkage and warpage in injection molding simulation". *Journal of Applied Polymer Science*, **123**(2), 1162–1168;
[208] Tao, R., Simon, S.L. (2015). „Pressure-volume-temperature and glass transition behavior of silica-polystyrene nanocomposites". *Journal of Polymer Science: Polymer Physics*, **53**(16), 1131–1138;
[209] Fetecău, C. (2007). „Injectarea materialelor plastice", 2nd ed.; *Editura Didactică şi Pedagogică R.A.,* ISBN 9789733019718;
[210] Stan, F., Stanciu, N.V., Constantinescu, A.M., Fetecău, C. (2021), „3D printing of flexible and stretchable parts using multiwall carbon nanotube/polyester-based thermoplastic polyurethane". *Journal of Manufacturing Science and Engineering Transactions of ASME*, **143**, 051002-1-9;

[211] Stanciu, N.V., Roşculeţ, T.R, Fetecău C., Ţapu C. (2020). „Forensic facial reconstruction using 3D printing". *Materiale Plastice*, **57**(4), 248–257;
[212] Stanciu, N.V., Stan, F., Sandu, I.L., Susac, F., Fetecău, C., Roşculeţ, T.R. (2019). „Mechanical, electrical and rheological behavior of ethylene-vinyl acetate/multi-walled carbon nanotube composites". *Polymers*, **11**, 1300;
[213] Stan, F., Stanciu, N.V., Fetecău, C., Sandu, I.L. (2019). „Mechanical recycling of low-density polyethylene/carbon nanotube composites and its effect on material properties". *Journal of Manufacturing Science and Engineering-Transactions of the ASME*, **141**, 091004-1-7;
[214] Stanciu, N.V., Stan, F., Fetecău, C. (2018). „Melt shear rheology and pVT behavior of polypropylene/multi-walled carbon nanotube composites". *Materiale Plastice*, **55**, 482–487;
[215] Stan, F., Stanciu, N.V., Fetecău, C. (2019). „On the 3D printability of multi-walled carbon nanotube/high density polyethylene composites". Proceedings of the 2019 Manufacturing Science and Engineering Conference (MSEC2019), Penn State Erie, The Behrend College, Erie, PA, USA, 10-14 June 2019, Paper No. MSEC2019-2776;
[216] Stanciu, N.V., Stan, F., Fetecău, C., Susac, F. (2019). „On the feasibility of printing 3D composite objects based on polypropylene/multi-walled carbon nanotubes". *MATEC Web of Conference*, **290**, 03017;
[217] Fetecău, C., Stan, F., Timotin, P., Stanciu, N.V., Roşculeţ, R.T. (2018). „Mechanical behavior of LDPE/MWCNT composites after fatigue and cryogenic treatment". Proceedings of the 2018 Manufacturing Science and Engineering Conference (MSEC2018), Collage Station, TX, USA, 18-22 June 2018, Paper No. MSEC2018-6532, V002T04A014;
[218] Stan, F., Fetecău, C., Stanciu, N.V., Roşculeţ, T.R., Sandu, I.L. (2017). „Investigation of structure-property relationships in thermoplastic polyurethane/multiwalled carbon nanotube composites". ASME 2017 12th International Manufacturing Science and Engineering Conference (MSEC2017), Vol. 2: Additive Manufacturing; Materials, Los Angeles, California, USA, 4-8 June 2017, Paper No. MSEC2017-2760, pp. V002T03A016;
[219] Fetecău, C., Stan, F., Cristea, N.V., Sandu, I.L. (2016). „An analysis of interfacial adhesion between TPU/MWCNT composites and ABS by over injection molding". ASME 2016 Manufacturing Science and Engineering Conference (MSEC2016) & 44rd North American Manufacturing Research Conference (NAMRC44) of SME, Virginia Tech University, USA, 27 June – 1 July 2016, Paper No. MSEC2016-8571, V001T02A050.